2011

INVESTIGATION OF BIOMOLECULAR INTERACTIONS FOR DEVELOPMENT OF SENSORS AND DIAGNOSTICS

Xiaojuan Zhang
Virginia Commonwealth University

INVESTIGATION OF BIOMOLECULAR INTERACTIONS FOR DEVELOPMENT OF SENSORS AND DIAGNOSTICS

A thesis submitted in partial fulfillment of the requirements for the degree of Doctor of Philosophy at Virginia Commonwealth University

By
Xiaojuan Zhang
Master of Engineering in Fermentation Engineering- Jiangnan University, China, 2007
Bachelor of Engineering in Biotechnology- Jiangnan University, China, 2005

Director: Vamsi K. Yadavalli, Ph.D
Assistant Professor of Chemical and Life Science Engineering

Virginia Commonwealth University
Richmond, Virginia
November, 2011

Acknowledgment

This dissertation would not have been possible without the guidance and the help of several individuals who contributed in one way or another and extended their valuable assistance in the completion of this study.

First and foremost I would like to thank my advisor, Dr. Vamsi Yadavalli, for giving me the opportunity to complete this thesis and for guiding me through research. He made his support in a number of ways: the sharing of his scientific expertise and extensive knowledge in many fields with me; extra effort on supervising my scientific writing, and his continuous encouragement and patience as I hurdle all the obstacles during these years.

I would like to express my appreciation to the rest of my thesis committee for their dedication along my research: Dr. Kenneth J. Wynne, for sharing his solid knowledge in the surface chemistry with me and also for the guidance for the fruitful and pleasant collaboration in a side project; Dr. Allison Johnson, for the vivid discussion on the biology side of my dissertation research, and technical support along my research; Dr. Stephen S. Fong, for his valuable suggestions regarding research direction and active support of my research, and Dr. Hu Yang, for his

valuable insight regarding the thesis writing and dedication along this research.

In addition, I would like to thank Dr. Ali Reza Siamaki for help with NMR measurements and analysis, and Dr. Wei Zhang for the assistance with the amination reaction system.

I am grateful to my lab mates: Nick Kurland, Zouheir Drira, Eric McCullough, and Chris Weigel for the vivid and fruitful discussion, the help at the bench and great company during all these years. Thank you for creating the joyful and encouraging working atmosphere in the lab.

Furthermore, I want to thank for my family: my parents, for always being there for me and generous support in many ways; my husband, Dr. Yu Deng, for the love and support, but also for being an academic buddy during these years of research.

Table of Contents

List of Tables

List of Figures

Abstract

INVESTIGATION OF BIOMOLECULAR INTERACTIONS FOR THE DEVELOPMENT OF SENSORS AND DIAGNOSTICS

By Xiaojuan Zhang, Ph.D

A thesis submitted in partial fulfillment of the requirements for the degree of Doctor of Philosophy at Virginia Commonwealth University

Virginia Commonwealth University, 2011

Major Director: Vamsi K. Yadavalli, Ph.D, Assistant Professor of Chemical and Life Science Engineering

The highly specific recognition processes between biomolecules mediate various crucial biological processes. Uncovering the molecular basis of these interactions is of great fundamental and applied importance. This research work focuses on understanding the interactions of several biomolecular recognition systems and processes that can provide fundamental information to aid in the rational design of sensing and molecular recognition tools. Initially, a reliable and versatile platform

was developed to investigate biomolecular interactions at a molecular level. This involved several techniques, including biomolecule functionalization to enable attachment to self-assembled monolayers as well as atomic force microscopy (AFM) based force spectroscopy to uncover the binding or rupture forces between the receptor and ligand pairs. It was shown that this platform allowed determination of molecular binding between single molecules with a high specificity. The platform was further adapted to a general sensing formulation utilizing a group of flexible and adaptive nucleic acid recognition elements (RNA and DNA aptamers) to detect specific target proteins. Investigation of interactions at the molecular level allowed characterization of the dynamics, specificity and the conformational properties of these functional nucleic acids in a manner inaccessible via traditional interaction studies.

These interactions were then adapted to aptamer-based detecting methods that at the ensemble or bulk scale, specifically taking advantage of mechanisms uncovered in the biophysical study of this system. A quartz crystal microbalance (QCM) was used to detect protein targets at the bulk level and the affinities and binding kinetics of these systems were analyzed. Along with AFM-based force spectroscopy, ensemble-averaging properties and molecular properties of these interactions could be correlated to contribute to bridging the gap across length scales.

Finally, more broadly applicable sensing platform was developed to take advantage of the unique properties of aptamers. DNA was employed both as a carrier and as a molecular recognition agent. DNA was used as a template for

nanoconstruction and fabricating unique shapes that could enhance the aptamer-based molecular recognition strategies. With aptamers tagged to distinct nanoconstructed DNA, a novel shape-based detecting method was enabled at the molecular level. The results demonstrated that this is a flexible strategy, which can be further developed as ultrasensitive single molecule sensing strategy in complex environments.

CHAPTER 1

INTRODUCTION

1.1 Introduction

The mystery of life has been an important intellectual focus for centuries. With the development of biochemistry and molecular biology, one can fundamentally regard the phenomenon of life as a complex interplay between a large numbers of biomolecules.[1, 2] The highly specific recognition processes between these biomolecules mediate various crucial biological processes, which are closely related to numerous essential functions, including genome transcription and translation, enzymatic reaction, cell proliferation, immune response, initiation of infections and so on.[3-5] On the other hand, many diseases, including cancers, genetic diseases and age-related diseases are closely associated to a malfunction in such molecular recognition processes.[6]

From an engineering perspective, besides the aim of understanding the fundamental principles of life, studying the processes of biomolecular interactions or

recognition can also assist in the development of bio-analytical and biomedical devices. [7] In order to rationally design effective biosensing agents or medical devices, a detailed understanding of the molecular binding processes, together with information about kinetics and conformation are necessary.

Over the years, ensemble-averaging properties of biomolecular interactions have been characterized using traditional analytical methods, such as surface plasmon resonance, nuclear magnetic resonance, mass spectrometry and fluorescence-based technologies.[4, 8] Recently, however, with the development of extremely sensitive methods, such as optical tweezers, magnetic tweezers and atomic force microscopy (AFM), it is possible to study systems at the single molecule level, without the ensemble-averaging inherent of traditional biochemical assays.[9] However, although these techniques are capable of performing highly precise descriptions of real-time progress of interactions at the molecular level, there are several methodological and technical difficulties limiting research carried out. Critical challenges include developing reliable experimental methodologies at the molecular level, extracting useful information from the data (often chaotic or having a low signal to noise ratio), and obtaining detailed biophysical information of the ligands. Another problem is the gap affecting the knowledge of interactions across length scales – from the molecular level to the ensemble level. How do the properties characterized from molecular level manifest themselves at the ensemble level? Can these correlations be used to design reliable sensing strategies or analytical tools? This research is intended to address these challenges and questions.

Broadly, the subject of this thesis is based on interdisciplinary research combining biology, chemistry, biophysics and nanotechnology with engineering principles. The goal is to provide detailed information about the binding processes at molecular level, and to further apply these properties for molecular recognition and sensing schemes. Initially, a versatile platform was established for conducting molecular interaction measurements using force spectroscopy. The interaction of a sugar-lectin system was detected and characterized using this platform, which verified the efficacy of the technique. The use of the platform was further adapted to investigate different interactions of short oligonucleotide sequences called aptamers and their protein targets. Using AFM as a primarily molecular tool, the energy landscapes, specificity, and structural stability of several aptamer/target protein systems was revealed. Based on this information, aptamer based sensors were fabricated and investigated by quartz crystal microbalance (QCM) measurements. The ensemble-averaging properties of aptamer/target protein interaction were characterized, and also correlated with molecular biophysical behaviors. These insights into the fundamental biophysical interactions between the aptamers and their target proteins provide useful information for the rational design of aptamer-based sensors or diagnostic tools. Furthermore, in order to apply them in more advanced applications such as ultrasensitive cellular sensors or therapeutic delivery systems, aptamers were organized into well defined DNA nanostructures. Using DNA nanoconstruction strategies, multiple aptamer-functionalized DNA nanostructure were designed and fabricated. The results indicated that aptamer-functionalized DNA

structures can facilitate the on-demand production of libraries of diverse shapes that can recognize and bind proteins or catalyze reactions via functional nucleic acid tags. These techniques can further enable the development of novel biosensing and therapeutic delivery tools.

1.2 Specific aims

1.2.1 Develop and characterize a platform to enable the study of biomolecular interactions at the molecular level

To enable the studies of biomolecular interactions at the molecular level, it is important to develop a versatile strategy to bring individual receptor-ligand pairs together and discriminate specific molecular interactions from non-specific ones. The initial portion of this research was to develop such a platform using a mixed self-assembled monolayer (SAM) approach. A model system (a carbohydrate and a sugar binding protein - lectin) was used in this research to test the efficacy of this strategy. The surface with immobilized biomolecules was characterized by AFM imaging, and followed by AFM-based force spectroscopy studies under different conditions to further verify the feasibility and flexibility of this platform.

1.2.2 Investigate the molecular interactions between aptamers and their protein targets via force spectroscopy

Built on the platform described above, a general formulation to investigate the

binding of flexible and adaptive molecular recognition elements was developed and tested. Specifically, engineered RNA and DNA ligands called aptamers are emerging as superior alternatives to antibodies for recognition and diagnostics. The goal of this research was to enable different aptamer-based molecular recognition strategies by understanding the interactions between them and their targets. Initially this interaction was studied at the single to few molecule level using AFM force spectroscopy. The rupture force, the dynamic bond under increasing external force, the specificity and the structural determinants of the interaction between the aptamer and target protein were revealed.

1.2.3 Translate specific biomolecular interaction events across length scales

Following the previous aim, the aptamer-based recognition investigated at the molecular level was studied at the ensemble level. First of all, it was necessary to optimize different strategies to immobilize aptamers on solid surfaces so that their binding with protein targets could be studied from a sensing perspective. Quartz crystal microbalance (QCM) measurements were used to evaluate the sensitivity and affinity of the aptamer sensors fabricated by these methods. AFM based force spectroscopy was performed to further verify the functional viability of the surface-tethered aptamers for biophysical analyses and protein binding. In order to correlate the information concluded from molecular level and ensemble level, the results obtained from QCM measurements and AFM force spectroscopy experiments were compared and discussed.

1.2.4 Utilize aptamer based molecular recognition to fabricate molecular sensing strategies

Since aptamers are functional nucleic acids, direct DNA modification by sequence extension or hybridization is easily performed. This allows enhancement of the aptamer-based molecular recognition strategies by developing novel aptamer tagged DNA nanostructures. The function of these DNA nanostructures as molecular sensors was evaluated by multiple techniques in biological condition. Furthermore, the flexibility and stability of these shapes were tested. By demonstrating multiple aptamer functionalized DNA nanostructures and complexes of these nanostructures with target proteins, functional DNA architectures were shown to be a powerful tool in enabling the development of ultrasensitive single molecule sensors.

1.3 Background and significance

This research is aimed at investigating biomolecular recognition processes, so that these specific interactions can be further applied and translated to general biosensing or diagnostic tools. In order to study biomolecule interaction, techniques and strategies from different disciplines were combined and applied in this research. This section is devoted to presenting the background and significance of this research, and introducing the techniques and disciplines merged in this thesis.

1.3.1 Biomolecular interaction or recognition in life science: the role and the principle

The last few decades have fundamentally changed the way people understand life. With the access to the information contained in biological macromolecules, now researchers can explain the phenomenon of death, infectious, inherited diseases by an extremely complex system of biochemical reactions.[10] It has become clear that biological functions of most macromolecules closely depend on their ability to interact with other molecules. Such specific interactions include those between antigens and antibodies, ligands and cell surface receptors, complementary strands of DNA, lectins and carbohydrates, as well as enzymes and substrates.[11] These interactions play crucial roles in various important biological processes, including genome replication and transcription, metabolic regulation, signaling transduction, immune response, and many other cellular functions.[12, 13] A thorough understanding of intermolecular interactions, such as the strength of the binding, stability of the complexes, and the conformational changes coupled with the binding processes, are of paramount importance. From an applied perspective, these investigations can further be used to guide our design of bio-analytical strategies and devices.

The non-covalent interaction between two biomolecules can be the result of electrostatic interactions, hydrogen bonding, hydrophobic effects or even ion induced binding. This binding process between biomolecules is a reversible thermodynamic

process.[14] There are three important properties commonly used to describe the binding phenomenon: 1) affinity, which is the summary of the thermodynamic property, can be interpreted as how strong the molecules in the pair adhere to each other; 2) kinetics, indicating how fast the association and dissociation happens between two biomolecules; 3) specificity, which describes how selectively a molecule binds to its target. Usually, this property closely associates with the conformational precision property of the biomolecule.[15]

Affinity related to Gibbs free energy of binding, is a macroscopic property indicating an averaged description of a large number of binding events. The thermodynamic behavior of biomolecules at steady state can be quantified by the equilibrium constant of binding, also known as association constant (K_A) over an effective concentration range. K_A is time- independent, and determines how much complex is formed at equilibrium. The kinetics of the binding can be described as the association constant rate (k_{+1}) or dissociation constant rate (k_{-1}). These two parameters describe how fast the molecules bind and fall apart. Hence, different interactions with different association/dissociation rates, possibly have the similar binding strength.

$$A+B \underset{k_d}{\overset{k_a}{\rightleftharpoons}} AB \tag{1.1}$$

$$d[AB]/dt = k_{+1}[A][B] - k_{-1}[AB] \tag{1.2}$$

At equilibrium,

$$k_1[A][B] = k_{-1}[AB] \tag{1.3}$$

K_A and K_D can be resolved by k_{+1} and k_{-1},

$$K_A = \frac{[AB]}{[A][B]} = \frac{k_{+1}}{k_{-1}} \tag{1.4}$$

$$K_D = \frac{[A][B]}{[AB]} = \frac{k_{-1}}{k_{+1}} \tag{1.5}$$

Biosensing and molecular recognition technologies utilize biomolecules (for example, proteins, oligonucleotides or even whole cells) as biological recognition elements to detect various target molecules.[16, 17] In the early 1960s, antibodies were first used to develop bioanalytical assays to detect plasma insulin.[18] Since then, biosensing studies applying antibodies as recognition elements for a wide range of target compounds have been continuously reported in the clinical, food, and environmental areas.[19] Besides antibodies, other biomolecules such as proteins and nucleic acids were also used as receptors in biosensing assays.[20, 21] Glucose sensors for example, which utilize the enzyme glucose oxidase as a biorecognition component, form the largest percentage of biosensors on the market because of their broad use in the diagnosis of diabetes.[22] In recent years, nucleic acid sensors, have gained increasing importance as well. The development of high density arrays of nucleic acid oligomers on chip have been successfully used to detect hybridization and further provide information about gene expression or to identify specific sequences.[23]

Current research and development in the area of bioanalytical sensing aim to improve their stability, selectivity and sensitivity. One approach to achieving this is to understand and control the biophysical properties of the recognition components to

achieve optimal performance. Since many biosensing designs are chip based, maintaining of the stability, recognition functionality, and specificity of these biomolecules at the interface between the biological layer and the analyte solution while minimizing effect of the substrate is a real challenge.

In this research, the initial focus was on investigating these interactions between various ligands and receptors, considering their immobilization on surfaces. The goal was to develop platforms for immobilizing different biomolecules to enable such investigations and further to study the biophysical determinants of their interactions. Much of the subsequent work focused on investigations of aptamers as recognition agents to identify and bind their target proteins in various formats and at various length scales. As new set of functional ligands, aptamers are rapidly emerging as attractive candidates for affinity-based biosensing applications. An introduction to aptamers and aptamer-based sensing is covered in the following section.

1.3.2 Nucleic acid aptamers and their targets interaction

Prior to the 1980s, nucleic acids, including both DNA and RNA, were typically understood as passive carriers of genetic information. However, the discovery that DNA and RNA can participate directly in catalysis in living cells greatly changed research in the area of nucleic acid research.[24, 25] Now, it is commonly recognized that DNA and RNA can also exist as a diversity of structures with a variety of sophisticated functions.[26] For example, riboswitches can directly bind small target molecules and affect gene activity. [27] RNA interference (RNAi) participates in

controlling gene expression activity by binding other specific mRNA.[28] These naturally existing functional nucleic acids have inspired scientists and engineers to utilize structural DNA or RNA as versatile tools to obtain artificial functions including recognizing and modulating the activity of proteins in biological systems.

Within a short period of time in the 1990s, three groups selected RNA and DNA molecules which could specifically bind to several protein targets using an evolutionary *in vitro* selection process, called systematic evolution of ligands by exponential Enrichment (SELEX).[29-31] Through this process, trillions of oligonucleotides are prepared simultaneously as a library, and subjected to a process of selective amplification to enrich the population with the ligands that bind to a particular protein target.[29] The resulting oligonucleotides were referred to as "aptamers", which derived from the Latin "*aptus"*, meaning "to fit".[32] As a new class of functional, ligand-binding biomolecules, aptamers usually have a high affinity with the K_D value in the picomolar range, and specificity comparable to, and often exceeding those of antibodies towards their targets. Another advantage of using aptamers instead of antibodies is the ease of synthesis, which does not require *in vivo* immunization of animals like antibodies. Besides, compared with antibodies aptamer do not cause significant immunogenicity.[33] Moving beyond protein targets, aptamers have been selected against a wide range of target molecules, from cells to low-molecular weight organic and inorganic substrates with a high degree of specificity, purity, and reproducibility.[34] There are advantages related to the chemical nature of aptamers, including enhanced stability and also the ability of

regeneration following denaturation, and ease of modification to contain specific chemical functionalities.[35] Aptamer technologies along with the SELEX process, have demonstrated that, in the laboratory, one can create DNA or RNA ligands which can fold into sophisticated 3D structures, and have exquisite recognition capabilities against a wide variety of targets including proteins and small molecules.[36] Recent progress in aptamer technology has verified that aptamers are a potentially powerful tool with applications in biosensors [37], diagnostics [38, 39], therapeutics [38] and targeted drug delivery.[39, 40] FDA approval of the first aptamer-based therapeutic agent Pegaptanib [41] for the treatment of nonvascular age-related macular degeneration was a milestone in the developmental history of aptamers and underscored the enormous potential of using RNA and DNA aptamers as therapeutics. Recently, researches have also shown the potential of using aptamer in analytical applications.[42, 43] Traditionally analytical strategies for detecting binding have typically used antibodies, in electrochemical detection, surface plasmon resonance (SPR) and gravimetric techniques including quartz crystal microbalance (QCM). Aptamers have been shown to be suitable replacements to antibodies in such applications. A unique structural property of aptamers, whereby they undergo significant conformational changes upon binding to their target molecules, was used to design novel optical sensing strategies.[44, 45] In these optical strategies, the aptamers were labeled with a fluorophore as reporter. By monitoring the fluorescence signal change (turning on or off upon binding), the conformational changes were used to indicate the binding of the target molecules to the aptamers. [45-47]

These various sensing schemes to date have focused on simply using aptamers as replacements for antibodies and have not exploited the unique properties of aptamers which could greatly enhance their role as biomolecular recognition agents. For example, aptamers have distinct properties such as structural flexibility and adaptive folding in the presence of their targets. More biophysical investigations are needed in order to utilize them for sensing applications compared to other recognition systems such as antibodies. Insights into the structure, dynamics, and the fundamental biophysics of these fundamental interactions and complex formations would greatly enhance the ability to engineer and deliver the next generation of "smart" drugs and diagnostic tools. Although several studies on the structure and function of receptor-ligand complexes have been reported, insight into the molecular dynamics within the complexes under non-equilibrium conditions is quite limited.[48-52] One of the goals of this research was to fill some of the gaps in this area.

1.3.3 Affinity analysis based ensemble-level sensing methods

As introduced above, affinity analyses at the ensemble level form an averaged description of the binding behavior of a large number of molecules, and are the most typical approaches to study molecular interactions. In general, sensing or detecting biomolecule interaction relies on a transducer that converts a chemical or biological interaction into a detectable signal. In theory, when biomolecular partners come together, there are several different phenomena that can be utilized as signal changes in biosensing applications, including physical parameters, mass, acoustic waves,

thermal capacity, enthalpy, heat transfer, optical signals, magnetic signals or electrical signals.[53] In reality, most of these signal changes are not operationally distinguishable, and difficult to apply to a qualitative affinity analysis. Until now, the most commonly applied signal transductions are based on electrochemical, optical, and acoustic waves.[19] The development of these interfaces of signal transduction technologies have resulted in various devices and techniques: for instance, electrochemical signal based techniques include mass spectrometer (MS)[54], potentiometric[55]; optical signal based technique including total internal reflectance fluorescence (TIRF)[56], surface plasmon resonance (SPR)[57]; acoustic wave based technique including quartz crystal microbalance (QCM)[58] and surface acoustic wave (SAW)[59].

Among all these techniques, QCM and SPR are among the most attractive sensing methods because they allow real-time analysis of reactions without labeling requirements and provide quantitative information on the equilibrium binding states as well as non-equilibrium states.[60] Both QCM and SPR detect binding between biomolecules immobilized on a surface and analyte in solution by a flow injection fashion, and they have the similar sensitivity and detection limits.[61] However, compared with SPR, QCM is typically much less expensive, and much easier to operate. Hence, the QCM has been adopted as a suitable analytical tool to measure bio-specific interactions, and has become one of the most leading strategies in biological binding measurements.[58] A broad range of biological molecules such as antibodies, proteins, nucleic acids, carbohydrate and drugs as receptor molecules have

been successfully investigated by QCM.[58] The interactions of aptamers and their targets have also been recently begun to be investigated by QCM techniques.[62-64]

The most important component of QCM is the quartz crystal sensor contacting a pair of electrodes. Due to the piezoelectric properties of quartz crystal, by applying an AC voltage across the electrodes, the crystal can be excited to oscillation. The resonance frequency *(f)* of the crystal depends on the total oscillating mass. QCM biosensors are integrated to a flow injection analysis (FIA) system. In this way, when the analyte molecules in the solution attach to the sensor crystal, the frequency of the sensor decreases, owing to the damping caused by the corresponding mass of the analytes. The decrease in frequency is proportional to the mass gain of the sensor, and the increase of mass due to the binding can be calculated according to the Sauerbrey equation [65]:

$$\Delta f = -C_f \times \Delta m / A \tag{6}$$

With

$$c_f = -\left[\left(f_R{}^2\right)/\left(\nu_q \rho_q\right)\right] \tag{7}$$

where Δf_r (Hz) is the frequency change of the quartz sensor, Δm (ng) is the mass change of the sensor, A (cm^2) is the area of the quartz surface, and c_f is the sensitivity constant. The constant c_f is determined by f_R, the original resonance frequency of the quartz, v_q, is the velocity of sound in the quartz crystal (3340 ms^{-1}); and ρ_q, is the quartz density (2648 kg m^{-3}).

QCM, has been utilized in a variety of different applications, such as monitoring and characterization of (bio)film deposition, detection of specific antigens,

biomolecule binding kinetics, cell adhesion, and DNA detection.[58, 66] Since 2000, aptamer based QCM sensing studies have reported as well. An anti-IgE DNA aptamer was used as a recognition component, and further compared with the monoclonal antibody for the same target (IgE) in a quartz crystal biosensor.[67] A DNA aptamer specific for human thrombin was used to detect binding of the target protein (thrombin).[62] The aptamer against the HIV-1 Tat protein was also used in a QCM based biosensor.[68] RNA and DNA aptamers specifically selected for interferon (IFN)-γ were studied and compared by QCM assay.[69] Recently, using aptamer based QCM sensing methods, IgE in human serum was successfully detected. [63] These previously reported studies indicate the feasibility of aptamer based QCM sensing techniques. However, optimizing the activity, simultaneously minimizing the loss in functionality and non-specific interactions are still major challenges in designing aptamer based sensors of high sensitivity and selectivity over a large dynamic range.

1.3.4 Measurement of single-molecule interaction based on AFM

At the other end of the length scale spectrum, the recent development of experimental tools allowing the precise description and measurement of single molecule binding events has greatly opened new perspectives in materials and life science.[70] As discussed above, ensemble level techniques such as QCM can provide valuable information about the affinity analysis of biomolecule interactions. However, due to the population-averaging inherent in these biochemical assays, subpopulations

and kinetic details of these interactions are typically hidden. Now however, distributions of molecular properties can be characterized and rare subpopulations can be identified with single molecule tools.[71] The second important benefit of the molecular approach is the ability to detect temporal transition states and binding/unfolding energy landscapes. Hence, the binding process can be precisely recorded as 'molecular movies', which usually happen during too short a period of time to be revealed in an ensemble asynchronous measurement.[70]

1.3.4.1 Force spectroscopy

Several techniques with different detecting principles and dynamical ranges have been developed to enable such single molecule measurements. These include magnetic beads [72], optical tweezers [73], biomembrane force probe (BFP) [74], and atomic force microscopy (AFM) [75]. In particular, one important biophysical parameter in these interactions has been the measurement of the binding (or rupture) forces of the interactions as well as the forces required to unzip or mechanically unfold various proteins.[76-78] Based on different molecular manipulation techniques, concepts related to single-molecule force spectroscopy technique have been developed. These are dynamic analytical techniques allowing the study of the physical properties of interactions from a force-displacement perspective,[79] and are performed by applying an external controlled force to the ligand/receptor system. The accuracy and temporal resolutions of these measurements has therefore been subject to the thermal fluctuations of micrometer-sized detecting elements (for example the

probes in the case of AFM technique, or the beads in the magnetic tweezers). [9, 71] Typically, precise thermal calibrations of the elements, and statistical analysis based on numerous of the measurements can improve the accuracy of applying these techniques.[9] With both an increasing understanding of the fundamental biophysics of molecular interactions as well as improving experiment tools, the development of force spectroscopy continues to be a rapidly evolving field of single molecule analyses.

1.3.4.2 Atomic force microscopy

Among all these methods, Atomic Force Microscopy (AFM) has emerged to be one of the most powerful and widely used tools for high precision imaging and force spectroscopy.[80] Since its invention by Binnig et al. in 1986 [81], the AFM has played a crucial role in nano-scale science and technology, and has been applied in a variety of research fields including physics, chemistry and biology.[82, 83]

Initially, AFM was a technique primarily used for imaging surface and characterizing its topography. This is achieved by feeling the force of atoms on a surface via a sharp probe, mounted at the end of a flexible cantilever. The precise lateral and vertical displacement control of the cantilever with respect to the sample is achieved by piezoelectric holders. During the scanning of probe with respect to the sample, by monitoring the deflection of a laser beam which is aligned on the back of the cantilever, the attractive or repulsive interaction forces between a few atoms attached at a tip on a cantilever and a sample are collected, and further used to create a

topographic image of the sample (Figure 1.1 A).[81, 83] Due to the important features of AFM, such as the simple and rapid sample preparation, the capability of manipulating individual molecules, real-time investigations and allowing the measurements of biological samples under near-physiological conditions, AFM has emerged as an ideal tool for biological applications compared to other scanning probe microscopes. [84, 85]

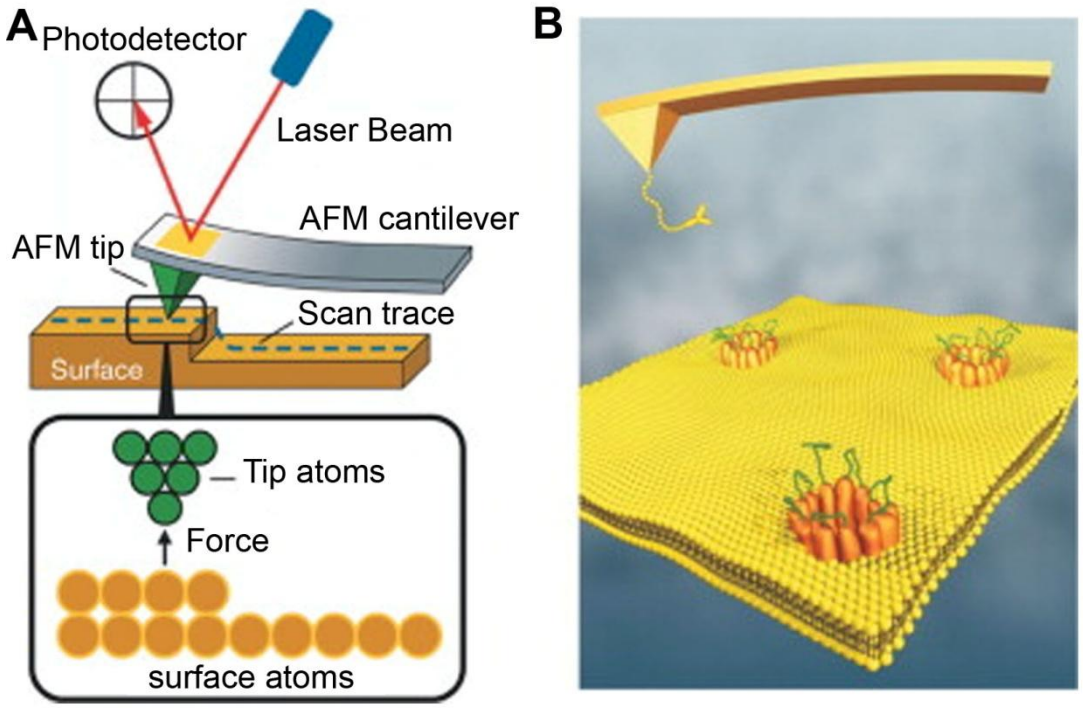

Figure 1.1. Principles of atomic force Microscopy. (A), during the scanning over the sample, the reflection of a laser beam from the AFM tip is recorded, and converted into height information. (B), interaction between a ligand and a receptor can be detected by immobilizing them on an AFM tip and surface respectively. [86]

1.3.4.3 Principle of AFM based force spectroscopy

Although AFM was primarily devised as an imaging tool, it also allows measurement of inter- and intra-molecular interaction forces with piconewton resolution.[71] Due to flexibility in the sample preparation, the ease of operation, and also the real time topographical information obtained from the imaging mode, AFM base force spectroscopy has quickly emerged as the most versatile tool for force spectroscopy compared with optical tweezers or magnetic tweezers.

In order to measure the force between the tip and a sample, an AFM cantilever is controlled to approach and retract form the surface (Figure 1.1 B). Once, the cantilever contacts the surface, further movement towards the surface results in bending of the cantilever due to the stiffness of the surface. After it touches the surface with designated force (referred as trigger point), the cantilever is retracted, and at the point that the pulling force is higher than the force required to dissociate the interaction between the tip and sample, a sudden change of deflection signal is detected. The deflection of the cantilever is monitored during this approach/withdrawal process, and is proportional to the interaction force between the tip and sample. The force can in turn, be estimated by Hooke's law: $F_c = -kx$, where k is the stiffness or spring constant of the cantilever and x is the deflection of the cantilever.[87-89] The entire path of the cantilever as it approaches and withdraws from the surface and its associated deflection as it contacts and interacts with the surface is recorded in the form of a force-displacement or force-distance curve (trace). (Figure 1.2)

Coupled with different immobilization strategies, the interaction forces between tip-bound ligands and surface-bound receptors (or vice-versa) can be measured using AFM- force spectroscopy based on the principles described above. The primary advantage of using the AFM is the ability to perform measurements under physiological conditions, in real-time and allowing investigations with controlled parameters including pH, salt concentration, inhibitors or other effectors.[82] Because of its high sensitivity (in piconewton (pN) force regime) and flexibility, AFM based force spectroscopy has evolved as an important technique to study the interactions of various biomolecular systems, including antigens/antibodies,[90] DNA hybridization,[91] biotin/avidin,[75] glycoproteins/carbohydrates,[92] formation of cadherin complexes,[93], integrin/fibronectin,[94] and DNA/peptides [95]. Moreover, the combined use of imaging, molecular manipulation and single-molecule force spectroscopy has been applied to conduct increasingly sophisticated measurements. There are several studies showing that both structural and functional insights of the bacterial and cell surfaces can be successfully characterized, and that specific proteins on the cell membrane can be localized.[96-98]

1.3.4.4 Challenges of AFM based force spectroscopy

Force spectroscopy using the AFM has proved to be a powerful tool to measure binding at a single molecule level (or the level of a few molecules), and can provide fundamental biophysical information on the biomolecule complex. However, there are several important challenges that need to be addressed:

a) It is difficult to discriminate the interactions of the AFM tip with the molecule of interest from nonspecific interactions. In typical AFM experiments, a large non-specific adhesive force is generally observed between the surface and the cantilever tip. A combination of factors such as hydrophobic, electrostatic, or Van der Waals interactions may result in these adhesive forces.[99] Such confounding factors make the selection and analysis of force–distance spectra considerably difficult.[100]

b) Another factor which affects the measurement is the non-consistent orientation of the ligand immobilized on the substrate, which might result in reduced accessibility of the ligand, and a broad distribution of the binding/rupture force. Defining and controlling the orientation of biomolecules on the surface is a significant challenge in molecular interaction studies.

c) The resolution of force measurements (or the force sensitivity) using AFM force spectroscopy is dependent on the small spring constants of the cantilever, (usually ranging from 10-500 pN/nm).[87] Generally, the softer the tip, the more sensitive the detection. However, different from ensemble-level affinity analysis, the dissociation process under an external force is far from equilibrium kinetics, and the rupture strengths for weak biochemical bonds are not constant, but depend on the rate of the force applied.[101] For example, the Bell model was used to describe the connection between rupture force and loading rate and verified in a set of pioneering measurements. [102, 103] This intrinsic difference between the techniques conducted at different levels results in the complexity of understanding the correlation between the affinity analysis at ensemble level and force spectroscopy analysis at the

molecular level.

Due to these challenges, using AFM and other single molecule tools to study molecular interactions can be quite limited in application. It is necessary to develop reliable platforms to study single molecule interaction using AFM, which can minimize nonspecific interactions and allow for direct measurement of the interactions between molecules of interest only. On the other hand, bridging the knowledge gap between the molecular level and the ensemble level can enable better understanding on steps to engineering these interactions, and optimize sensor designs. Consequently, there is clearly a need to fill up the deficiency of the research in this area.

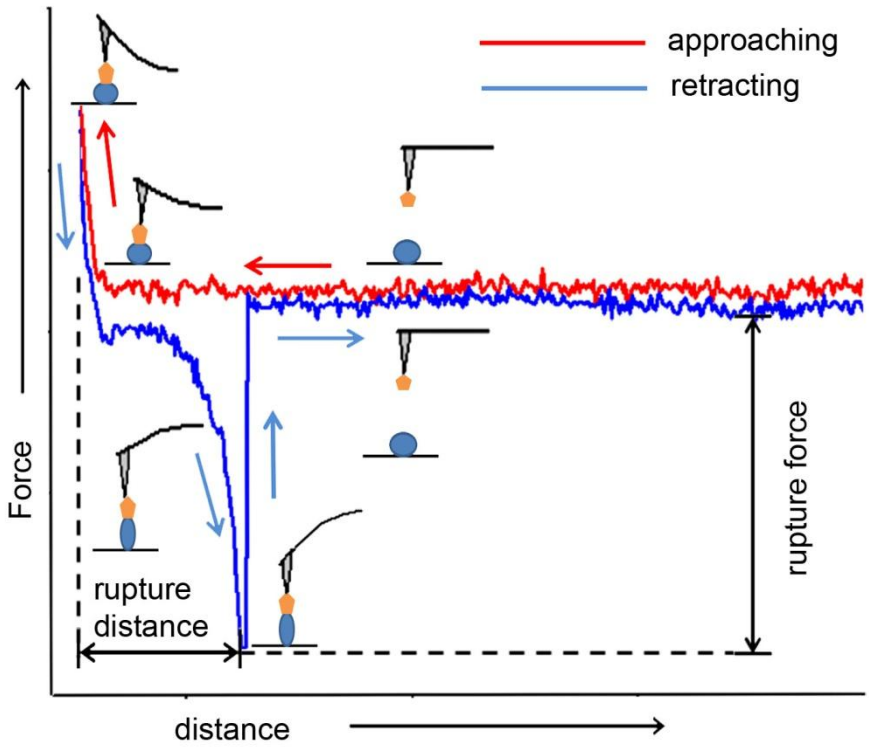

Figure 1.2. Typical force-distance curves obtained indicating a binding/rupture event. The schematic of AFM cantilevers shown represents the bending state of the cantilever during the approach and retraction steps.

1.3.5 Development of platforms for immobilizing biomolecules

Generally, the biosensing strategies are integrated with an electrochemical, optical or piezoelectric transducer, making it necessary to attach the biomolecule component to a solid substrate. For example, in the case of QCM sensing, the ligands are usually immobilize on a quartz crystal sensor surface. In the case of using AFM for single molecule recognition, the molecules under study are attached to two surfaces (the AFM tip and a solid surface that the tip contacts). Consequently, suitably immobilizing the ligands or receptors to different substrates is also of paramount importance. Challenges in the design of such strategies include: a) minimization of the loss of affinity towards the target during this procedure and b) reduction of the nonspecific interaction between substrate and analyte.

1.3.5.1 General strategies for biomolecule attachment

There are various possible methods for biomolecule attachment, ranging from nonspecific adsorption (which may be non-covalent) to specific covalent attachments.[9, 104, 105] Due to the simplicity and ease of experiment, nonspecific adsorption of biomolecules has been the most commonly used method for AFM based force spectroscopy in the last decade. [9, 13] Since this is not a reliable platform, and usually associates with artifacts and uncertainty in the data collection, strategies based on specific covalent reactions have been developed and applied. For example, nucleotides modified with a spacer, terminated in a reactive moiety, can react and

further attach to the functional group in the substrates.[106, 107] Utilizing the tight binding between well characterized ligand-receptor pairs such as biotin-avidin or antibody-antigen are also commonly used to provide attachment sites on the surface and to the probe.[108] Proteins are more challenging to modify, but by introducing biotin and hexahistidine tags, attachments of proteins to different surfaces have been reported.[109, 110]

1.3.5.2 Self-assembled monolayers

For biosensing applications, developing sophisticated immobilization strategies which can provide reproducibility, durability and precision control over a surface are of great importance. It is advantageous to attach biomolecules to surfaces through an organized molecular layer with defined orientation. A versatile strategy to achieve this is via self-assembled monolayers (SAMs).

SAMs have become popular in scientific consciousness and well studied since the 1980s.[111] They have been widely applied to studies of interfacial phenomena and biosensing applications due to their ability to create precisely controlled and functionalized surfaces. The SAM is formed by the strong adsorption of disulfides (R–S–S–R), sulfides (R–S–R) and thiols (R–SH) on a metal surface.[112] These thiol molecules can spontaneously form a highly ordered, densely packed monolayer on metal surfaces (Fig. 1.3). The surfaces functionalized with SAM can have hydrocarbon chains extended with an angle between 40-90^{o} to the surface.[113] Gold surfaces are particularly efficient at forming SAMs via strong, covalent sulfur-Au

bonds.[114] This well-studied thiol chemistry allows the selection of thiols with various exposed functional groups, such as –OH, $–SO_3H$, $–PO_4H_2$ and –COOH, which makes SAM strategy applicable for a numerous purposes, including the attachment of different biomolecules via covalent bond formation. [115, 116]

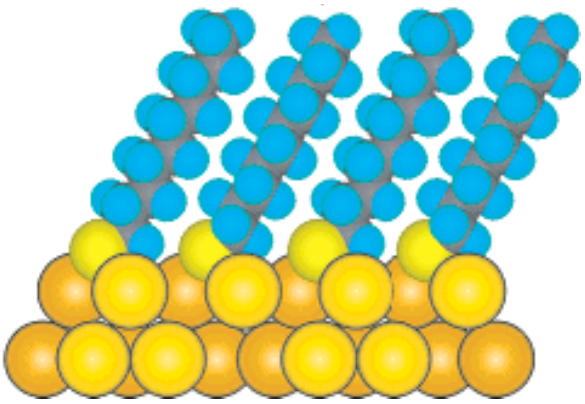

Figure 1.3. Schematic diagram depicting the arrangement of decanethiolates on Au when maximum coverage of the thiolates is attained.[112]

In contrast to SAMs formed from a single adsorbent, mixed SAMs have been synthesized by co-adsorption to a surface from a mixture of thiols solution. In this manner, multiple functional groups can be displayed on the substrate, which greatly expands the functionality of the SAM.[117] In this research, we take advantage of this by using a mixed SAM to control and tune the density of a biomolecule immobilized on this functionalized surface.[118]

In the case of aptamer based sensors, direct attachment of aptamers to a gold surface via S-Au bond was earlier demonstrated using different alkane thiol linkers.[119] However, for these ligands with high degree of structural flexibility,

questions remain as to the activity and accessibility of the ligand for various biosensing applications, as well as on how to minimize the nonspecific adhesion between surfaces that come in contact (for example in AFM spectroscopy).

1.3.6 Self assembly of programmable DNA nanostructures

The theme of self-assembly was further explored in this research by considering the assembly of DNA into programmable nanostructures. Multiple aptamer-based sensing methods were explored in this research primarily using the conventional strategies of surface immobilization. It was found that advanced sensing applications can be enabled by using distinct tags to label these aptamers. Various strategies exist on labeling aptamers using radiolabels or fluorescent tags for different applications.[42, 120, 121] However, owing to the chemical nature of aptamer-nucleic acids, a novel research direction was pursued in using DNA itself to act as both the tag and the sensing agent. In this manner, DNA nanostructures via sequence extension or hybridization can be used to develop a novel shape-based ultrasensitive aptamer-sensing strategy. The concept of this method originated from structural DNA nanotechnology. As introduced above, it is well understood that DNA can exist in a diversity of structures and with sophisticated functions.[26] Functional nucleic acids such as aptamers represent one of the most important examples in this area. Similarly another exciting area of research has been developments in structural DNA nanotechnologies. Structural DNA nanotechnology entails the use of the diverse DNA motifs for the construction of novel materials with specific geometrical properties on

the nanometer scales.[122] Seeman et al. first proposed the concept of using DNA to yield junction structures in 1982, [123] which formed the beginning of a brand new research field of structural DNA nanotechnology. Over the last decade, it has emerged as one of the most promising and exciting paths to developing productive nanosystems.

DNA has been considered as the top choice for programmable construction of supramolecular structures using a 'bottom-up' approach on the nanoscale due to the following properties: a) precise size; b) ease of synthesis and continually dropping costs; c) chemical robustness which leads to structural stability under a variety of environments; d) a precise periodical-helix structure, which enable using different computational methods to design and predict synthetic DNA nanostructures; e) specificity of the Watson-Crick base pairing and self-recognition properties, which may be utilized as site-specific molecular glues and f) well characterized 3D motifs with diverse structures. [122, 124]

A number of well defined DNA nanoarchitectures with a large variety of geometries, topologies, and periodicities have been fabricated. [125, 126] These nanoconstructs include holiday junctions,[127] DNA nanowires,[128] 3-point and 4-point stars,[129] cubes,[130] supramolecular polyhedra.[131] Inspired by DNA nanotechnology, RNA was also applied to construct nanostructures, such as tecto-squares [132] and polyhedra.[133] The DNA origami technique, which is achieved by folding long, single-stranded DNA into 2 and 3D shapes, is another important milestone in the field of structural DNA nanotechnology. [134, 135] These

shapes have been proposed for applications ranging from enabling spatially periodic networks [136] and nanoarrays [137] and as molecular cages for drug delivery applications.[138]

The two fields of structural DNA nanotechnology and functional nucleic acids have been independently coevolving. With the tremendous achievements established by the pioneers in both fields, merging and integrating functional nucleic acid modules into the DNA architectures is a new challenge.[122] The research on fundamental biophysical interactions of aptamers conducted at ensemble and single molecule scales provided the impetus to develop new strategies to take advantage of the unique properties uncovered (flexibility, adaptive binding, switchability). Our goal was to develop a new generation of functional DNA structures that can fully exploit aptamers in novel sensing strategies. Recently several studies were reported on using DNA nanoarray to organize other species and providing precise control of the spacing between individual molecules by programming the self-assembly of DNA tile, especially with the development of DNA "origami" technique.[139] Our goal was to demonstrate the functionalization of DNA nanostructure with a functional nucleic acid motif. In this research, a facile strategy to construct aptamer-functionalized 2D DNA shapes for molecular recognition is developed, which enables the visual sensing of aptamer-based recognition.

CHAPTER 2

DEVELOPMENT AND CHARACTERIZATION OF A PLATFORM TO STUDY BIOMOLECULAR INTERACTIONS USING FORCE SPECTROSCOPY

2.1 Introduction

AFM force spectroscopy is a powerful tool to study interactions between diverse pairs of molecules. These measurements are based on the interactions between the two molecules: one attached to the AFM tip and the other bound to the surface of interest. However, as has been extensively reported,[99, 140] and also observed in these experiments, the nonspecific adhesion between AFM probe and surface, usually caused by Born repulsion, van der Waals attractions, and electrostatic repulsions, can often obscure the analysis of the specific intermolecular binding forces between the molecules of interest.[141]

In this research, we are interested in measuring the interactions between diverse biomolecular systems at the molecular level, preferably at a single molecule level. To achieve this, various strategies are needed to immobilize the molecules on the AFM

tip and a surface. Two general approaches to immobilize biomolecules on such substrates or AFM tips have been commonly reported in the literature: a) direct amination of the surface by silanization or esterification, and b) amination via a thiol-based self-assembled monolayer (SAM). The first approach is a direct functionalization of a silicon or silicon nitride surface (or AFM tip). The reaction ends up with a formation of an organosilane layer, with functional amine groups on the surface. [142] Although it has been used in many pioneering works, the silanization reaction is difficult to control, sensitive to contamination, and not stable. [143-145]

The second approach is particularly suited for surfaces that are coated with gold. In this case, a thiol-based SAM is easily obtained by immersing the gold coated surface or AFM tip in selected alkanethiol solutions. The proteins can be further immobilized by different ways depending on the functional group of the SAM. For example, alkanethiols that terminate in carboxyl groups are most commonly used. These can further couple with amino groups of proteins via 1-ethyl-3-(3-dimethylaminopropyl) carbodiimide (EDC) and N-hydroxysuccinimide (NHS) in aqueous solution.[146, 147] However, both these approaches generate surfaces fully covered with active groups and also result in a high surface density of ligands which increases the possibility for nonspecific adhesion. These densely packed biomolecules on the surface make it difficult to discriminate a single molecule binding event from extensive multiple binding events.[13] It has also been suggested that increasing the spacing between molecules on a surface can not only reduce such multiple binding events, but also helps preserve their binding capacity since they are

less likely to be denatured and can freely interact.[148]

Hence, it is necessary to develop an optimal platform based on a suitable SAM approach to carry out measurements of single molecule interactions using an AFM. The ideal surface is one which can eliminate the nonspecific adhesion between the surface and sample, as well as dilute the surface density of the ligands. Inspired by thiol-based monolayers described above, a platform consisting of two thiol molecules to form a mixed SAM was found to be ideal for such investigations. This strategy involved using a mixture of two thiols to form a functional surface - one thiol acts as a reactive capturing agent for the biomolecule, while a second thiol is incorporated within the SAMs to space out the reactive groups on the functionalized surface.

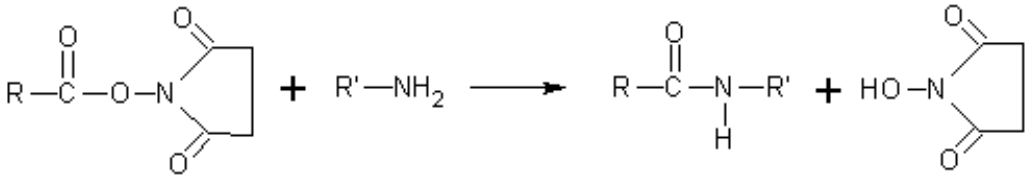

Figure 2.1. Covalent reaction between NHS and amine groups. NHS-Esters can react with amine groups present on the N-termini of proteins or amines on lysine residues to form amide bonds

An NHS-terminated thiol was used as the first thiol to present reactive groups for biomolecule attachment (Figure 2.1).[149] To act as a spacer and to reduce non-specific protein absorption, an inert oligo (ethylene glycol) (OEG) terminated thiol was chosen as the second thiol. OEG thiols have been extensively used to fabricate protein resistant SAMs on gold.[150] Although the mechanisms of the

protein resistance have not yet been fully established, such OEG terminated alkane thiol SAMs on gold have been shown to reduce nonspecific protein adsorption in many applications including biosensing, cell adhesion studies, and fabrication of protein biochips.[117, 151, 152]

To test the feasibility of this platform for single molecule interaction analysis, an important biomolecular interaction system between a sugar (mannose) and its specific binding protein (lectin) was chosen. The specific interactions between lectins present on cell surfaces and their complementary carbohydrates mediate diverse processes in living organisms such as cell-cell recognition, cellular adhesion or mediation of signaling events at the cell surface.[153] Carbohydrate-lectin recognition events are also found to play key roles in diverse pathological processes, including infection, cancer cell metastasis, and inflammation.[154, 155]

Due to the importance of this system in life science, understanding and utilizing these interactions have been the subject of active research to develop and engineer bioanalytical strategies and devices.[156] The molecular recognition between lectin and carbohydrate is an intriguing process because the binding is due to relatively weak, noncovalent interactions. However the strength and specificity required for proper cellular targeting is high.[157] To date, lectin-carbohydrate interactions have been studied primarily on surfaces using bulk measurement methods including fluorescence, surface plasmon resonance (SPR) [158] and evanescent-field detection.[159] Assessing protein-carbohydrate interactions has typically been difficult because of the weak affinities observed and associated complications arising

from the importance of multivalency in these interactions.

This research focused on using the lectin – Concanavalin A, as a ligand to bind sugar molecules immobilized on surfaces. Concanavalin A (Con A) is a widely investigated lectin isolated from the jack bean (*Canavalia Ensiformis*), that binds specifically to α-D-mannosyl and α-D-glucosyl residues. Lekka et al. studied the interaction force occurring between Con A and the carbohydrate component of the glycoproteins using AFM. [160] Touhami et al. also conducted force spectroscopy via AFM and reported the unbinding force between Con A and oligo-glucose saccharides to be 96±55 pN.[161] Ratto et al. measured the force required to rupture a polymer tethered Con A and a similar tethered mannopyranosylphenyl isothiocyanate bond as 47±9 pN.[92] Importantly, all these studies applied densely packed ligand-immobilization methods, and consequently reported a wide range in force values.

This system therefore provides an ideal opportunity to investigate the strategy of using mixed SAMs to a) create functional groups for attachment of the lectin or the sugar on a solid surface b) create an inert (non-functional) spacing between molecules of interest to prevent non-specific adhesion and c) immobilize the complementary molecule on the AFM cantilever tip (for example, lectin on surface, sugar on tip or lectin on tip, sugar on surface). Using a mixed SAM platform not only allows covalent immobilization of an amine containing molecule (specifically mannosylamine or the lectin Con A in these experiments), but also provides an inert surface over the surrounding area that minimizes non-specific interactions and

provides a well separated and homogeneous environment for binding. In this study, AFM as a versatile technique was applied for both imaging and measurement of the specific interaction forces between the Con A and mannose. In order to enable covalent attachment to a surface via active $–NH_2$ groups, this work used a one-step synthesis protocol to create an amine-functionalized sugar by a novel amination reaction. The flexibility and reliability of this platform was tested by conducting the measurements under varying environmental conditions, and the specificity of the binding interactions could be confirmed via the blocking of binding sites on the Con A with *free* mannose. Combined with the functionality of the mixed SAM platform described above, Con A and mannose were immobilized on the substrates (surface and AFM tip) to investigate the specific interaction at the single molecule level.

2.2 Experimental section

2.2.1Materials and instrumentation

(1-Mercaptoundec-11-yl) hexaethylene glycol (Oligoethylene glycol (OEG) terminated thiol), $HS\text{-}C_{11}\text{-}(EG)_6OH$, and (1-mercaptonhexanedecanoic acid)-N-Succinimidyl ester (NHS-terminated thiol) $HS\text{-}C_{15}COO\text{-}NHS$, were purchased from Asemblon Inc (Redmond, WA) and SensoPath Technologies (Bozeman, MT) respectively. Ethanol (200-proof) was purchased from Decon Labs, Inc. (King of Prussia, PA). Epoxy glue was purchased from Epoxy Technology (Avon, OH). Tetrahydrofuran (THF), highly purified Concanavalin A from *Canavalia ensiformis* (Jack bean), type IV, D-(+)-mannose and ammonium carbonate were

purchased from Sigma-Aldrich (St. Louis, MO). Phosphate-buffered saline (PBS pH 7.4) (11.9 mM phosphates, 137 mM sodium chloride and 2.7 mM potassium chloride) was obtained from Fisher Scientific. Ultrapure water (resistivity 18.2 MΩ-cm) obtained from a MilliQ water purification system (Millipore Scientific, MA). Gold coated PPP-CONTCSAu cantilevers from Nanosensors (Neuchatel, Switzerland) and TR800PSA cantilever form Olympus (Tokyo, Japan) were used for force measurement and imaging. All force spectroscopy experiments were performed using an Asylum MFP-3D atomic force microscope (Asylum Research, Santa Barbara, CA). NMR experiments were carried out on a Varian ((Palo Alto, CA) spectrometer.

2.2.2 Preparation and characterization of glycosylamines of mannose

Since the mixed SAM strategy involved functional NHS groups on the surface, it was necessary to form a variant of the sugar molecule with pendant amine groups to enable attachment to the platform. Amination of mannose was performed using a Kochetkov reaction involving the treatment of reducing sugars with ammonium carbonate to create anomeric amines.[162, 163] A solution of mannose (1%) in saturated aqueous ammonium carbonate was stirred at room temperature for 5 days at room temperature (20 ^{o}C). Solid $(NH_4)_2CO_3$ was added in fractions during the course of the reaction to ensure saturation. After the reaction, the solution was dried in vacuum for 2 days. Excess solid $(NH_4)_2CO_3$ was removed by dissolving the crude glycosylamine in warm methanol. After termination of CO_2 evolution, the methanol was slowly evaporated and the residual material dried in vacuum overnight. 50 mg

freshly prepared sample was dissolved in 1 ml D_2O, and further characterized by NMR working at 300 MHz for proton to verify the formation of the glycosylamine.

2.2.3 Functionalized substrate and probe preparation

To easily locate single protein molecules immobilized on the surface, and further optimize their surface density, it is important that the substrate should have large flat area. Gold is a popular substrate, because it is stable in various conditions, and can be easily functionalized by organic thiols to from SAMs. Typically gold surfaces are obtained by the physical vapor deposition of gold on mica surfaces. However, gold surfaces formed in this manner can be irregular, with unpredictable terrace features ranging from tens to hundreds of nanometer formed during the vaporizing process. This causes difficulty to clearly visualize features smaller than the terraces. In this part of research, in order to clearly distinguish proteins from the underlying substrates, and further to optimize the protein immobilization strategy, it was important to develop a technique to form ultraflat surfaces that presented a flat, defect free substrate over a large area (around 5-10 μm^2). Since the vapor deposition of the gold on mica surfaces follows an epitaxial deposition process, ultraflat surfaces can be formed by using the gold surface in closest contact with the mica. This "template-stripped" gold (TSG) is formed by stripping the mica layer using a solvent such as tetrahydrofuran (THF) method.[164] The resulting gold surfaces, with the roughness similar to mica, were then washed several times with ethanol prior to formation of the mixed SAMs.

Mixed thiol SAMs were prepared by the incubation of the freshly prepared gold surfaces in a 5 mM mixed thiol solution (the molar ratio of OEG and NHS thiol was maintained at 10000:1 to ensure separation of attachment sites for protein on the surface) in ethanol for 20 hours at room temperature. After incubation, the surfaces were rinsed with ethanol, and placed in a 10 ng/ml solution of Con A in PBS buffer for 1 hour at room temperature. Gold coated cantilevers (PPP-CONTCSAu) with mixed SAM coatings were prepared in the same manner. The cantilevers were incubated with mannosylamine in PBS buffer for 1 hour to obtain sugar functionalized AFM tips.

Following the incubation, the resulting surface and cantilever were washed with PBS buffer to remove any unattached protein and glycosylamine. The surfaces were then placed in a fluid cell containing 500 µl of PBS for AFM imaging and force measurements. Experiments were also performed with the lectin attached to the cantilever and the aminated sugar linked to a surface via the same chemistry and identical procedure as that described above.

2.2.4 AFM imaging of surfaces and force spectroscopy

Spring constants of functionalized cantilevers were measured using the thermal fluctuation method.[165] TR800PSA cantilever (spring constant ~0.15 N/m, resonance frequency 24 kHz) were cleaned using high-intensity UV light to remove organic contamination and used for imaging the surfaces in noncontact mode. A PPP-CONTCSAu cantilever (spring constant ~0.2 N/m, resonance frequency 24 kHz)

functionalized with the SAM and the sugar or protein (as described above) was used for measurement of interaction forces. Regions containing protein molecules were identified prior to force spectroscopy by imaging and force-distance curves were obtained by moving the tip to these locations, holding it in place for 5 seconds to allow binding to occur and then retracting in a repeated, cyclic manner. Several hundred curves were obtained for each experiment by moving the tip to different points on the surface, including areas where no protein was previously observed as a control. The force of contact was kept <500 pN to avoid damaging the surface protein.

2.3 Results and discussion

2.3.1 Synthesis and verification of mannosylamine

In order to study the interaction between a carbohydrate and a carbohydrate-binding protein (lectin), an important prerequisite is to activate or modify the carbohydrate so that it can be covalently attached to a substrate or probe without a changing either its conformation or properties. Touhami and colleagues reported using thiol-terminated hexasaccharide to create carbohydrate surface.[161] Lekka et al. reported using 3-aminopropyltriethoxysilane (APTES) silanized glass slide to immobilized glycoprotein with mannose unit present.[160] However, these methods usually involve several synthesis steps, or result in disturbing the reducing termini of the sugar. It is important to note that the unmodified hydroxyl groups at the C3, C4 and C6 positions of D-glucopyranosyl or D-mannopyranosyl rings are hypothesized to be essential for binding saccharides.[166] Studies have shown that the modifications of

hydroxyl groups significantly affect the binding between the sugar and the lectin. More specifically, the C2 position is crucial for Con A binding, which is reflected in the 5 times higher affinity of Con A towards mannose than glucose, which are C2 epimers.[167] Hence, the specific position of the functionalization on the mannose molecule was considered an important criterion for choosing a modification method. In this study, a one step animation reaction was chosen to modify the mannose. The reaction starts with an unprotected mannose and results in a 1-amino-1-deoxy sugar. An amine group substituting the hydroxyl group at C1 allowing it to be easily linked to a surface containing –COOH or –CONHS groups, and also avoiding any loss in binding ability (Figure 2.3 A).

This conversion of the mannose to the aminated form was confirmed by comparison to the ^{1}H NMR spectroscopy between the product of the amination reaction and the native mannose. The mannose 1H NMR spectroscopy was reported as follows[162]: Mannose $C_6H_{12}O_6$: 1H NMR (300MHz, D_2O), δ 5.00 (s, 1H, corresponds to OH group on C1 position), δ 4.67 (s, 1H), δ3.76–3.47 (m, 7H).

The product of the reaction ($C_6H_{13}NO_5$) (Figure 2.2): 1H NMR (300MHz, D_2O): δ 5.00 (s, 1H corresponds to the OH group of the C1 position of the residual mannose), δ 4.66 (s, 1H), δ 4.36 (s, 2H, corresponds toNH_2 group), δ 4.16 (s, 1H), δ 3.79–3.36 (m, 7H).

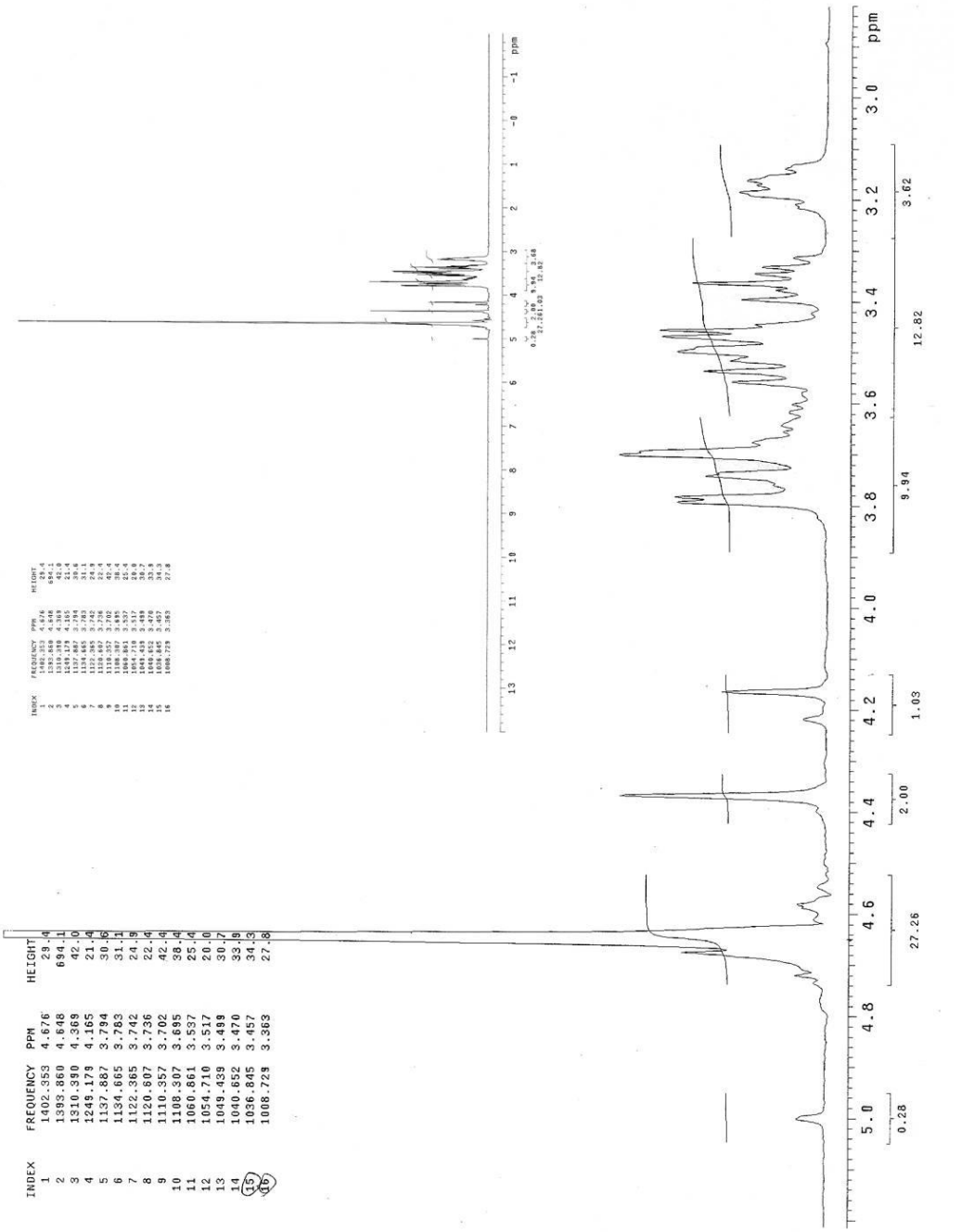

Figure 2.2. NMR Analysis of mannosylamine prepared by Kotchetkov amination. The NMR spectra of mannosylamine, δ=5.00 (s, 1 H from the OH(C1) group of residue mannose), δ=4.66 (s, 1 H), δ=4.36 (s, 2 H from NH_2 group), δ=4.16 (s, 1 H), δ=3.79-3.36 (m, 7 H). From these results, the molar ratio of NH_2 group to OH (C1) group is estimated to be ~ 4:1 (molar fraction) in rough mannosylamine product, showing that NH_2 group successfully replaced most of the OH (C1) group of mannose. The inset shows the NMR spectrum over the entire range.

The appearance of a peak at δ 4.36 suggests the successful amination reaction, leading to the formation of the mannosylamine. However, the smaller peak at δ 5.00 indicates that a small amount of the starting mannose remained unreacted in the final product. The molar ratio of NH_2 group to OH (C1) group can be estimated as ~ 4:1 in the mannosylamine product, showing that the majority of the starting mannose was converted. Since the residual unmodified mannose does not react with the NHS group of thiol, it can be easily removed by rinsing. While diglycosylamines are also produced as byproducts in this reaction (reported yield is around 5-10%) [162], however, the presence of the NH group of diglycoslamines prevents covalent attachment to the self-assembled monolayers and they can be removed by rinsing with buffer as well.

2.3.2 Self assembled monolayer on gold and immobilization of Con A and mannose

Mixed SAMs utilizing binary mixtures of functionalized thiols are generally synthesized by co-adsorption to a surface from a mixture of thiols.[168] The mixed SAM platform provides an ideal surface to attach single molecules and study their interactions without the interference of non-specific adhesion. Since many carbohydrate-carbohydrate and protein-carbohydrate interactions are polyvalent in nature, the precisely controlled surface density of the ligands is especially important to analyze the data, and reduce the complexity of the interaction experiment. [118]

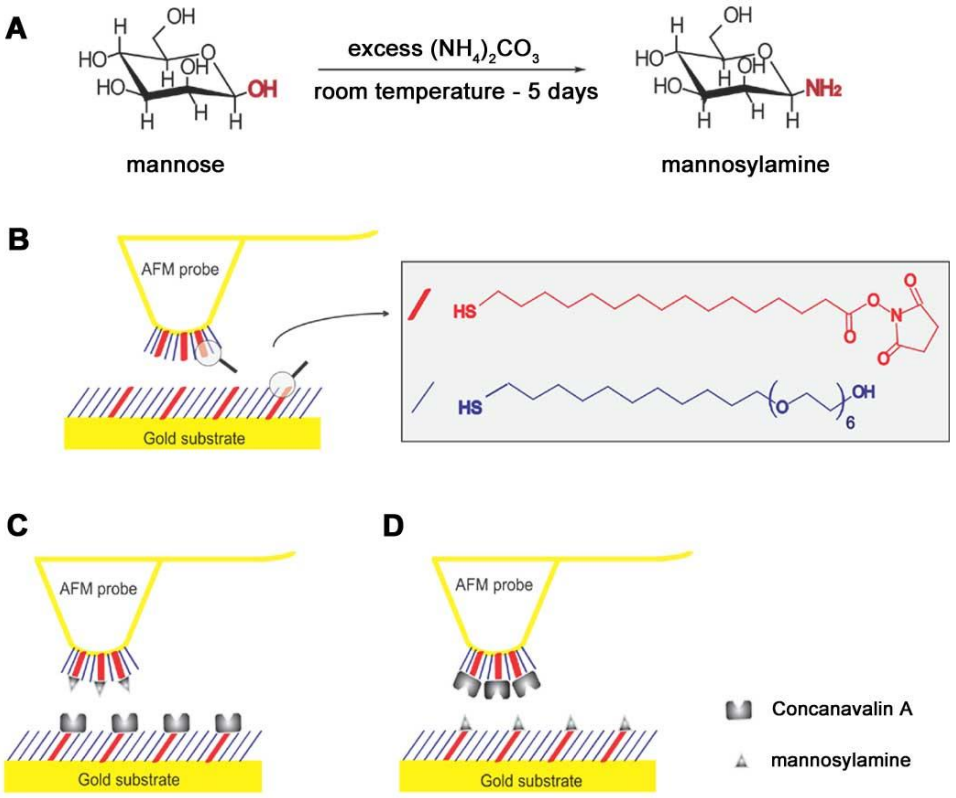

Figure 2.3. Schematic representation of the strategy used for immobilization of concanavalin A and mannose on substrates. (A) amination of mannose; (B), structure of NHS-terminated thiol, OEG terminated thiol and the self-assembled monolayers formed on the surface and probe; (C) and (D) adsorption of Con A and mannose on the functionalized substrates.

Here, a mixed thiol approach consisting of two alkyl thiols - a protein-resistant oligoethylene glycol (OEG) thiol SAM along with a sparsely populated N-hydroxysuccinimide (NHS) thiol was used to form the molecular platform. The NHS terminated thiol (HS-C_{15}COO-NHS) can react with amine groups, and thus act as covalent tethers for the biomolecules. In this study, amine groups exist in the lysine residues present on Con A or via the mannosylamine obtained by the

described method above. Concurrently, the OEG terminated thiol ($HS\text{-}C_{11}\text{-}(EG)_6OH$) has been shown to be resistant to protein adhesion [169] as well as to non-specific tip-surface interactions [118]. Utilizing this OEG thiol allows spacing the position of the active NHS groups. By simply changing the proportion of the two thiols in the ethanol solution, the ligand density could be easily tuned to obtain the optimal surface density of proteins or sugar molecules. A previously optimized NHS to OEG thiols ratio (1:10000) was used in this research.[118]

Besides using OEG thiols to space the position of the active NHS groups, the concentration of the protein used for the immobilization process is also critical to obtain a platform surface with protein features well separated from each other. Hence, in this research, the concentration of the protein solution was also modulated to minimize the probability of multiple molecules interacting with the AFM cantilever. Con A solution with varying concentrations ranging from 1-1000 ng/ml were used to incubate Au surface functionalized with mixed SAMs. Figure 2.4 A and B are the AFM images showing the functional gold surface incubated with 10 ng/ml and 200 ng/ml Con A respectively. The features surface density significantly increased with the protein concentration. In comparison, a relatively low concentration of protein solution (1-10 ng/ml) is optimal to obtain a surface with well-separated protein immobilized on. The following experiments were conducted with 10 ng/ml protein solution.

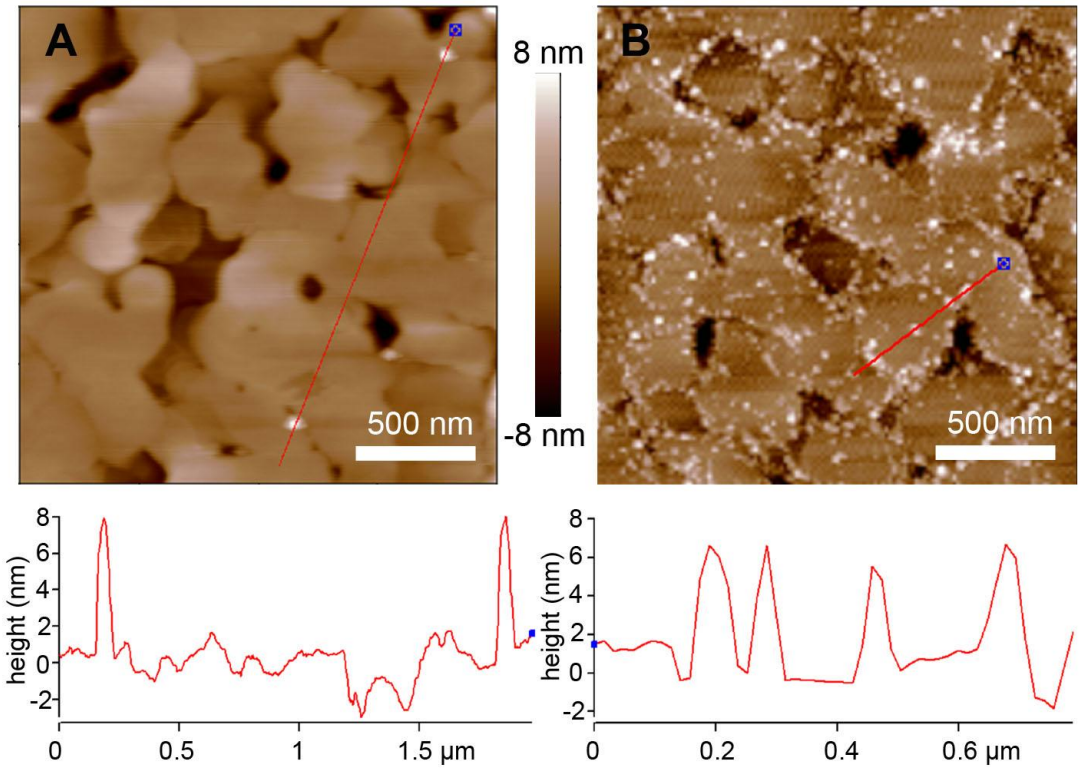

Figure 2.4. AFM images of the mixed SAM functional gold surface incubated with different concentration of concanavalin A solution. (A) with 10 ng/ml Con A; (B) 200 ng/ml Con A.

The lectin used in this study, Concanavalin A (Con A) is isolated from the jack bean (*Canavalia Ensiformis*) and binds specifically to mannosyl and glucosyl residues of polysaccharides and glycoproteins. The monomeric molecular weight of unit of Con A is 25.5 kDa. At pH < 5.5 Con-A exists as a dimer (two-protomer unit with overall dimensions of about 30 x 45 x 89 Å), and at a pH>7 it exists as a tetramer. [170, 171] Experiments were conducted at a pH of 4.8 to minimize the probability of multivalent interactions from a Con A tetramer.

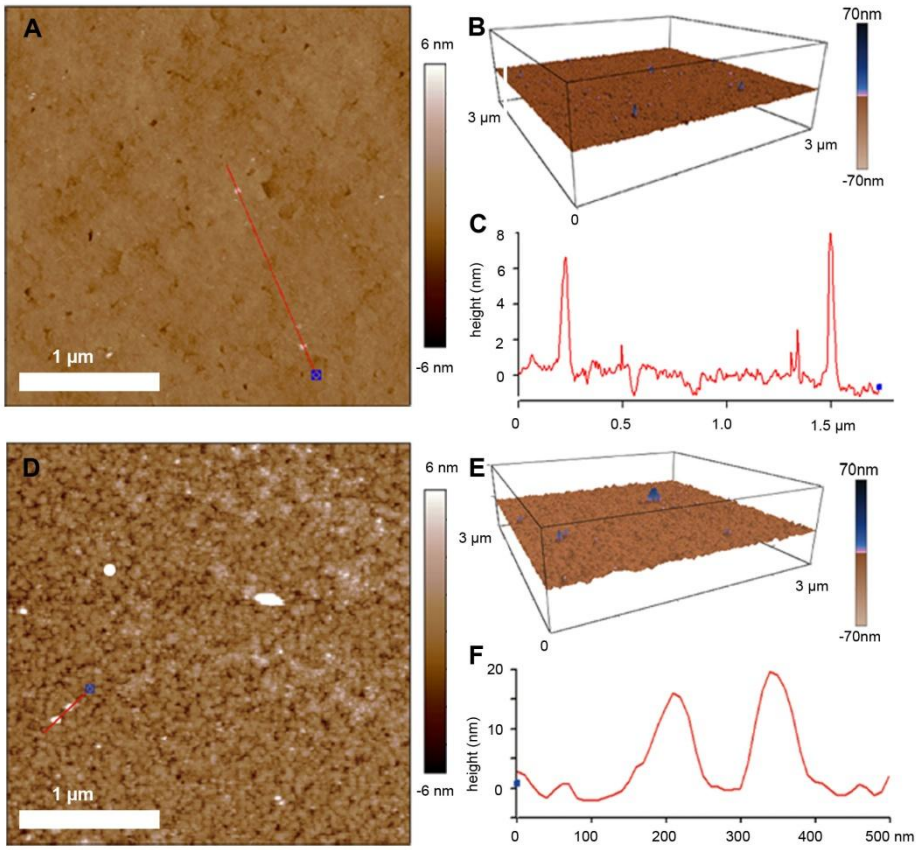

Figure 2.5. AFM images of concanavalin A on ultraflat gold surfaces functionalized with mixed SAMs in PBS at different pH. At pH 4.8, AFM topographic image (A) and 3D image (B), and the corresponding section (C). At pH 7.4, AFM topographic image (D) and 3D image (E), and the corresponding section (F).

In order to clearly assess the dimensions of the Con A in different multimeric states (dimer, tetramer) via AFM imaging under different pH, ultraflat gold surfaces need to be used to avoid the terrace features on the regular gold surface. Ultraflat gold is defined as one having a roughness of < 1 nm over a 5 μm^2 area. As prepared by template stripping, flat gold surfaces with a mean surface roughness value of ±0.40 nm over a 5 μm^2 area were obtained, following the formation of the mixed thiol SAM as described above. This enabled a clear visualization of the attached protein. Figure

2.5 A and B show the non-contact AFM image of a SAM surface with a typical concentration of Con A. on a mixed SAM functionalized gold surface. The morphology of the platform with the Con A was observed to be homogeneous and stable upon repeated AFM imaging with surface features in the range of 3-8 nm in height. (Mean roughness was estimated to be ±0.68 nm at an optimal concentration of Con A on the surface). Figure 2.5 C shows a 2 μm line profile across the SAM surface with the immobilized lectin. The height values correspond well with the dimensions of the Con A molecule obtained using X-ray crystallography.[170] As a comparison, the morphology of Con A on the surface at a pH of 7.4 was also recorded by AFM image (Figure 2.5 D and E), where the molecule is expected to be a tetramer, was observed to display feature sizes on the order of 10-20 nm (Figure 2.5 F). Subsequent to the imaging, gold coated AFM cantilever was also functionalized with mannosylamine in a similar fashion and used for collection of force curves on a surface that had Con A immobilized on it.

2.3.3 Force measurement between the Con A and the mannose

To minimize the deviation among the experiments, a 300 pN force was designated as trigger point, and 5 seconds as dwelling time. This means that during the force measurements, after the tip touched the surface with 300 pN force, the tip remains on the surface for 5 seconds before retracting from the surface. This step is to ensure a higher probability of an interaction between the carbohydrate and lectin immobilized on each interacting surface (the platform and the AFM cantilever tip).

For each set of force spectroscopy experiment, hundreds of force-distance curves were measured. Each measurement was recorded as force-distance curve. The force measurements were converted from the deflection signal of the cantilever using the slope of the cantilever on a hard surface and the cantilever spring constant calibrated using the thermal noise method in fluid.[165, 172] Rupture distances are determined from the force-distance curves from the point at which the tip contacts the hard substrate, to the point where the force jump returns to zero. It is important to note that this is not the bond length of the biomolecule pair, but the distance between the AFM tip and the substrate, which includes deflection of cantilever as the bound complex is pulled apart, the length of the linker tethered with biomolecules and the bond length. [87]

In typical AFM experiments, a large nonspecific adhesive force is generally observed between the surface and the cantilever tip (Figure 2.6 C). This is manifested in a cantilever deflection that is observed as a linear non-delayed retraction curve with the same slope as that of the contact region. A combination of factors such as hydrophobic, electrostatic, or Van der Waals interactions may result in adhesive forces of magnitudes that are on the order of the binding event between an antibody and antigen or receptor and ligand and often obscures specific interactions.[173] Such confounding factors make the selection and analysis of force-distance spectra considerably difficult. As reported earlier, the use of an OEG terminated thiol surrounding NHS tethers is a simple and effective strategy to significantly reduce the incidence of non-specific tip-surface adhesion, and the inherent water layer around

OEG groups is hypothesized to preserve the protein conformation and binding ability.[118] This enabled us to clearly observe and analyze molecular recognition events that are distinguishable from areas on the surface where there is no interaction and formed the basis for the single molecule platform described in this chapter.

Although the mixed SAM modification minimizes the nonspecific adhesion, the presence of defects in the mixed SAM still causes a small portion of the force-curve to show non-specific interactions which affect the final rupture force analysis. Hence, criteria are needed for the determination of specific versus nonspecific interactions in hundreds of the force-distance curves obtained in each set of the experiments, and over 1000 curves with one tip. First, the adhesive interactions within 10 nm rupture length are neglected, since the nonspecific adhesion usually takes place at this length scale.[92] Second, interactions at a rupture length between 10 to 50 nm were used for the analysis which is proposed specific interaction between the tethered Con A and the mannose; Third, if both specific and nonspecific interaction exist in the same trace, only the ones with a small nonspecific interaction and also with a well separated interaction event are used for analysis. These selection criteria greatly streamline the process of analyzing force curves and also enable discrimination of data in an unbiased manner for the determination of rupture forces.

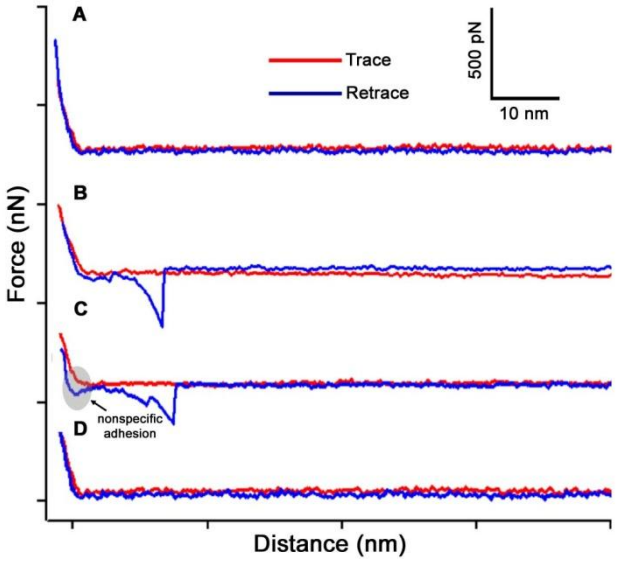

Figure 2.6. Typical AFM force–distance curves obtained in the experiments: (A) No tip surface sticking when the tip encounters the OEG SAM on the surface (B) typical selected traces indicating a molecular recognition event and (C) ~10% of the traces showed a small non-specific adhesion force and were selected for analysis. Traces where the tip-surface sticking was >200 pN were not used (D) in the presence of free mannose in the solution, the force dropped to zero.

Typical force-distance curves obtained the experiments are shown in Figure 2.6. In the absence of any interaction, the retraction curve did not show any rupture force as seen in Figure 2.6A. Figure 2.6B shows the typical specific interaction forces of the curves that were selected for analysis. In a small percentage of observed force-distance curves (typically ~ 10%), we observe a small tip surface adhesion (Figure 2.6C). These curves were also selected for analysis because of a clearly discernible interaction event. Around 10 % of the total number of curves obtained had large non-specific forces that were > 200 pN and were discarded. It is likely that the

tip becomes contaminated after collection of a large number of force curves resulting in larger non-specific forces over time. However, an additional advantage of functionalization is that the OEG SAM also prolongs the useful life of the tip allowing several measurements to be taken (for a typical experiment n ~ 1000). Selected force curves were analyzed by histogram analysis in IgorPro to determine the rupture force and rupture lengths.

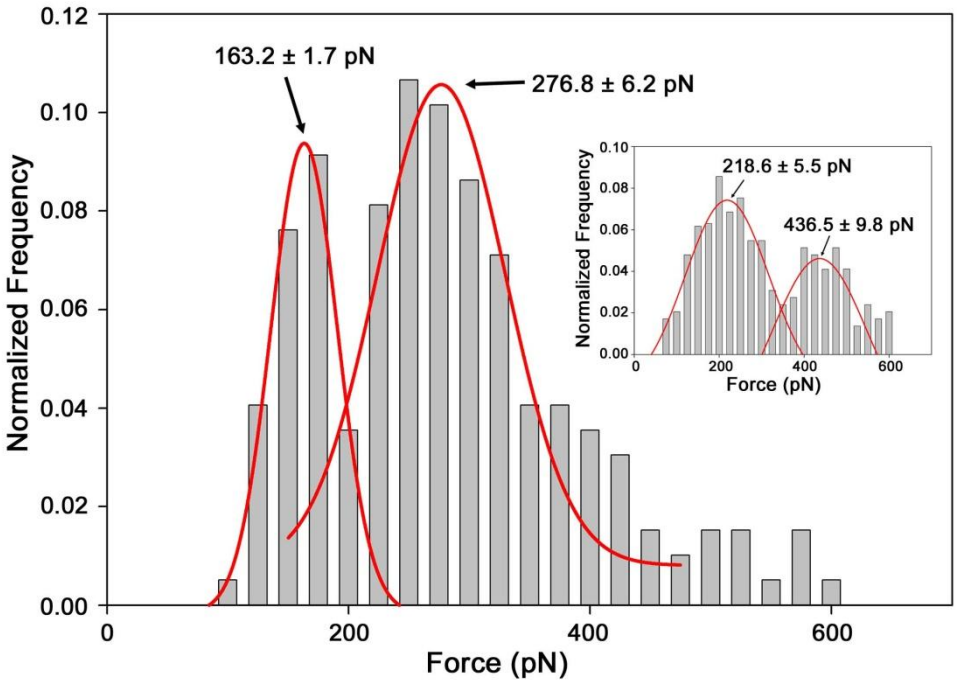

Figure 2.7. Single molecule force spectroscopy showing the distribution of rupture forces for the concanavalin A-sugar complexes. The Gaussians showed quantized binding events at 163±2 pN and 276±6 pN at a pH of 4.8 (n = 200). The inset shows the corresponding values at a higher pH of 7.4 (n = 300) where the Con A exists as a tetramer. Quantization of forces shows peaks at 218±6 pN and 436±10 pN.

To statistically analyze the force data, a bin size of 25 pN was used to construct

histograms and multiple Gaussians curves were fit to the data. Goodness of fit was determined by the χ^2 statistic for each Gaussian. The distribution of the forces is shown in Figure 2.7. At a pH of 4.8, the rupture forces show a clear quantization of force with peaks around 163 pN and 276 pN. The inset of Figure 2.7 shows the analysis of force curves at a pH of 7.4, where multivalent interactions are likely to dominate. The peaks were obtained around 218 pN and 436 pN. Despite the use of the mixed SAM platform and low concentration of the lectin and sugar, we still obtained a small percentage of multivalent interactions. However, the percentage of such events was much lower than that observed without any such surface modification, showing the usefulness of this platform.

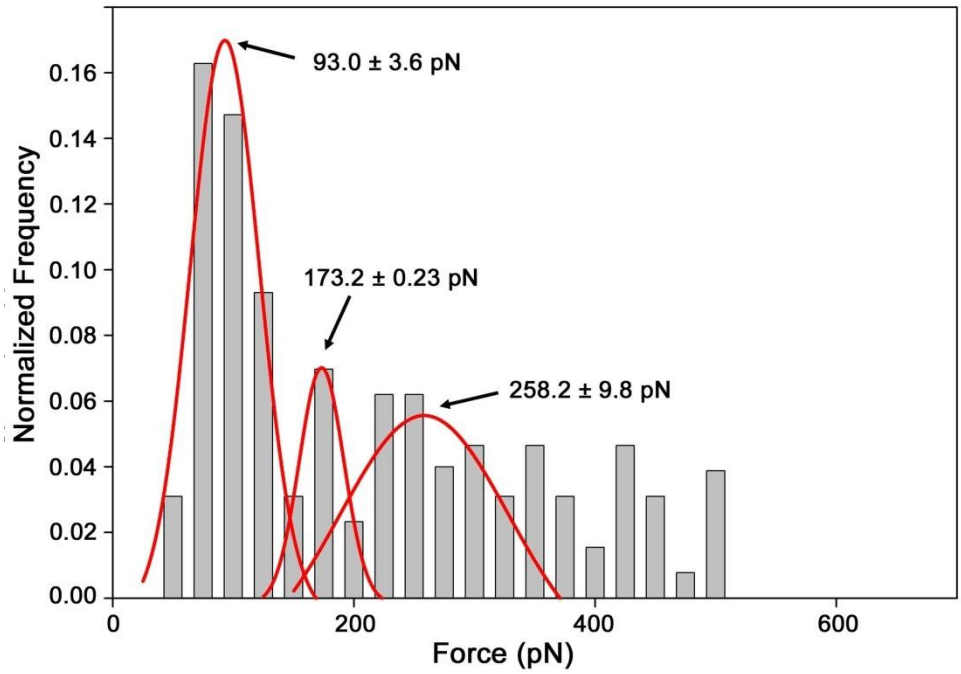

Figure 2.8. Histogram analysis of single molecule force spectroscopy experiments with the Con A on the AFM tip and the mannosylamine on the surface (n = 128). The Gaussians showed quantized binding events at 102.5 ±5.2 and 218 ±20 pN.

2.3.4 Carbohydrate immobilized on the platform surface

To understand the effect of immobilization as well as to probe the multivalency of interactions, the positions of the Con A and the mannosylamine were switched. These experiments consisted of a functionalized AFM cantilever with Con A tethered via a mixed SAM and the platform with mannosylamine covalently bound via NHS linkages as described in the experimental section above, the mannosylamine could be attached to the mixed SAM surface via the same chemistry that enabled the tethering of Con A. The distribution of forces is shown in Figure 2.8. Clear quantized peaks can be observed via the fit Gaussians at 93, 173 and 258 pN corresponding to single and multiple interactions respectively. The number of multivalent interactions in these experiments was much lower than those observed when the lectin was on the platform surface and the sugar on the AFM cantilever surface. This may be due to the fact the binding sites on Con A are 6.5 nm apart from each other, which reduce the possibility of multiple interaction with mannose immobilized on the cantilever surface.

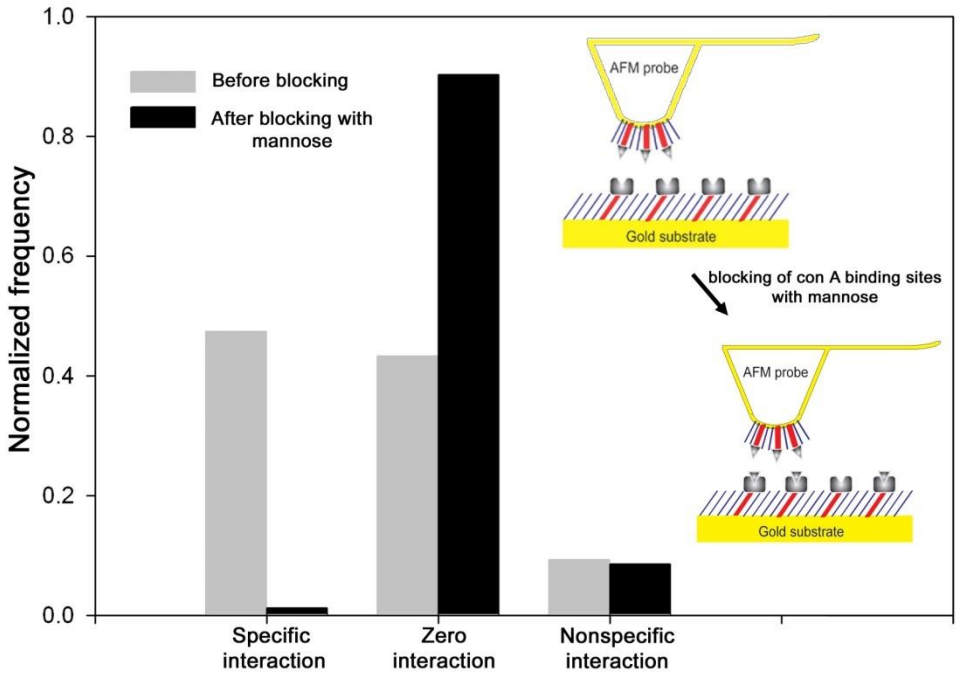

Figure 2.9. Control experiment showing the decrease in binding on blocking with a 0.1mM solution of mannose. The graph shows the percentage of curves obtained with specific, zero and non-specific interactions before blocking (n = 344) and after blocking (n = 482). These results clearly shows that the free mannose blocks the binding sites of the Con A, and prevents the further interaction with the mannose immobilized on the AFM cantilever, and further confirmed the specific binding between the Con A and mannose in the previous experiments.

2.3.5 Blocking with free sugar

Following the measurement of the interaction forces between Con A and the mannose sugar, blocking experiments were conducted to verify that the interactions were indeed specific. Binding sites on the Con A tethered to the SAM surface on the platform were blocked by the addition of 0.1M mannose solution prior to measurements of force with a mannosylamine functionalized cantilever. The change

in binding is shown in Figure 2.9. Both the frequency as well as magnitude of the forces dropped as shown in the figure. In each experiment, there was at least an order of magnitude decrease in the binding of the lectin and the sugar as a result of the blocking with the mannose. Thus we can hypothesize that free sugar blocks the binding sites of the lectin preventing any further interactions with the sugar conjugated to the AFM cantilever. This indicates that the binding between the mannose and the lectin was specific as designed.

2.3.6 Force analysis

Based on the force values obtained, the rupture force for a single Con A – mannose bond was estimated to be 95 ± 10 pN. The Con A dimers and tetramers possess two and four binding sites that can act independently. A sugar functionalized AFM tip (with a typical radius of curvature of ~ 10 nm) is large enough to span multiple binding sites on a lectin. Thus at a pH of 4.8, with the dimeric Con A on the surface and the mannosylamine on the AFM tip, it is possible that are many "double" interactions. At a pH of 7.4, where the Con A exists as a tetramer, more multivalent interactions (3 and 4) are seen. At a pH of 4.8, the force peaks around 163 pN and 276 pN correspond to 2 and 3 interactions. The higher peak around 420 pN at a pH of 7.4 would likely indicate that the possibility of ~ 2 tetramers of Con A that might be binding to 2 sugar molecules on the tip. When the Con A is on the AFM tip, there is a lesser likelihood of multiple interactions because of the size of the lectin in comparison to the tip radius (~ 10-20 nm) is such that the probability of a single Con

A molecule interacting with single mannose is higher.

The possibility of more than one sugar molecule in close proximity cannot be ruled out despite the SAM approach taken in this work. However, as can be seen from the distribution of forces, the majority of interactions are single or double interactions as expected, with single interactions predominating when the Con A is on the AFM tip and the mannose on the surface. The use of this versatile, functionalized SAM platform allows investigation of these multivalent interactions and thereby calculation of the rupture force for a single Con A and mannose bond. It must also be noted that there is a wide range of forces estimated due to the uncertainty in the determination of the spring constant of the cantilever. The measured values of the spring constants often differed by as much as 20 % from the value supplied by the manufacturer. As has been observed by several studies, this leads to an inherent uncertainty in determination of an accurate force value.[174]

Experiments to determine the rupture forces were conducted at a loading rate of ~150 nN/sec. Ratto et al. estimated the unbinding force for a polymer-tethered concanavalin A with a tethered mannose molecule to be 47 ± 6.9 pN. The loading rate in their experiment was ~ 10 nN/sec. The unbinding force for a single Con A -mannose bond obtained here is almost twice this value and may be attributed to the significantly higher loading in these experiments. Although the unbinding force is dependent on the loading rate, with an increased loading rate resulting in a higher force [175], a consistent increase on increasing the loading rate to 300 nN/sec was not observed. This suggests that the unbinding energy landscape for this system seems to

level off at higher loading. In addition, the effect of glycoside clustering and introduction of multivalent binding as has been studied in previous studies is also intriguing and may play a significant role in these interactions at the single molecule level. [176]

2.4 Conclusions

In this chapter, an effective platform was established and used to study single molecule interaction. The efficacy of this platform was tested with a well characterized and important lectin and carbohydrate binding system. This strategy involved biomolecule immobilization using mixed SAMs, to enable AFM force spectroscopy with improved accuracy and specificity. The results show that the functionalized SAM surfaces reduce the incidence of non-specific tip-surface adhesion artifacts as well as allow the positioning of molecules at a sufficiently low concentration to enable single molecule monitoring. The reduction in non-specific adhesion forces permit using unbiased criteria and easier analysis of force-distance curves. A novel method to synthesize functionalized carbohydrates was developed which has implications in the investigation of lectin-carbohydrate interactions in glucoarrays as well as lectin arrays. By changing the pH of the interaction environment, the multimeric state of concanavalin A (dimer, tetramer) could be observed both via AFM imaging and in the distribution of rupture force analyzed from each state. The binding events are strongly influenced by introducing with free sugars to block the binding site of the Con A.

The combination of the SAM with the amination protocol makes this a versatile strategy for probing lectin and sugar binding under different environmental conditions. It was hypothesized that this is a versatile platform, which allows determination of the single molecule bond strength with high specificity for different biological recognition system. In the subsequent chapter, this platform is applied extensively in the investigation of various newly developed biorecognition systems, such as aptamer/target protein systems.

[This chapter contains results that have been previously published in the paper "Functionalized self-assembled monolayers for measuring single molecule lectin carbohydrate interactions" in Analytica Chimica Acta, 2009]

CHAPTER 3

INVESTIGATION OF THE MOLECULAR INTERACTION BETWEEN AN APTAMER AND ITS PROTEIN TARGET VIA FORCE SPECTROSCOPY

3.1 Introduction

Building on the platform for studying molecular interaction described above, a general formulation to investigate the binding of flexible and adaptive molecular recognition elements was developed in this chapter. As shown in this and subsequent chapters, using oligonucleotides as functional elements have enormous potential for molecular recognition. It was the goal of this work to further develop this field. As a test system, an important angiogenic protein, vascular endothelial growth factor (VEGF) and its corresponding aptamers were selected as model systems. The experiments and results detailed below focused on understanding the binding behavior of this aptamer/target protein system at molecular scales.

As previously introduced in Chapter 1, aptamers are a class of synthesized, functional, ligand-binding nucleic acids, whose affinity and specificity is comparable

to, and can often exceed those of antibodies towards their targets. The evolutionary selection of aptamers by a process called Systematic Evolution of Ligands by Exponential Enrichment (SELEX) [177, 178], allows us to synthetically create nucleotide sequences with exquisite recognition capabilities against a wide variety of targets including proteins and small molecules.[179] Aptamer technology has been proven to be a potentially powerful tool with applications in biosensors [43], diagnostics and therapeutics [38], such as the FDA approved aptamer-based therapeutic agent Pegaptanib for the treatment of nonvascular age-related macular degeneration.[41]

As aptamers gain widespread utility in biotechnological applications, understanding the mechanisms of interaction with their targets is of vital importance. Insights into the structure, dynamics, and the biophysics of the fundamental interactions and complex formation would greatly enhance the ability to rationally engineer and design the next generation of aptamer-based tools. Typically, the interactions between aptamers and their targets have been investigated at a molecular level primarily using NMR spectroscopy and X-ray diffraction.[44] Recently, surface plasmon resonance [180] and fluorescence resonance energy transfer [181] were applied to study the mechanisms of aptamer interactions. However, these represent observations of ensemble scale interactions by essentially "capturing" a DNA aptamer-protein complex and studying steady states averaged over millions of molecules. As discussed in Chapter 1, these ensemble level techniques cannot provide detailed kinetic information, including subpopulation properties. In

comparison, single molecule techniques such as using AFM force spectroscopy allow us to detect temporal transitions, spatial states and binding/unfolding energy landscapes which are normally obscured in ensemble scale studies.[71]

To date, there have been limited studies on the binding of aptamers with their targets using AFM and other single molecule tools. Basnar et al. investigated the rupture force between an aptamer functionalized AFM tip and a thrombin modified Au surface.[182] Jiang et al. studied the specific interaction between immunoglobulin E (IgE) and its binding aptamer and obtained a rupture force of 160 ± 29 pN. In comparison, the binding force between IgE and its monoclonal antibody was reported to be 139 ± 43 pN.[49] However, questions on aptamer affinity at the molecular level remain unanswered. For example, owing to the flexible, adaptive binding of aptamers, higher-affinity binding aptamers are not necessarily more specific to their target ligands.[183] In addition, environmental parameters can have a strong influence on the specificity and selectivity of aptamers to their targets and has not been probed at the molecular level.

A comprehensive study was carried out on the molecular level interactions between an RNA aptamer and its protein target. Specifically, vascular endothelial growth factor (VEGF) and anti-VEGF RNA aptamer was investigated. VEGF is a disulfide-linked dimeric glycoprotein serving as a crucial mediator of angiogenesis. It can stimulate blood vessel growth and plays an important role in pathological processes such as tumor growth, rheumatoid arthritis, and age-related macular degeneration.[184] VEGF induces proliferation of endothelial cells through binding

to the kinase domain receptor and the Fms-like tyrosine kinase receptor. There are four principal isoforms of VEGF expressed in humans, which contain 121, 165, 189 and 206 amino acids respectively.[185] $VEGF_{165}$ (containing 165 amino acids) is the predominant and most physiologically relevant isoform, with a molecular weight about 45 kDa. $VEGF_{165}$ has a heparin binding domain (pdb: 1KMX) formed by 111-165 residues, which is not present in the $VEGF_{121}$ isoform.[186] Aptamers selected to bind to VEGF were in turn, shown to be capable of inhibiting the binding of VEGF to its receptors and therefore regulating angiogenesis and metastasis, with clinical implications.[187]

The binding of $VEGF_{165}$ and the anti-$VEGF_{165}$ aptamer was observed by force spectroscopy using an AFM to capture fundamental interaction information at the molecular level. The use of the mixed self-assembled monolayer platform described in the previous chapter provided the ideal platform to enable such investigations. As shown, functional groups in the monolayers allowed control over the attachment of the protein to the surface and the mitigation of non-specific tip-surface adhesion forces. An isoform of the target VEGF protein – $VEGF_{121}$ with 121 amino acids, deficient in a critical heparin binding domain[188] and a $VEGF_{165}$ isoform blocked with heparin were used to study the specificity of the aptamer. [189] Control experiments were conducted to measure the interaction forces between the aptamer and protein using bare (no aptamer attached) cantilevers and surfaces as well as a random sequence (nonbinding) RNA ligand. These experiments revealed the degree of nonspecific adhesion between the aptamer and protein. In addition, the

extremely important effect of the loading rate on the rupture forces between the aptamer and its target were studied. Finally, the relationship between stability and binding force of aptamer towards its target was investigated by varying the concentration of a metal ion (Mg^{2+}) in the binding buffer.

3.2 Experimental section

3.2.1 Materials and instrumentation

RNA aptamers with a 5′ dithiol S-S modifier and a $(CH_2)_6$ spacer with RNase free HPLC purification were custom synthesized by Integrated DNA Technologies, Inc. (Coralville, IA). Recombinant $VEGF_{165}$ and $VEGF_{121}$ were obtained from Biovision, Inc. (Mountain view, CA). The specific aptamer for $VEGF_{165}$ is referred to as the anti-$VEGF_{165}$ aptamer in the rest of the manuscript. The sequence of the anti-$VEGF_{165}$ RNA aptamer and a random RNA ligands used as a control aptamer was used in this chapter, and the sequences are: 5′-CCG GUA GUC GCA UGG CCC AUC GCG CCC GG-3′ and 5′-UAC AGA CGA CAC AUA GAG AUA GAC CGA GA-3′ respectively.

(1-Mercaptoundec-11-yl) hexaethylene glycol (Oligoethylene glycol (OEG) terminated thiol), HS-C_{11}-$(EG)_6$OH, and (1-mercaptohexadecanoic acid)-N-succinimidyl ester (NHS-terminated thiol), HS-C_{15}COO-NHS, were purchased from Asemblon Inc (Redmond, WA) and SensoPath Technologies (Bozeman, MT) respectively. Tetrahydrofuran (THF), Phosphate-buffered saline (PBS pH 7.4) (11.9 mM phosphates, 137 mM sodium chloride and 2.7 mM potassium

chloride, 1 M $MgCl_2$ solution (molecular biology grade) and Ethanol (200-proof) were purchased from Fisher Scientific. DEPC treated RNase free water was used for all experiments. Gold surfaces were purchased from Agilent Technologies, Inc. (Foster City, CA) Gold coated PPP-CONTCSAu cantilevers from Nanosensors (Neuchatel, Switzerland), TR400 PB and TR800PSA cantilevers from Olympus (Tokyo, Japan) were used for force measurement and imaging respectively. All AFM imaging and force spectroscopy experiments were performed using an Asylum MFP-3D atomic force microscope (Asylum Research, Santa Barbara, CA).

3.2.2 Functionalized substrate and probe preparation

Gold surfaces were cleaned by washing several times with ethanol prior to formation of the self-assembled monolayers (SAMs). Functionalized SAM platforms were prepared as described in Chapter 2. After monolayer formation, the surfaces were rinsed with ethanol, and incubated in a 0.2 μg/ml solution of VEGF in PBS buffer for 1 hour at room temperature to take advantage of binding by the lysine groups. The unreacted NHS groups were then quenched for 1 hour in 0.1M ethanolamine solution at pH 7.4.

In contrast to the preparation procedure described in Chapter 2, the AFM cantilever was functionalized by aptamer thiol directly. The aptamer was synthesized with a thiol linker, so that it could be directly attached to a gold substrate. Specifically, gold coated cantilevers (PPP-CONTCSAu and TR 400 PSA) were used to take advantage of this chemistry by incubating with 5 μM 5′- thiol modified aptamers

(aptamer-$(CH_2)_6$-S-S-$(CH_2)_6$-OH) in PBS buffer for 1 hour to obtain aptamer-functionalized AFM tips. Following the incubation, the resulting surfaces were washed with PBS buffer to remove any unattached aptamer. The surfaces were then placed in a fluid cell containing 500 µl of PBS for AFM imaging and force measurements. Control experiments without aptamers were performed using the bare gold coated cantilevers directly with the modified platform surfaces.

3.2.3 AFM imaging of platform surfaces and force spectroscopy

Spring constants of functionalized cantilevers were measured using the thermal fluctuation method.[165] TR800PSA cantilever (spring constant ~0.15 N/m, resonance frequency 24 kHz) were cleaned using high-intensity UV light to remove any organic contamination and used for imaging the surfaces in noncontact (tapping) mode. PPP-CONTCSAu cantilever (spring constant ~0.2 N/m, resonance frequency 24 kHz) and TR400 PB cantilever (spring constant~0.09 N/m, resonance frequency 24 kHz) functionalized with the aptamer as described above, was used for measurement of interaction forces. Regions containing VEGF molecules were identified on the platform surfaces by imaging prior to force spectroscopy.

Force-distance curves were obtained using the same procedures described in the previous chapter. To verify the specificity of the interaction curves obtained by AFM, multiple control experiments were performed. The first set of control experiments consisted of measuring the interaction of an un-functionalized (bare) Au-cantilever and a mixed SAM surface with attached $VEGF_{165}$ protein. The second

set of experiments measured the interaction of an anti-$VEGF_{165}$ aptamer with a mixed SAM surface without any attached protein. The third set of control experiments involved measuring the interactions of a nonbinding (control) aptamer with a 'random' sequence and a mixed SAM surface with attached $VEGF_{165}$ protein.

The bonds between biological receptor molecules and their ligands are not constants but instead are dependent upon the rate of force that is applied to the ligand−receptor complex (referred as loading rate).[190] The effect of loading rate was studied using cantilevers with different stiffness values and also by altering the velocity of approach and retraction during force spectroscopy. The specificity of the aptamer was investigated using two isoforms of VEGF - $VEGF_{121}$ and $VEGF_{165}$, covalently attached to two different surfaces as described above. Earlier interaction studies at the bulk scale, showed RNA-based aptamers capable of binding $VEGF_{165}$ but not to $VEGF_{121}$.[189] Interaction forces were then measured under identical conditions using a cantilever functionalized with the anti-$VEGF_{165}$ aptamer. Blocking experiments were conducted to further verify the specificity and binding site of the anti-$VEGF_{165}$ aptamer. The platform surface with attached $VEGF_{165}$ was incubated with 5 μg/ml heparin solution for 15 min to block the heparin binding sites. Following rinsing with PBS, interaction forces were measured. The effect of metal ions on the stability and binding of the aptamer/protein complex was investigating using binding buffers with different concentrations of Mg^{2+}. Surfaces from each experiment were repeatedly rinsed followed by a buffer exchange. After allowing the system to equilibrate for a few hours, the interaction forces were measured as

described above.

3.3 Results and discussion

3.3.1 Surface modification and protein/aptamer immobilization

As verified in the previous chapter, the mixed SAMs synthesized via co-adsorption from solutions containing two different thiols provided a useful strategy for the incorporation of properties from different molecular species. [115] In this chapter, this technique was used to immobilize the VEGF protein on the platform. An AFM cantilever was directly functionalized with the corresponding thiol modified aptamer. The scheme of the AFM force spectroscopy is shown in Figure 3.1.

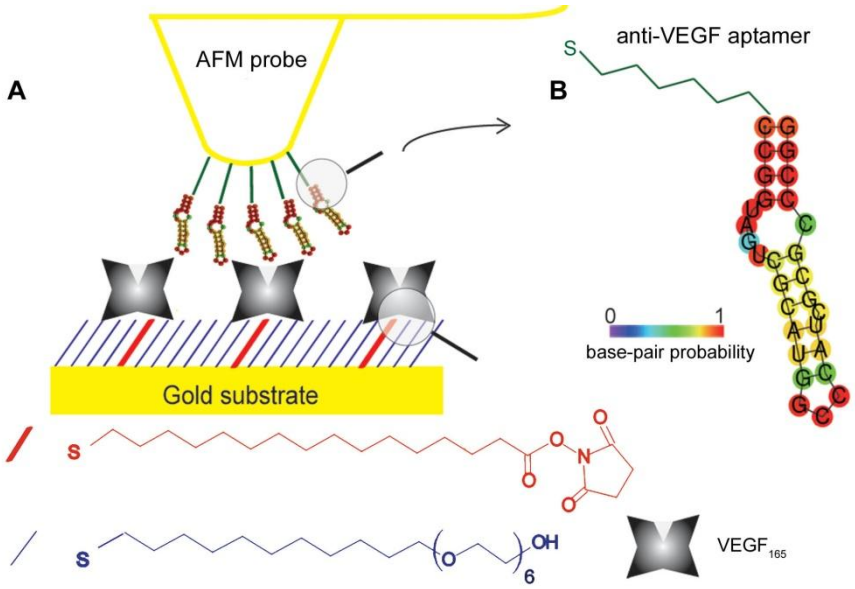

Figure 3.1. Schematic of experiment showing the functionalization of the surface and AFM tip with a SAM strategy. (A) The gold surface with a mixed SAM modification and an AFM probe immobilized with $VEGF_{165}$ and thiol terminated

aptamer correspondingly. (B) Secondary structure of anti-$VEGF_{165}$ aptamer predicted by RNAfold web server with thiol modification at the 5′ end.

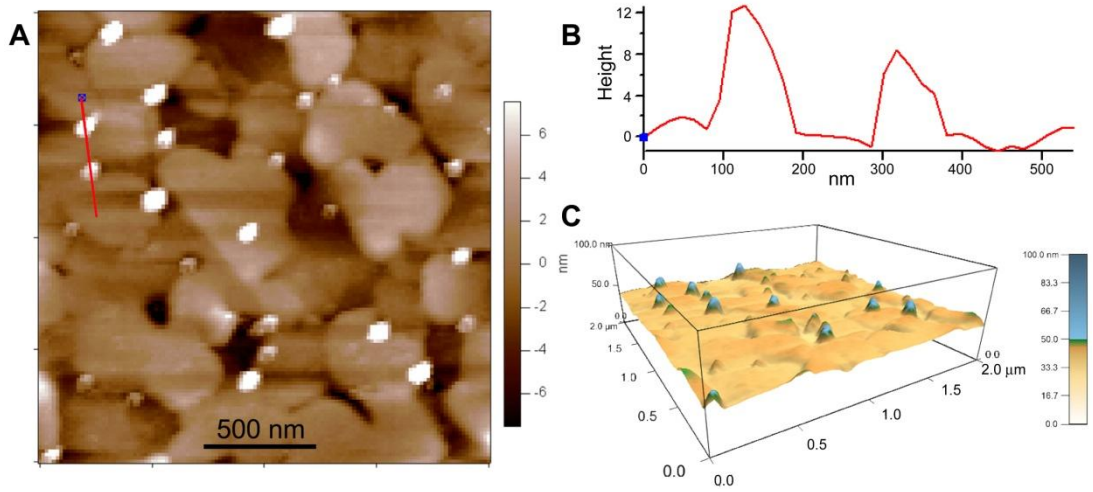

Figure 3.2. AFM characterization of $VEGF_{165}$ on the mixed SAMs surface. An AFM topography image (A) and a 3 D image (B) recorded in PBS buffer of $VEGF_{165}$ on the mixed SAMs surface. (C) A line profile across a 500 nm section showing the height of the $VEGF_{165}$ molecules observed on the surface.

3.3.2 Binding of RNA Ligands with $VEGF_{165}$

The oligonucleotide aptamers specific to $VEGF_{165}$ were first identified by Jellinek et al.[187], and grouped into six families. After deletion analysis, the minimal sequences required for high affinity binding were minimized to 29-36 nucleotides. One of the aptamers identified as 100t, a truncated high-affinity aptamer, with a K_D ~0.42 nM was used as the basis for the anti-$VEGF_{165}$ aptamer reported in this research. The affinity selections of the aptamers were performed in PBS, which is the reaction buffer in our experiments. Figure 3.1B shows the secondary structure

predicted by RNAfold.[194] This aptamer was also successfully applied in an RNA aptamer microarray used to detect protein biomarkers including VEGF.[195]

More than 1500 curves were obtained from each experiment, and approximately 20% of the curves showed a specific adhesion event. Typical force-distance curves obtained are presented in Figure 3.3. The criteria for selecting the proper force curves to analyze the rupture forces from the set of all data collected were the same as those used in Chapter 2.

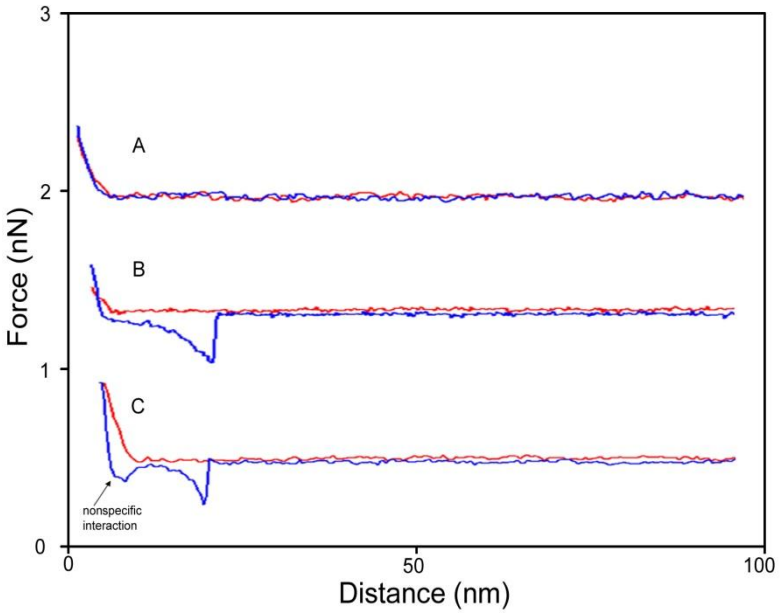

Figure 3.3. Typical AFM force–distance curves obtained in the experiments: (A) No tip surface adhesion when the tip encounters the OEG SAM on the surface (B) typical selected traces indicating a molecular recognition event and (C) a small amount of the traces showed a small non-specific adhesion force and were selected for analysis. Traces where the tip-surface sticking was >200 pN were not used.

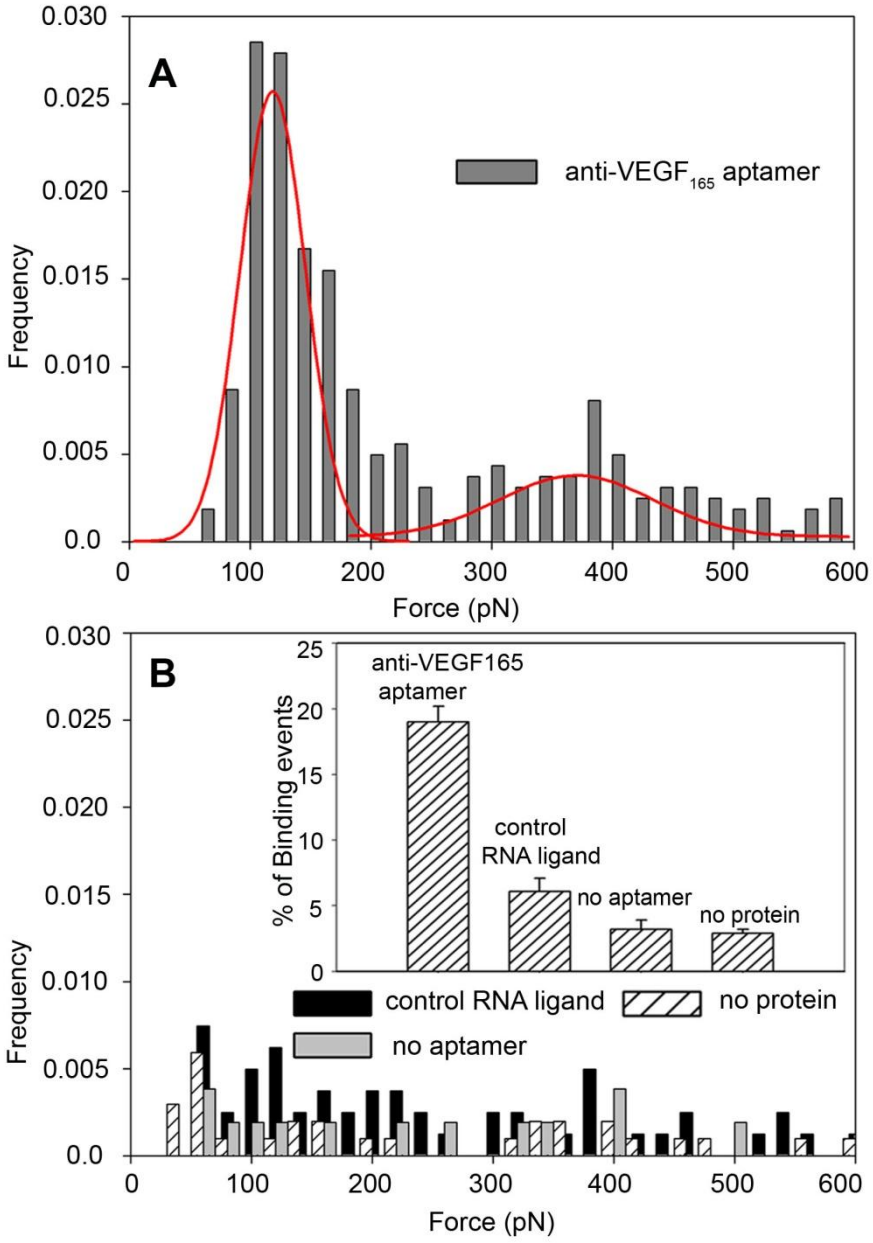

Figure 3.4. Histogram analysis of rupture forces for $VEGF_{165}$ and anti-$VEGF_{165}$ RNA aptamer complexes (A), and series of control systems (B), including the system with a cantilever functionalized with a random RNA sequence as a control RNA ligand, a tip without aptamer functionalization, and an aptamer functionalized tip against a bare surface modified with mixed SAMs but without protein immobilized on. The solid lines are the fit Gaussian distributions for anti-$VEGF_{165}$ aptamer**,** showing quantized binding events with anti-$VEGF_{165}$ aptamer at 119.3±2.5 pN and

371±12.7 pN, and the force spectroscopy experiments conducted with different control systems show a random distribution. The inset of B is the binding percentages of all the force spectroscopy experiments mentioned above.

The force distribution histogram for aptamers and $VEGF_{165}$ rupture force at a loading rate of ~150 nN/s is shown in Figure 3.4A. The distribution of the rupture force between the anti-$VEGF_{165}$ aptamer and $VEGF_{165}$ shows a clear peak at 119.3±2.5 pN, and a broad peak at 371±12.7 pN. A small percentage of curves showed that multivalent interactions still occurred, with a much lower probability, which could contribute to the broad distribution between 280-500 pN

Three different control experiments were carried out to confirm the measured forces were indeed caused by the anti-$VEGF_{165}$ aptamer/ $VEGF_{165}$ interaction (Figure 3.4B). First, a bare cantilever without attached aptamer was used to interrogate a surface with immobilized $VEGF_{165}$. In these experiments, the binding percentage decreased to 3.2±0.7% (in contrast to 19.0±1.2% for the anti-$VEGF_{165}$ aptamer/$VEGF_{165}$ system). Second, a cantilever with an attached anti-$VEGF_{165}$ aptamer was used to interrogate a surface without any attached $VEGF_{165}$ protein (The surface was covered with the mixed SAM thiols as described above without any attached protein). The binding percentage in this case showed a decrease to 2.9%. The significant decrease of the binding percentage (Figure 3.4B inset) and the distinct force distribution of these two control experiments compared with anti-$VEGF_{165}$ aptamer/$VEGF_{165}$ system demonstrated that the observed interactions

between the functionalized cantilever and the surface are likely caused by specific binding events between the aptamer and protein.

Finally, an RNA ligand, with the same length as the anti-$VEGF_{165}$ aptamer but with a random sequence, was designed in this study as a control aptamer to further discriminate between the binding events of the aptamer and its specific target from the nonspecific adhesion between a nucleic acid sequence and protein. This control aptamer did not contain the consensus binding sequence of aptamer Family 1[187], and did not assume an intricate secondary structure as determined by RNAfold.[196] However, interestingly the detected binding percentage was 6.1 ± 1.0 %, which was significantly lower than that observed with the anti-$VEGF_{165}$ aptamer, but higher than that observed with a bare cantilever. The histogram revealed a broad peak of rupture force at 125.8 ± 17.2 pN and a roughly uniform distribution >250 pN. The lower binding probability and distinct force distribution further confirmed that the forces measured between the anti-$VEGF_{165}$ aptamer and $VEGF_{165}$ were caused by a sequence-specific interaction. They also indicated that the anti-$VEGF_{165}$ aptamer selected through SELEX showed a higher affinity towards $VEGF_{165}$ compared with other RNA ligands as manifested by a considerably higher binding probability.

These results showed that even though the control aptamer did not adopt a specific secondary structure corresponding to the $VEGF_{165}$ molecule, an adhesion force could still exist between this RNA motif and the protein at the molecular level. It is known that positively charged amino acid residues (Arg82, Lys84 and His86)

that mediate binding to the kinase domain receptor,[197] cluster to form a positively charged surface at the end of the VEGF monomer. One possible hypothesis is that the control aptamer may bind to this positively charged region owing to charge interactions. In addition, the control aptamer was predicted as a linear structure instead of a stable secondary structure, and with a higher minimal free energy than the anti-$VEGF_{165}$ aptamer (calculated by RNAfold [196]). This linear unstable structure may result in more nucleotides in each aptamer molecule coming in contact with the protein, thereby contributing to the non-specific adhesion observed between this control aptamer and the protein at the molecular level.

3.3.3 Dynamic force spectroscopy of anti-$VEGF_{165}$ aptamer and $VEGF_{165}$

The bond strength of a ligand-receptor is a dynamic property that depends on the force loading rate applied during bond rupture. [198] Single molecule dynamic force spectroscopy of a ligand-receptor bond can provide valuable information about the dissociation dynamics and prominent barriers traversed in the bond energy landscape.[101, 102] In these experiments, the dependence of the rupture force on the loading rate for the anti-$VEGF_{165}$ aptamer/ $VEGF_{165}$ was investigated. At each loading rate, the molecular rupture force was obtained by the Gaussian fit of force histograms from independent experiments (for example, the value of first peak in Figure 3.4A). Under similar experimental conditions, the rupture forces were measured at different loading rates ranging from 25 nN/s to 600 nN/s. The trend and linear dependence of bond strength on the logarithm of loading rate are illustrated in

Figure 3.5A. These values represent typical loading rates used in the study of receptor-ligand interaction systems via AFM.[199] The unbinding force between aptamer and protein shifted toward higher values with increasing pulling velocity, with an increasing slope at the higher loading rate. An increase in peak width of the force distribution with higher loading rate was also observed in these experiments. For example, two force distributions at loading rates of 50 nN/s and 550 nN/s showed force peaks at 112.3±2.4 pN and 181.5±4.7pN, with widths of 34.4±3.8 pN and 55.7±6.0 pN respectively (Figure 3.5B). Thermal fluctuations of solvent molecules play a more effective role in bond dissociation under lower loading rate, resulting in lower force and sharp force distribution. On the other hand, at a higher loading rate, less high-energy thermal fluctuations occur in a relatively shorter time, resulting in a higher rupture force and wider peak. [101, 198]

The presence of two linear regimes indicates that the dissociation of the aptamer/VEGF complex likely passes through different energy barriers from the bound state to the dissociation state according to the Bell model.[101, 102, 200] While the rupture force did not increase significantly at lower loading rates (25 nN/s to 270 nN/s), there was a significant increase in rupture force as a function of the loading rate at higher loading rates (270 nN/s to 600 nN/s). Similar energy regimes were observed in the unbinding of the biotin-streptavidin bond over 9 orders of magnitude in loading rate.[190]

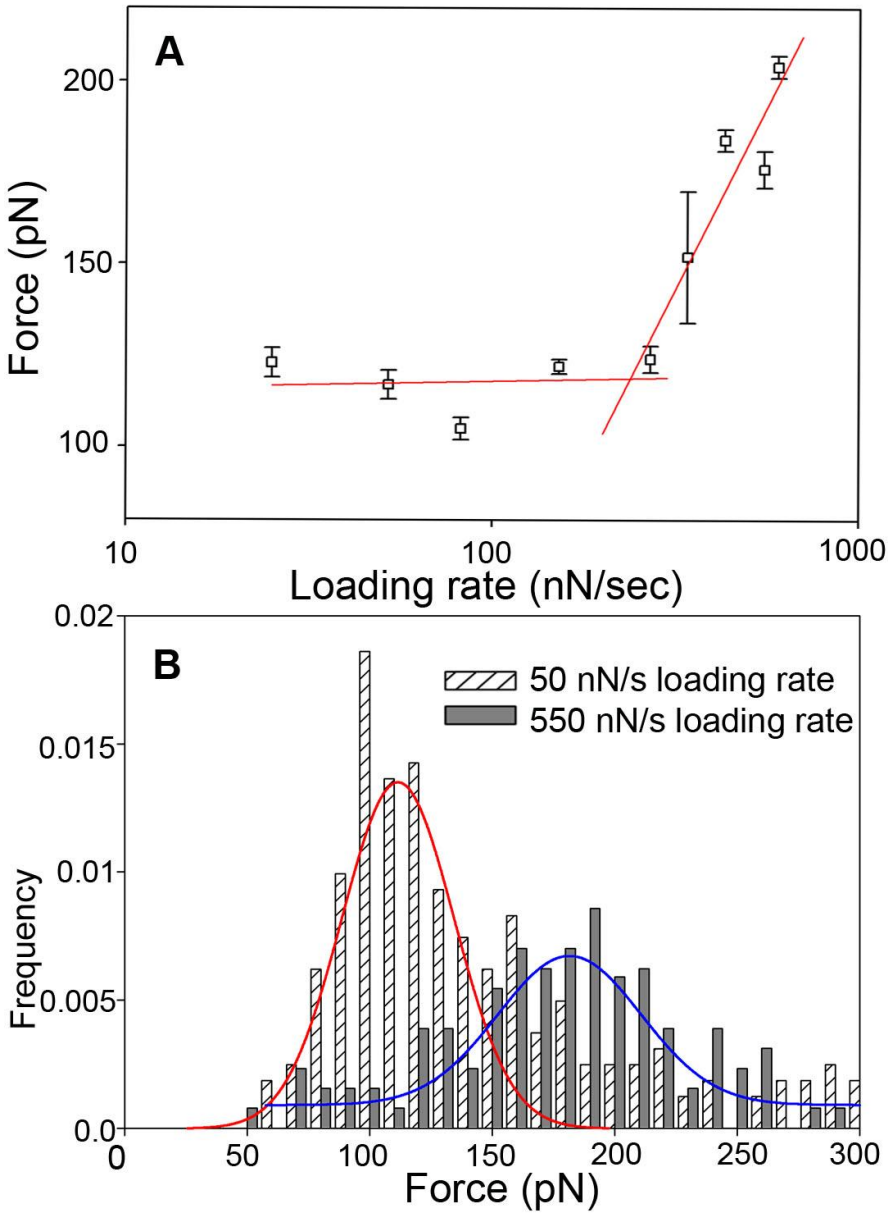

Figure 3.5 The dependence of rupture force between $VEGF_{165}$ and anti-$VEGF_{165}$ aptamer on loading rate. (A) Dynamic force spectra for $VEGF_{165}$ and anti-$VEGF_{165}$ aptamer interaction at different loading rates (25 nN/s - 600 nN/s). The peak forces obtained at the respective loading rates are plotted along with the standard deviations for each experiment. (B) Two examples of rupture force distributions of force spectroscopy experiments conducted at a low and a high loading rate.

In this loading scale, the measured rupture force is in the range of 85.0±3.0 pN to 184.2±3.0. Jiang et al.[49] determined the rupture force between IgE and its aptamer as 160 ± 29 pN in the loading rate range from 80-210 nN/s, which is at a comparable order of magnitude. Basnar et al.[182] measured the force to separate thrombin and its aptamer complex; however, their experiments revealed a very low separation value (4.45 pN), and the low force value was attributed to the melting of the H-bonded G-quadruplexes conducted at a low loading rate of 3 nN/s. A higher loading can therefore be postulated to help maintain the integrity of the RNA aptamer structure. In a recent study, Yu et al.[201] studied the stability of G-quadruplexes in the insulin linked polymorphism region sequence via laser tweezers, and obtained a rupture force for parallel and antiparallel structures ~30 pN, also under a low loading rate of 5 pN/s.

3.3.4 Specificity of the anti-$VEGF_{165}$ aptamer

Experiments performed by Jellinek et al. to study the specificity and competition of aptamers, revealed that the aptamer can be displaced by heparin from the protein. This suggested that the heparin binding domain of $VEGF_{165}$ is crucial for aptamer binding.[187] Since the isoform $VEGF_{121}$ (with 121 amino acids) does not have a heparin binding domain, it is expected that the lack of this domain would reduce the binding behavior between the protein and the anti-$VEGF_{165}$ aptamer. Similarly, an experiment where the heparin binding site of $VEGF_{165}$ was blocked would also be expected to show reduced binding. We therefore used $VEGF_{121}$ and

blocking experiments as a comparison to study the specificity of the interaction between anti-$VEGF_{165}$ aptamer and $VEGF_{165}$.

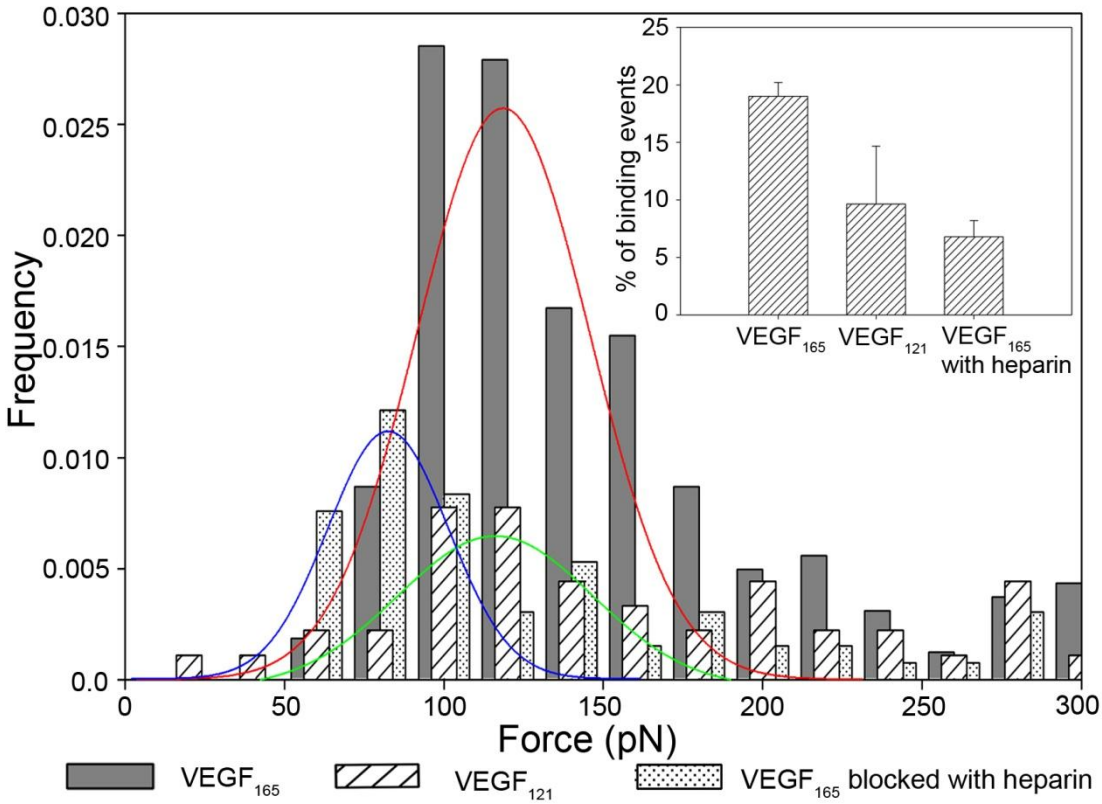

Figure 3.6. Specificity of anti-$VEGF_{165}$ RNA aptamer analysis. Histogram analysis of rupture forces of anti-$VEGF_{165}$ RNA aptamer against $VEGF_{165}$, $VEGF_{121}$ and $VEGF_{165}$ in presence of 5 µg/ml heparin. The solid lines are the fit Gaussian distributions for $VEGF_{165}$ (red), $VEGF_{121}$ (green) and $VEGF_{165}$ blocked with heparin (blue), showed binding events with anti-$VEGF_{165}$ aptamer at 119.3±2.5 pN, 116.2±6.6 pN and 82.6±2.5 pN, respectively. The inset is the binding percentages for force spectroscopy experiments conducted with these different systems.

The force distribution of the interaction of the anti-$VEGF_{165}$ aptamer with $VEGF_{165}$ that had been blocked with heparin is shown in Figure 3.6. While the

rupture force dropped to 82.6±2.5 pN, the binding percentage dropped significantly to 6.8±1.4% (Figure 3.6 inset). The force distribution histogram for anti-$VEGF_{165}$ aptamer and the two VEGF isoforms at a loading rate of ~150 nN/s was also analyzed. For the $VEGF_{165}$/anti-$VEGF_{165}$ aptamer system, clear and sharp peak was observed via the Gaussian fit at 119.3±2.5 pN, with a binding percentage of 19.0±1.2%. On the other hand, for the anti-$VEGF_{165}$ aptamer/ $VEGF_{121}$ system, the forces exhibited a similar distribution with a peak ~116.2±6.6 pN estimated from the histogram distribution, but the binding percentage dropped by half to 9.6±0.5%. The much fewer binding events, concluded from the experiments conducted with $VEGF_{121}$, and $VEGF_{165}$ blocked with heparin, verified that the absence of the heparin binding domain does indeed affect the interaction between anti-$VEGF_{165}$ aptamer and VEGF, and confirmed that the heparin binding site is critical for the binding of the anti-$VEGF_{165}$ aptamer.

However, similar to the random sequence RNA ligand-$VEGF_{165}$ system, there are a small number of force curves for the anti-$VEGF_{165}$ aptamer/$VEGF_{121}$ system and anti-$VEGF_{165}$ aptamer/$VEGF_{165}$ blocked by heparin system that exhibit binding events, especially evident at the molecular level. This shows that the specificity of this particular RNA aptamer is limited to some extent. Since aptamers are known to exhibit a high degree of structural flexibility, they can frequently undergo significant conformational alterations in the presence of their ligands.[44] Some aptamers selected by SELEX might change their secondary structure upon binding to other non-preferential targets, while it is possible that aptamers with a

more rigid and stable structure could have higher specificity compared with flexible aptamers.

Indeed, Carothers et al. [183] first questioned this specificity based on analysis of the interaction between aptamers selected to bind to GTP, and 16 different analogues of GTP. Their results indicated that the binding affinity and specificity were not closely related to each other. They further suggested that increasing the stability of aptamer could be an effective way to improve affinity, whereas the specificity of aptamer depended on the direct selection procedure.[183] The result in this work, that the anti-$VEGF_{165}$ aptamer also binds $VEGF_{121}$, even though at a lower frequency, may be explained by this hypothesis.

3.3.5 Binding in the presence of Mg^{2+}

It was previously demonstrated that positively charged ions have a strong influence on RNA folding into functional structure. They can neutralize negatively charged phosphate groups on RNA [202]; moreover, positively charged ions, especially divalent ions (such as Mg^{2+}) can further reduced the negative potential by binding to pre-formed binding sites, which only exist in tertiary structure, therefore, they act as stabilizers to enhance the formation of tertiary structure of RNA.[203, 204] By nuclear magnetic resonance (NMR) assay, Gonzalez et al. identified that a short, two-nucleotide loop and the major groove of a stem formed a pocket which is the specific binding site for Mg^{2+} and Co^{2+} in an RNA pseudoknot tertiary structure.[205] Cho et al. studied the effect of Mg^{2+} on a multiplexed aptamer microarray generated

by printing two RNA aptamers (anti-lysozyme and anti-ricin) and two DNA aptamers (anti-IgE and anti-thrombin). It was observed that a single buffer containing 5 mM $MgCl_2$ was suitable for all the aptamers, despite the fact that the aptamers were originally selected under diverse buffer conditions.[206] Taylor et al. used single-molecule fluorescence resonance energy transfer to study the interaction between a DNA aptamer and its target (VEGF) under different Mg^{2+} concentrations, and the analysis revealed that a higher Mg^{2+} concentration (2 mM compared to 0.2 mM) resulted in a more closed conformation for the aptamer.[181]

As discussed above, the stability of the aptamer is an important factor in determining its affinity. To investigate Mg^{2+} ions as a stabilizer of aptamers, we studied the effect of ionic strength on the interaction between the anti-$VEGF_{165}$ aptamer and $VEGF_{165}$. The rupture force distribution of this interaction under different Mg^{2+} concentration at a loading rate of ~80 nN/s is shown in Figure 3.7. As the Mg^{2+} concentration increased, the number of binding events observed decreased. This was manifested in a general decreasing trend in binding percentage from 19.7 % in the absence of Mg^{2+} ions to 4% at 100 mM Mg^{2+}. However, as the concentration of Mg^{2+} increased, the peak of the rupture force distribution shifted to higher values, which were 116.7±2.74 pN, 132.2±2.7 pN 131.2±5.8 pN, 138.2±6.2 pN and 146.0±19.4 pN in buffers with 0 mM, 0.1 mM, 1 mM, 5 mM and 10 mM Mg^{2+}, respectively. While the effect of 100 mM Mg^{2+} was also investigated, however, since the binding events were too rare (less than 4%), no significant peak can be concluded from the rupture force distribution.

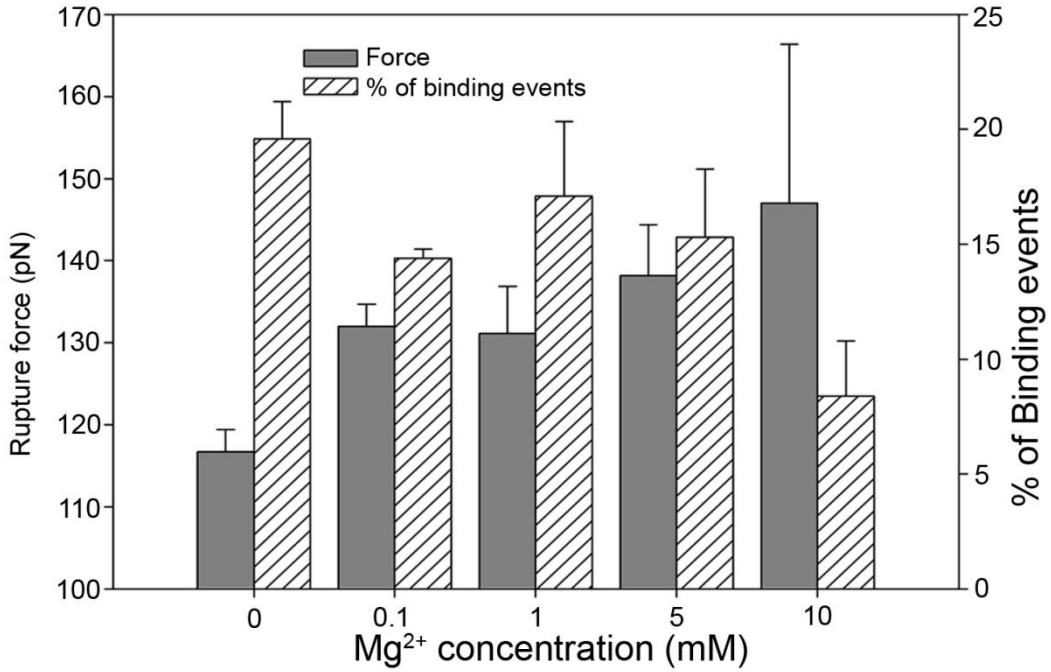

Figure 3.7. The effect of varying Mg^{2+} concentration on the detected binding percentage and rupture force of $VEGF_{165}$ and anti-$VEGF_{165}$ aptamer system. Mg^{2+} concentration was altered in the reaction buffer from 0 – 10 mM.

It is important to note that aptamers are designed to function optimally in the buffer system in which they are selected and changing the ionic strength may impair their molecular recognition and binding ability.[207] As mentioned above, the affinity selections of the aptamers were performed in PBS, which is the reaction buffer in our experiments. We hypothesize that in the absence of Mg^{2+} ions, the aptamers are in a more flexible state, whereby they can adjust their structure and direction upon binding to their targets, resulting in more frequent binding events. On the other hand, this flexible structure also readily gives up its preferential structure under external physical forces, which explains lower binding forces. In the presence of Mg^{2+}, the

aptamers assume a putative tertiary structure, which might result in reduced flexibility to adaptively folding in response to its target, but, on the other hand, it also requires higher energy to yield to an external force, explaining the higher binding forces but reduced binding probabilities.[203, 204] From the force spectroscopy experiments conducted in different Mg^{2+} concentration, it can be concluded that the rigidity of the aptamer significantly affects the binding behavior of the anti-$VEGF_{165}$ RNA aptamer and $VEGF_{165}$ protein. These experiments therefore show the optimization of the interplay between the binding forces and probabilities of aptamers is required to design better aptamer-based sensor systems and nanodevices.

Finally, it is important to note that recent bulk biophysical studies on a 25-mer DNA aptamer to $VEGF_{165}$ using fluorescence anisotropy and isothermal titration calorimetry (ITC) also concluded that aptamer stabilization is key to molecular recognition of the aptamer to its target.[180] A mutant aptamer with an improvement of aptamer stability by a sequence extension at the 5′ shows a higher association rates, and higher affinity towards its target. The force spectroscopy results showed that the anti-$VEGF_{165}$ RNA aptamers behave in a similar manner. To obtain aptamers with a higher affinity towards their targets, a selection strategy with selection pressure of stability may offer better results than a post selection improvement. These experiments show the advantages of single molecule experiments as sub-population and rare events can be uncovered. In contrast, bulk experiments provide the ensemble averages of large populations (several million molecules) and cannot show how certain non-specific events or certain blocking experiments affect aptamer behavior.

3.3.6 Monitoring the aptamer/target protein binding based on AFM nanografting

To further evaluate the feasibility of using this aptamer as biosensing component, anti-$VEGF_{165}$ aptamer nanoarrays and nanoshapes were fabricated on Au surface to facilitate visualization of the binding between this aptamer/target protein pair. As previously introduced, aptamers can be immobilized on gold surfaces via thiol modification to form SAM, therefore, the binding of the target protein to the aptamer can be reflected as a increased height of the features on the substrate.

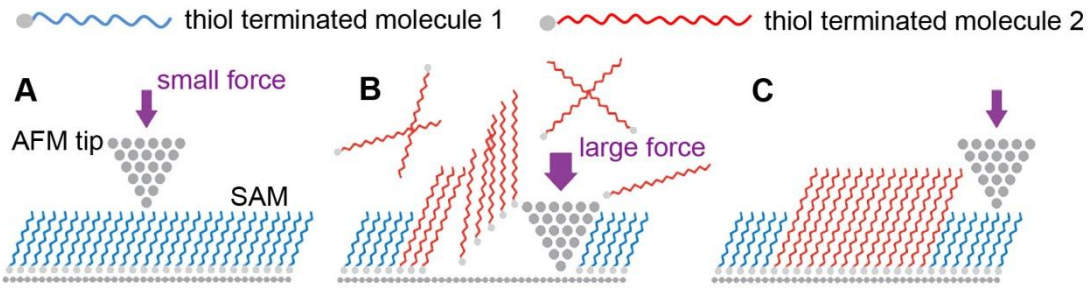

Figure 3.8. Schematic showing the process of nanografting.[208] (A) SAM functionalized surface is imaged with a low force; (B) with a force greater than the displacement threshold, the thiol terminated molecule 1 is removed at designated area, and the second thiol molecules attached onto the exposed Au surface; (C) the grafted area is imaged with a low force.

However, in order to clearly visualize the height difference by AFM imaging, it is necessary to precisely locate the aptamer on the surface within nanometer

regime. AFM nanografting is a suitable lithography technique to fabricate such patterns on a monolayer surface.[209] The procedure is relatively simple, starting from forming an alkanethiol functionalized monolayer surface. By applying a high force against such a surface during the scanning step, the thiol molecules are removed by the AFM tip, and meanwhile, the second thiol molecules contained in the solution immediately adsorb on the freshly exposed area.(Figure 3.8)[208] This technique was applied for the fabrication of DNA nanoarrays[208, 210] and DNA-directed immobilization of semi-synthetic protein-DNA conjugates. [211, 212]

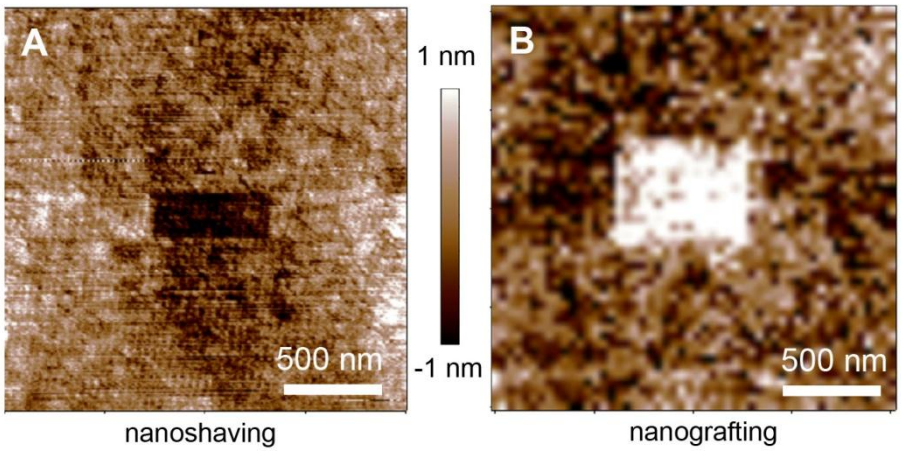

Figure 3.9. AFM images of the Au surface with OEG SAM modification after nanoshaving (A) and nanografting with aptamer thiols (B). The only difference between nanoshaving and nanografting procedures is whether the AFM tip scanned cross the surface with the second thiol (in this case, aptamer thiol) in presence.

In this research, an inert SAM was formed on gold surface by HS-C_{11}-$(EG)_3OH$ (EG_3) thiols to prevent nonspecific protein adhesion. An AFM probe was then scanned across the designated area with a relatively high force (typically, above 500 pN). This

scanning process was conducted in the solution of a thiol terminated aptamer, to enable the aptamer grafting. Basically, this step consists of removing the original EG_3 thiol molecules, exposing the underlying gold surface, which then acts as a substrate for the attachment of thiol terminated aptamer. Figure 3.9 A shows a surface prepared by a similar procedure as described above. This process referred to as "nanoshaving" was conducted in a PBS buffer instead of an aptamer thiol solution to demonstrate the process of EG_3 removal.[209] In this case, a lowered feature (around 1 nm lower than surrounding area) appeared in the designated area, indicating the success in removal of the OEG thiol. It is important to note that the thickness of (EG_3) thiol used in this research is about 2.2 nm, which is larger than the height difference observed after the nanoshaving procedure. It is possible that the $(EG)_3$ thiol molecules were not completely removed with the force applied in this case (500 pN). It was also observed that using AFM tips with different sharpness or applying different forces to the AFM tip, could result in variable depths of the patches (from 0.8-3.0 nm). "Nanografting" is essentially the subsequent step where the patches created by "nanoshaving" are filled by the secondary thiol. In the case of nanografting (Figure 3.9 B), a raised feature was observed, with around 1-2 nm height difference comparing with the surrounding OEG thiol, demonstrating the achievement of the aptamer grafting.

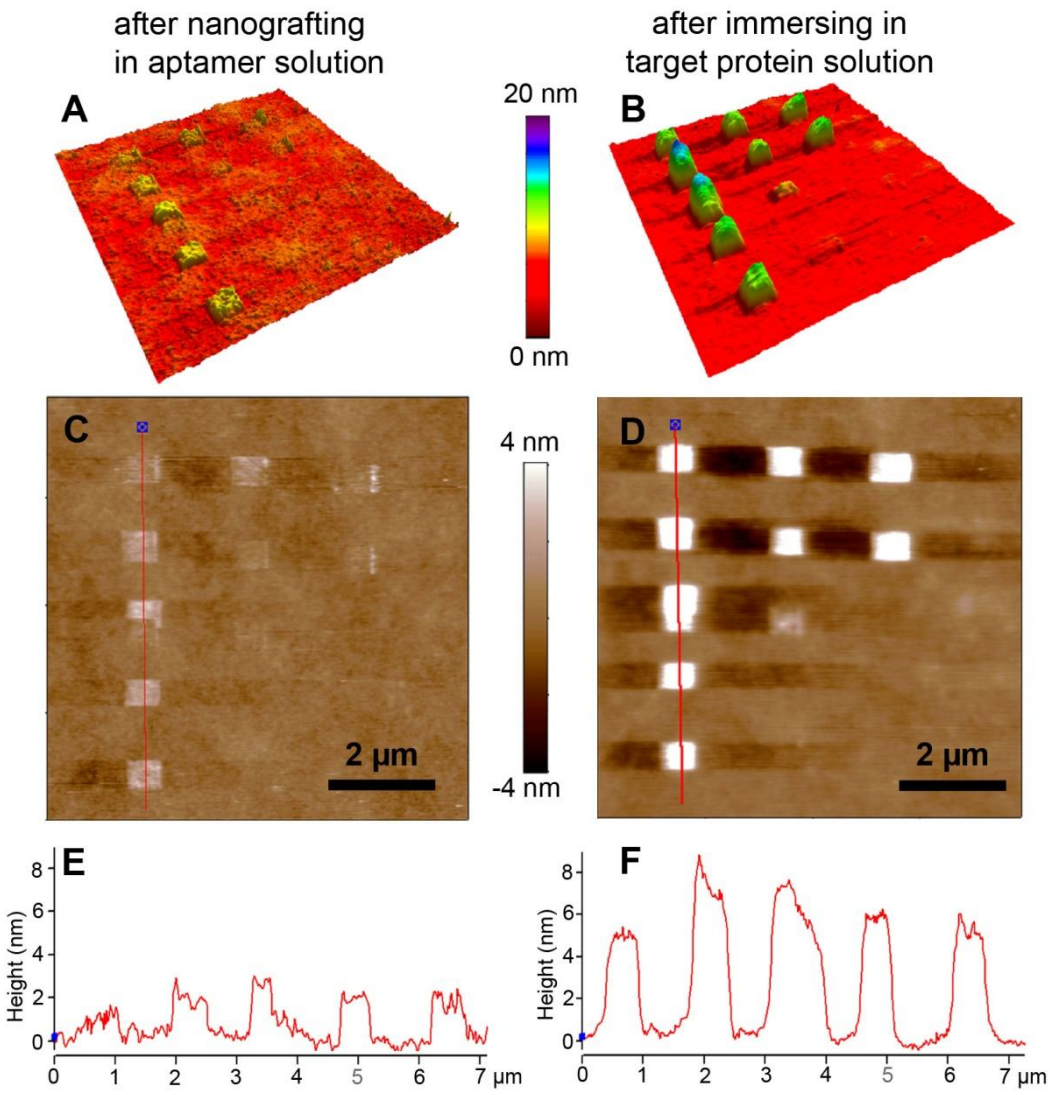

Figure 3.10. AFM characterization of the area grafted with anti-$VEGF_{165}$ aptamer before and after immersing with $VEGF_{165}$ protein solution. 3D (A, B) and 2D (C, D) AFM images; (E, F), the cross section analyses of the patches.

After the fabrication of the aptamer pattern via AFM nanografting, 10 nM $VEGF_{165}$ solution was deposited on this surface for 2 min, followed by rinsing with buffer to remove the unbound protein. Figure 3.10 shows the topography of the surface grafted by anti-$VEGF_{165}$ aptamer (patches patterns) before and after

immersing into the $VEGF_{165}$ solution. The height of the patches increased from 2 nm to 5-8 nm, which demonstrated the binding the protein onto the aptamer patch due to the aptamer recognition. Furthermore, sophisticated patterns of aptamer could be created using this AFM nanografting technique. As shown in Figure 3.11, thiol terminated anti-$VEGF_{165}$ aptamer molecules were grafted as the letters "VCU". This pattern was clearly visualized after immersing in the $VEGF_{165}$ solution, with an increased height about 2 nm. It is interesting to note that the height increase in the line shape pattern is smaller than that of the patch pattern. It is possible that in the case of line shape pattern, the steric hindrance caused by surrounding OEG thiol to the aptamer/protein binding is more significant due to an edge effect.

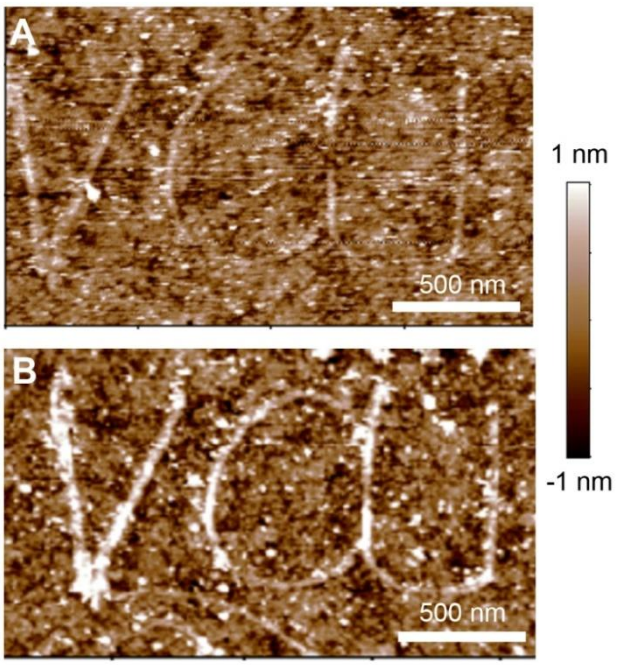

Figure 3.11. Anti-$VEGF_{165}$ aptamer grafted as "VCU" showing increased height after immersing in $VEGF_{165}$ protein solution.

3.4 Conclusions

The specific interaction of an aptamer and its target was successfully measured by single molecule force spectroscopy via an AFM. The results of varying binding probabilities and force distributions by different RNA ligands against the angiogenic protein VEGF and by other control systems confirmed that binding between the AFM probe and surface indee caused by the interaction between the aptamer and its target. The specificity of the anti-$VEGF_{165}$ aptamer was investigated using $VEGF_{121}$ as a target lacking an essential binding domain and using $VEGF_{165}$ blocked by heparin. The lower frequency of binding compared with $VEGF_{165}$ reflected that despite the high affinity to its preferential target-$VEGF_{165}$, the specificity of this aptamer may be impaired to some extent at the molecular level. Dynamic force spectra reflected that the binding force between anti-$VEGF_{165}$ aptamer and $VEGF_{165}$ increased at a higher loading rate. By changing the concentration of the stabilizing metal ion-Mg^{2+} in the binding buffer, it was observed that a rigid tertiary structure required a higher force to unbind the aptamer/protein complex, although the frequency of the corresponding binding events decreased. Optimizing the interplay of these parameters - binding probabilities and affinities, can be used in the engineering and design of more effective aptamer based devices and diagnostic tools.

Finally, in order to develop strategies to use this aptamer as a biosensing component, the formation of anti-$VEGF_{165}$ aptamer nanoarrays was demonstrated using an AFM nanografting technique. The binding between this aptamer/target

protein system was successfully assessed by AFM height measurements, and showed how aptamers immobilized in this manner could be used to feasibly detect and bind their protein targets.

[This chapter contains results that have been previously published in the paper "Molecular interaction studies of vascular endothelial growth factor with RNA aptamers" in Analyst, 2010]

CHAPTER 4

SPECIFIC DETECTION BY APTAMERS CONDUCTED AT DIFFERENT LENGTH SCALES

4.1 Introduction

As discussed in the previous chapter, aptamers are a group of promising bio-components for molecular recognition applications due to advantages including ease of synthesis and modification, high stability, low immunogenicity and availability against a wide variety of targets (proteins, inorganics and even whole cells). The research shown in previous chapter confirmed the recognition of aptamer-target protein at the molecular level by exploring aspects of the energy landscape, the specificity and the conformations. Patterning of aptamers to fabricate nanoscale arrays was also shown. Importantly, these fundamental characteristics mentioned above, can only be obtained by the high-precision analytical tools at the molecular scale. However, in order to create systems that can use aptamers in various diagnostic devices, it is also necessary to investigate their kinetic behavior at multiple length scales. A significant challenge is in trying to bridge the gap between

these two scales – the molecular scale at the level of a few molecules and the ensemble scale – at the level of millions of molecules.

In this chapter, work on trying to correlate this binding information across scales is presented so that we can take advantage of all this data to optimize the design of aptamer based tools. However, based on a review of the literature, there has been very limited work on establishing direct correlations between the affinity properties (ensemble level) and the rupture forces (single molecular level) to characterize the binding of the biomolecular pair. In order to address on this problem, different aptamer-target protein systems were investigated by ensemble level methods along with AFM force spectroscopy at single molecule level. By comparing the results from these two levels, the possible correlation and translation between these two scales was discussed.

At the ensemble level, several studies on aptamer-based biosensors have been reported including both optical methods and label free methods. The former designs typically take advantage of the ligand-induced conformational change of aptamers. By introducing optical reporters in the labile region of the aptamer, conformational change upon binding to the target can be detected by the fluorescence characteristics such as intensity and anisotropy. [35, 62, 213] In this fashion, several signaling aptamers have been created. For example, Bai et al. reported a signaling aptamer sensor by intercalating luminescence signal change of $[Ru(phen)_2(dppz)]^{2+}$ in a 37-nt DNA aptamer against immunoglobulin E (IgE).[120] Signaling aptamers against anticocaine [121] and platelet-derived growth factor (PDGF) [214] were also

designed by truncating one of the stems of a three way junction and introducing a fluorophore and a quencher at the 5′ and 3′ termini respectively. However, a loss in binding affinity is a general problem for these label-based designs.[42] For example, the equilibrium dissociation constant K_D of a fluorescently labeled DNA -signaling aptamer was 5 times higher than that of the original (unmodified) aptamer.[215] [216] Another potential problem with a labeling strategy is that the optical signals might be interfered by a variety of ligands or solvents, resulting in a false positive or high noise background.[216]

On the other hand, label-free methods, such as surface plasmon resonance (SPR) and quartz crystal microbalance (QCM) can minimize these problems. Besides, these chemical-electric methods have the advantages including high sensitivities, ease of operation, and real time measurement. In particular, QCM is much less expensive, and much easier to operate, and has become of the leading strategies in biological binding measurements.[58] (See Section 1.3.3 for a detailed introduction) Due to these reasons, QCM was chosen as an ensemble level analytical method to investigate the aptamer recognition at ensemble level.

QCM methods come with their own set of challenges. For example, to utilize a QCM to investigate the binding kinetics of aptamers, the first step involves the immobilization of the aptamer to the sensor (crystal) surface. Design challenges include minimization of non-specific binding, loss of affinity and increasing the accessibility of the aptamer. Strategies for DNA immobilization for QCM detection of hybridization were developed several years ago in various formats including

biotin attachment and direct adsorption.[217, 218] These were adapted to aptamers in QCM biosensors, for example, biotin labeled anti-IgE aptamer [64, 67] and anti-thrombin aptamer [62] immobilized on a streptavidin modified Au. However, the methods described take multiple steps to immobilize the aptamer, which can result in a higher risk for chemical contamination and loss of specificity of the sensor.[219] It is therefore vital to develop methods for the attachment of aptamers to surfaces for use in such biosensors or diagnostics that involve minimal loss in functionality and non-specific interactions. Direct attachment of anti-thrombin aptamers to a gold surface was earlier demonstrated using alkane thiol linkers to form a thiol terminated aptamer SAM, SPR and ellipsometry analysis were used to compare different co-adsorbent thiols and different aptamer linkers.[119] However, optimizing the activity and accessibility of the aptamer for various biosensing applications still remains unsolved.

From earlier experience and investigations at the molecular level shown in Chapter 2 and 3, using a direct Au-S bond to attach the aptamer was found to be a reliable strategy to address these challenges. As previously described, the thiol chemistry allows the selection of functional groups that may be used as co-adsorbents to form mixed monolayers with different surface properties.[115] Inspired by the mixed SAM platform developed earlier, here, three strategies (Figure 4.1) for the direct attachment of aptamers to gold surfaces were investigated.

The first is the direct formation of an aptamer monolayer via thiol attachment to a gold surface. The second is a two-step mixed-SAM formation: aptamer

monolayer self-assembly, followed by backfilling of the unmodified surface with an oligoethylene glycol (OEG) thiol. The third involves the formation of a mixed-SAM in a single step via co-adsorption from a solution of a thiol-modified aptamer and OEG thiol. The aptamer is modified at the 5′-end with a $(CH_2)_6$ spacer and an –SH linker, for direct covalent immobilization to gold.

Prior to application in more useful biological systems, the well characterized immunoglobulin E (IgE) DNA aptamer/IgE system was chosen as a model system to evaluate and optimize the methods in an initial set of experiments. DNA is more stable and less prone to nuclease attack experimentally compared to RNA.[220] Consequently, instead of the RNA aptamer characterized in Chapter 3, more stable DNA aptamer/target protein systems were chosen to investigate these strategies. To further verify the functional viability of the surface-tethered aptamers for biophysical analyses and protein binding, AFM based force spectroscopy of the binding pairs was performed. Once an optimal strategy was identified, the angiogenic VEGF and the VEGF-binding aptamer system was investigated with the strategy evaluated. The optimization of these surface modification strategies is reported here along with correlation between affinities and rupture forces. Furthermore, the effect of the Mg^{2+} on the binding between anti-VEGF RNA aptamer and VEGF protein was also investigated at ensemble level in this chapter in order to correlate with the previous results obtained at single molecule level.

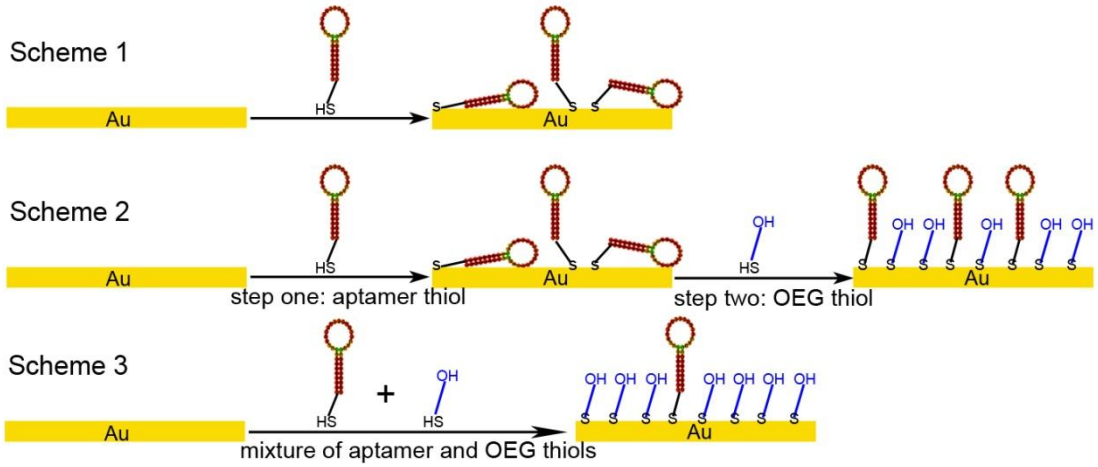

Figure 4.1. Schematic of different sensor configurations investigated.

4.2 Experimental section

4.2.1 Materials and instrumentation

IgE binding DNA aptamer (anti-IgE DNA) (5′- GGG GCA CGT TTATCC GTC CCT CCT AGT GGC GTG CCC C -3′), $VEGF_{165}$ binding DNA aptamer (anti-$VEGF_{165}$ DNA) (5′- CCGTCTTCCAGACAAGAGTGCAGGG -3′), and Anti-$VEGF_{165}$ RNA (anti-VEGF RNA) (5′-CCG GUA GUC GCA UGG CCC AUC GCG CCC GG-3′) with 5' dithiol S-S modifiers and $(CH_2)_6$ spacers were custom synthesized by Integrated DNA Technologies, Inc. (Coralville, IA). Anti-Human IgE produced in goat was purchased from Sigma Aldrich, and recombinant $VEGF_{165}$ was obtained from Biovision, Inc. (Mountain view, CA). Since this research primarily focused on the VEGF protein isoform with 165 amino acids, the designation "VEGF" is used subsequently to refer to "$VEGF_{165}$".

(1-Mercaptoundec-11-yl) hexaethylene glycol ($HS\text{-}C_{11}\text{-}(EG)_6OH$), (1-Mercaptoundec-11-yl) triethylene glycol ($HS\text{-}C_{11}\text{-}(EG)_3OH$) and

(1-mercaptohexadecanoic acid)-N-succinimidyl ester (NHS-terminated thiol), HS-C_{15}-COO-NHS, were purchased from Nanoscience Instruments (Phoenix, AZ). We refer to HS-C_{11}-$(EG)_6OH$ and HS-C_{11}-$(EG)_3OH$ thiols as EG_6 and EG_3 respectively. Phosphate-buffered saline (PBS pH 7.4) (11.9 mM phosphates, 137 mM sodium chloride and 2.7 mM potassium chloride), 1 M $MgCl_2$ solution (molecular biology grade) and Ethanol (200-proof) were purchased from Fisher Scientific. DEPC treated RNase free water was used for all experiments.

QCM measurements were performed using a Q-Sense E4 system (Q-Sense AB, Gothenburg, Sweden). Gold coated QCM crystal sensors (QSX 301) were purchased from QSense. Gold surfaces were purchased from Agilent Technologies, Inc. (Foster City, CA).

4.2.2 Functionalized sensor, substrate and probe preparation

Gold sensors and substrates were cleaned by UV/ozone treatment for 10 min, rinsing with ethanol and RNase free water, followed by UV/ozone treatment for 10 min. The resulting clean surfaces were modified by different strategies (Figure 4.1). **Scheme 1:** immersion in 2.5 µM solution of a thiolated aptamer (HS-C_6-aptamer) in RNase free water overnight, and rinsing with RNase free water; **Scheme 2:** two-step mixed monolayer modification: immersion in a thiolated aptamer (HS-C_6-aptamer) water solution for two hours, followed by rinsing with water. Subsequent immersion in either HS-C_{11}-$(EG)_3OH$ or HS-C_{11}-$(EG)_6OH$ ethanol solution overnight, and rinsing with ethanol. **Scheme 3:** one-step mixed monolayer modification: immersion

in a water solution containing both thiolated aptamer (HS-C_6-aptamer) and HS-C_{11}-$(EG)_3OH$ overnight, then rinsing with water.

Gold coated AFM cantilevers were UV/ozone cleaned for 10 min. Cantilevers were functionalized by self-assembled monolayers prepared as described [118] - immersion in mixed thiol solution (HS-C_{11}-$(EG)_6OH$ and HS-C_{15}COO-NHS) in ethanol for 16 hours. Surfaces were then rinsed with ethanol, and incubated in a 100 nM solution of protein (IgE or VEGF) in PBS buffer for 1 hour at room temperature.

4.2.3 Quartz crystal microbalance measurements

The QCM sensors used are 14 mm diameter discs, optically polished quartz crystals with Au coating (10 mm diameter) on both sides. Sensors operate at a fundamental frequency of 4.95 MHz. Before each measurement, buffer (without any protein) was passed through the QCM flow module for 2-4 hours to obtain a stable baseline. All measurements were carried out under constant flow rates of 8.6 µl/min, and at 20 ℃.

4.2.4 AFM imaging of surfaces and force spectroscopy

Gold coated PPP-CONTCSAu cantilevers from Nanosensors (Neuchatel, Switzerland), TR400 PB and TR800PSA cantilevers from Olympus (Tokyo, Japan) were used for force measurement and imaging respectively. TR800PSA cantilevers (k ~0.15 N/m, frequency 24 kHz) was used for imaging the surfaces in noncontact

(tapping) mode. TR400 PB cantilevers (k~0.09 N/m, frequency 24 kHz) functionalized with the aptamer as described, were used for measurement of interaction forces. Force-distance curves were obtained by collected and analyzed by the same method as described in Chapter 2.

4.3 Results and discussion

4.3.1 QCM measurements to investigate binding kinetics

The QCM is based on the change in resonance frequency of the quartz crystal sensor due to changes of its mass load. From the Sauerbrey equation, the change of frequency, Δf, can be is linearly correlated to its mass change, Δm, (as equation (6) in section 13.2). The sensitivity constant c_f can be calculated by equation (7), from a original resonance frequency (here, 4.95 MHz), velocity of sound in the quartz crystal (3340 ms^{-1}) and the quartz density (2648 kg m^{-3}).[67] Hence, the relation between the change of frequency, Δf, and its mass change, Δm, can be described as:

$$\Delta f = -56.5 \times 10^{-3} \Delta m / A \qquad (8)$$

Issues with QCM: While the QCM is a highly sensitive detecting technique, measurements can be significantly influenced by numerous effects, such as the liquid's density and viscosity, flow rate, temperature fluctuations, environmental noise, pressure fluctuations etc. These influences were observed frequently during the reported experiments. Figure 4.2A is an example of QCM measurement showing a sudden spike signal, which could be caused by several possible reasons, such as an air bubble trapped on the sensor surface during the injection of analyte solution to

the sensor, contamination in the analyte solution, or a pressure shock experienced by the sensor. Figure 4.2B shows an example of baseline shift caused by adding small amount of $MgCl_2$ to the PBS buffer. The baseline shifts is often caused by different viscosity and/or density of the solution, referred as "bulk property".[221] In order to conduct accurate measurements, it is therefore necessary to distinguish the shift caused by the bulk property of the solution from the weight gain due to the binding between the analyte in the solution and receptor immobilized on the sensor.

Due to these challenges, the QCM measurements were carefully designed. Various strict criteria were set up in order to obtain reliable quantitative results: (a) Only clean and new sensors were used. This is an important criterion because typically QCM manufacturers indicate that sensors can be cleaned using various protocols and reused; (b) Baselines were obtained in the same buffer used for making analyte solution; (c) The binding between the aptamer and protein is dependent on the analyte concentration. Typically, the QCM measurements are conducted by observing frequency response with different sensors under different analyte concentration. In order to minimize the system error, and accurately quantify this concentration-dependence, instead of separate experiments, the frequency responses with increasing analyte concentration were recorded in a sequential fashion using the same sensor.

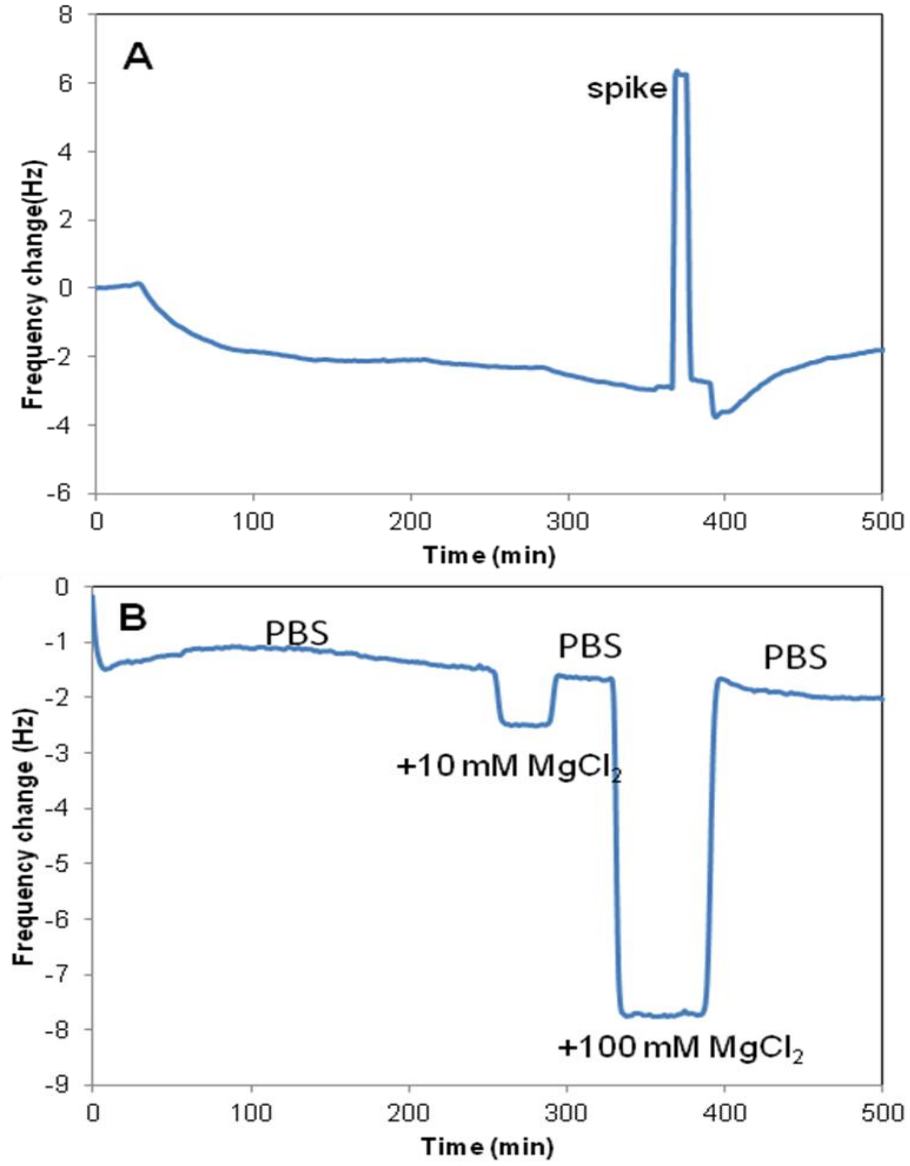

Figure 4.2. Examples of frequency change during the QCM measurements which were not caused by ligand/receptor binding. (A) Example of sensor showing a sudden spike peak during the binding measurement. Instability measurements similar to this were discarded. (B) Baseline shift caused by the bulk property of solution. Specifically, the baseline shifted 0.9 Hz, and 6.3 Hz right after the injection of PBS buffer with 10 mM and 100 mM $MgCl_2$ added.

4.3.1 IgE Binding to Thiolated anti-IgE Aptamer Monolayer

In the initial set of experiments, the binding of IgE to a sensor with anti-IgE aptamers immobilized on the surface was studied (Figure 4.1, Scheme 1). Different concentrations of the protein (IgE) were flowed over the sensor and the value of the steady-state frequency was used to estimate the corresponding binding affinity of IgE. In all experiments, a steady-state is defined as when the frequency change of the signal is <0.5 Hz/hr. Based on the frequency response at different IgE concentrations, the binding affinity between two biomolecules at equilibrium, K_A was estimated. The relationship between frequency changes and the affinity constant was derived:[60]

$$1/\Delta f_e = 1/\Delta f_{max} + 1/\Delta f_{max} K_A C_{IgE} \quad (9)$$

Where Δf_e is the frequency change of crystal sensor after it reaches equilibrium, and Δf_{max} represents the maximum frequency drop, which is an ideal state in which all accessible aptamers are bound to the target. Therefore, the plot of $1/\Delta f_e$ as a function of $1/ C_{IgE}$ is a straight line, and the K_A is determined as the quotient of the intercept and the slope.

This linear relationship between $1/\Delta f_e$ and $1/ C_{IgE}$ is supported by the experimental observations (Figure 4.3). The affinity K_A = 0.64 nM^{-1}. In earlier reported works, the dissociation constant K_D for this aptamer and IgE was earlier measured as 10 nM through nitrocellulose filter partitioning analysis [222] and 8.4 nM via QCM measurements.[67] K_A can be calculated from these K_D values as 0.10 nM^{-1} and 0.12 nM^{-1} respectively. Compared to these reported values, this sensor shows a higher binding affinity, while maintaining a low detection limit <10nM.

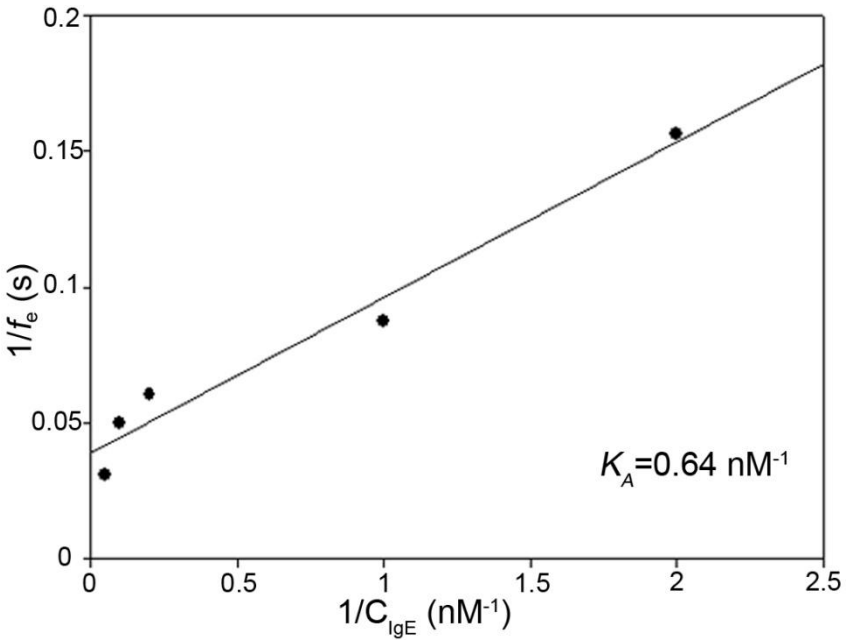

Figure 4.3. Relationship between $1/C_{IgE}$ and $1/\Delta f_e$ from QCM measurements on sensors modified by thiolated aptamer SAM alone. Δf_e is the frequency change of crystal sensor after it reaches equilibrium. The plot of $1/\Delta f_e$ as a function of $1/ C_{IgE}$ is a straight line, and the binding affinity K_A is determined as the quotient of the intercept and the slope of this line.

However, this immobilization strategy with direct attachment of thiolated DNA monolayers on gold was earlier shown by hybridization studies to be non-optimal.[119, 223] First, interactions between the Au surface and the DNA are not exclusively through thiol groups modified at the 5′-end, but also through nitrogen moieties within the nucleotide bases. The DNA therefore, tends to nonspecifically bind to the gold surface, resulting in reduced accessibility of the aptamer and a disordered orientation. Second, the repulsion between DNA chains may result in poorer surface coverage, especially at low ionic strength buffer

conditions.[119, 223] The resulting uneven coverage results in nonspecific adsorption of analytes to the bare Au surface. It can therefore be expected that, for aptamer-based protein sensors, both the nonspecific adsorption and reduced accessibility can affect its function, and cause inaccuracy of measurement. In order to minimize these effects, inspired by the previous established mixed SAMs surface modification for protein attachment, a thiolated aptamer surface with passivating thiols as co-adsorbents to fabricate stable, specific aptasensors was used.

4.3.2 IgE binding to mixed self-assembled monolayers

To form mixed self-assembled monolayers, a co-adsorbent thiol can be used to fill the Au surface between the thiolated DNA molecules and thereby reduce nonspecific interactions between the gold and DNA.[223, 224] Oligo-ethylene glycol (OEG) thiols as co-adsorbents with thiol-modified aptamers were used to form mixed SAMs for QCM based aptasensors. SAMs of OEG-terminated thiols have been well documented as effective protein-resistant monolayers, with EG_3 and EG_6 being most widely used.[169, 225] particularly, as shown in Chapters 2 and 3, the OEG thiol shows great resistance to nonspecific interaction.

Two different strategies to form mixed SAMs were studied: 1. A two-step method where the aptamer thiol was first immobilized on a gold surface, followed by backfilling of the bare gold area with an OEG thiol (Figure 4.1 Scheme 2 – Sensors A and B - backfilling with EG_6 and EG_3 respectively). This strategy can enhance the utilization of the aptamer and minimize possible contamination caused by the mixing

process. 2. A single step method using a mixture of the aptamer-thiol and OEG-thiol in water (Figure 4.1, Scheme 3 - Sensor C) to form the SAM. Previous studies have shown that water is also a suitable solvent for the formation of ordered mixed SAMs of ssDNA and OEG on Au surface.[224] This strategy allows control of the aptamer coverage on the surface by simply changing the molar ratio of the two thiols in solution. In contrast to using ethanol as a solvent to form these monolayers, the use of water was considered a significant advantage because it also allows subsequent adsorption of proteins without the need for any solvent exchange or fear of denaturation. Control sensors (containing no sensing aptamer) modified by EG_3 or EG_6 alone were used to determine the extent of non-specific adsorption to the sensor surfaces.

Typical QCM curves obtained are shown in Figure 4.4. Binding affinities were analyzed based on the changes in frequency observed (Figure 4.4 insets). K_A values for sensors A, B and C are calculated as 0.065 nM^{-1}, 0.029 nM^{-1} and 0.042 nM^{-1} respectively. Compared to the K_A values analyzed by the sensor modified by aptamer thiol alone (Scheme 1), these results are consistent with that measured by previous studies (K_A=0.10 nM^{-1}). Sensor A shows the highest IgE affinity but a low frequency response at each IgE concentration. Sensors B and C were modified with mixed SAMs of aptamer and EG_3, by Scheme 2 and 3 respectively. While the K_A values are similar, Sensor C shows a reduced frequency response at each IgE concentration, although the concentration of aptamer in the thiol solution is 100 times the aptamer concentration for Sensor B. In all sensors, low concentrations <

10nM of the IgE can be reliably detected, showing that this strategy is useful to create sensitive sensors with reduced non-specificity. Figure 4.5 A and B show AFM images of sensors before and after QCM experiments respectively. Figure 4.5 B shows coverage of the surface with IgE, bound to the immobilized aptamer.

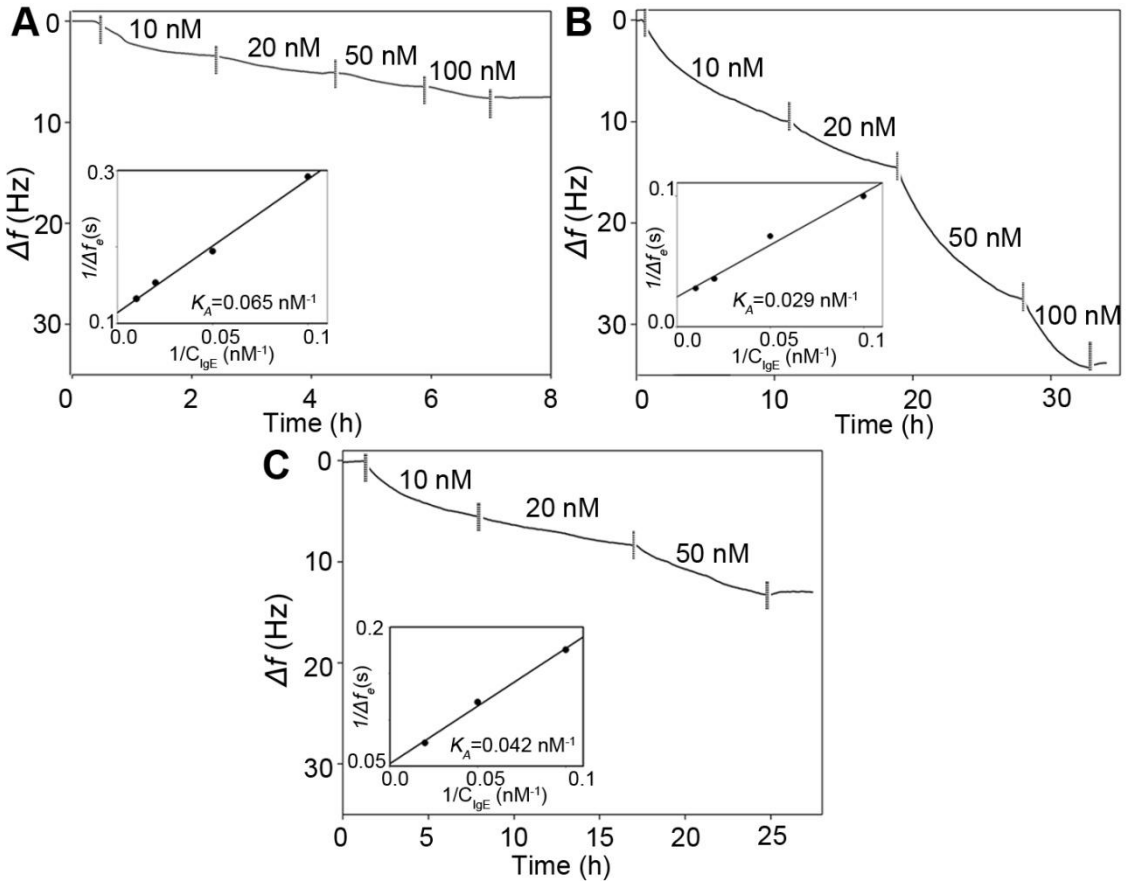

Figure 4.4. QCM frequency response to IgE for each modification strategy. Sensor A: two-step modification, aptamer 0.25 µM, EG_6 1 mM; Sensor B: two-step modification, aptamer 0.25 µM, EG_3 1 mM; Sensor C: one-step modification, 25 µM, EG_3 1 mM; Insets - K_A estimated from $1/\Delta f_e$ as a function of $1/C_{IgE}$ for each sensor.

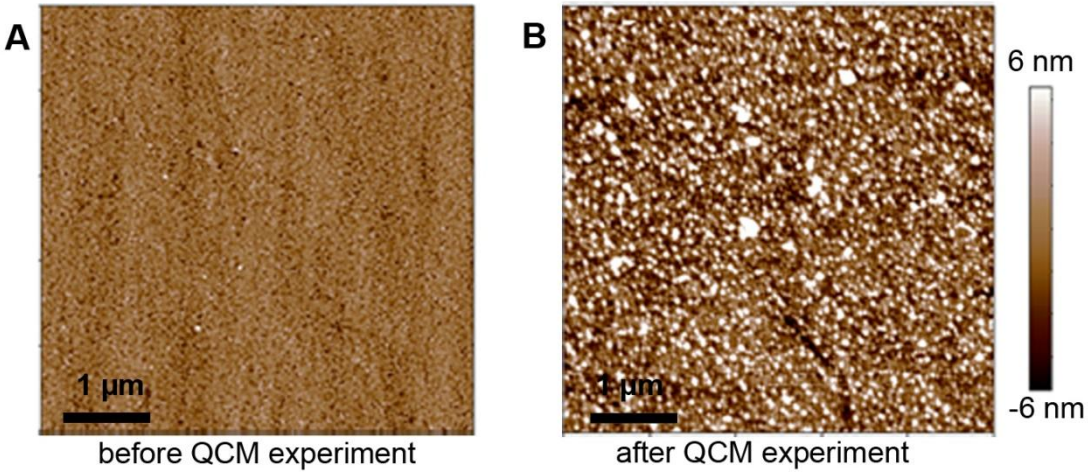

Figure 4.5. AFM image of the gold surface of QCM sensor modified with a mixed thiol SAMs modification by scheme 2 (sensor B), which were conducted before (A) and after (B) QCM experiments.

The frequency drop of sensors at equilibrium at a flow of 20 nM IgE is shown in Figure 4.6 (other concentrations exhibited similar values – data not shown), where the frequency drop is directly correlated to the amount of bound protein. As expected, sensors modified by OEG thiols alone have a much smaller frequency drop compared with those modified with aptamer thiol SAMs. While longer chain EG_6 has been shown to exhibit a better resistance to protein adsorption than EG_3.[169] In these experiments, the Sensor A with immobilized aptamer thiol and EG_6 thiol does not show significant response compared to EG_6 thiol alone. With the EG_3 thiol as co-adsorbent, the sensor modified by the aptamer and EG_3 thiol (sensor B) has significantly increased response toward IgE (Figure 4.6). This is likely because the aptamer surrounded by the longer chain EG_6 may result in poorer accessibility of the aptamer. On the contrary, the shorter chain EG_3 thiol has considerably less impact on

the accessibility of aptamer, making it a better choice for sensor fabrication.

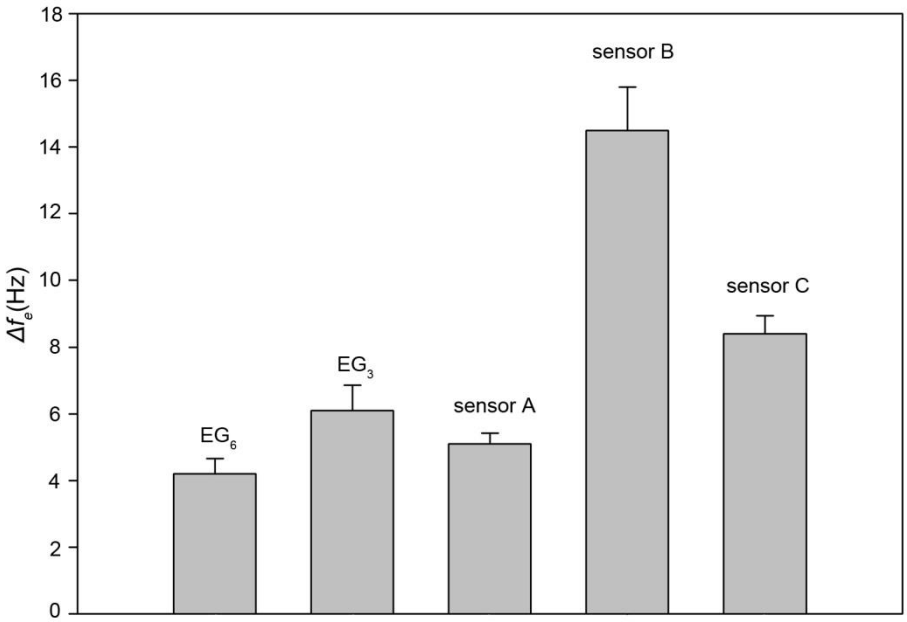

Figure 4.6. QCM frequency response to 20 nM IgE for each modification strategy of control sensors modified by 1mM EG_6 or EG_3 thiol alone and sensors modified by both aptamer thiol and OEG thiol (sensor A, B and C). Sensor A: two-step modification, aptamer 0.25 μM, EG_6 1 mM; Sensor B: two-step modification, aptamer 0.25 μM, EG_3 1 mM; Sensor C: one-step modification, 25 μM, EG_3 1 mM. The value Δf_e is the average value of three individual normalized frequency changes obtained from multiple overtones.

4.3.3 AFM force spectroscopy of IgE/Anti-IgE aptamer system on mixed SAMs

By QCM measurements, different strategies display different abilities to resist nonspecific adsorption. All of the strategies used above showed a better *binding* to IgE (measured by the absolute value of the frequency change) than a

surface with just the immobilized aptamer. However, sensors functionalized in different conditions showed different *affinity* towards IgE (measured by the value of the determined K_A) (Figure 4.5). One underlying reason for this could be due to the difference in the biological activity of the aptamer caused by different immobilization strategies. Another reason could be due to the differences in accessibility of aptamer caused by different length of OEG thiol, or surface thiol coverage.

To uncover the reason for these different affinities, molecular force spectroscopy using AFM was applied to study the rupture forces between IgE and the immobilized aptamer in each sensor. The biophysical differences of aptamer immobilized by different strategies could therefore be observed through force spectroscopy as described in previous chapters.

Rupture forces were measured and analyzed on the surfaces modified, corresponding to the Sensors A, B and C, respectively. As shown in Figure 4.7, similar rupture force distributions were obtained from all three sensors, at 64.1±0.9 pN, 64.0±2.9 pN and 61.7±0.7 pN. However, the frequency of binding events is different, especially for Scheme 3 (Sensor C) where the percentage of total binding events is 3.2%, which is much lower than 27.5% (Sensor B) and 16.7% (Sensor A) for two-step modification strategies. This result is consistent with the low frequency response of QCM sensors modified by an identical strategy. It appears that in the presence of a mixture of OEG and aptamer thiol, the surface coverage of the aptamer is significantly lower. For two-step modifications, aptamer/EG_3 surface (Sensor B)

has a higher percentage of total binding events compared to aptamer/EG_6 (Sensor A). This could be explained by considering the better accessibility of aptamer towards IgE because of the shorter chain of EG_3 compared with EG_6.

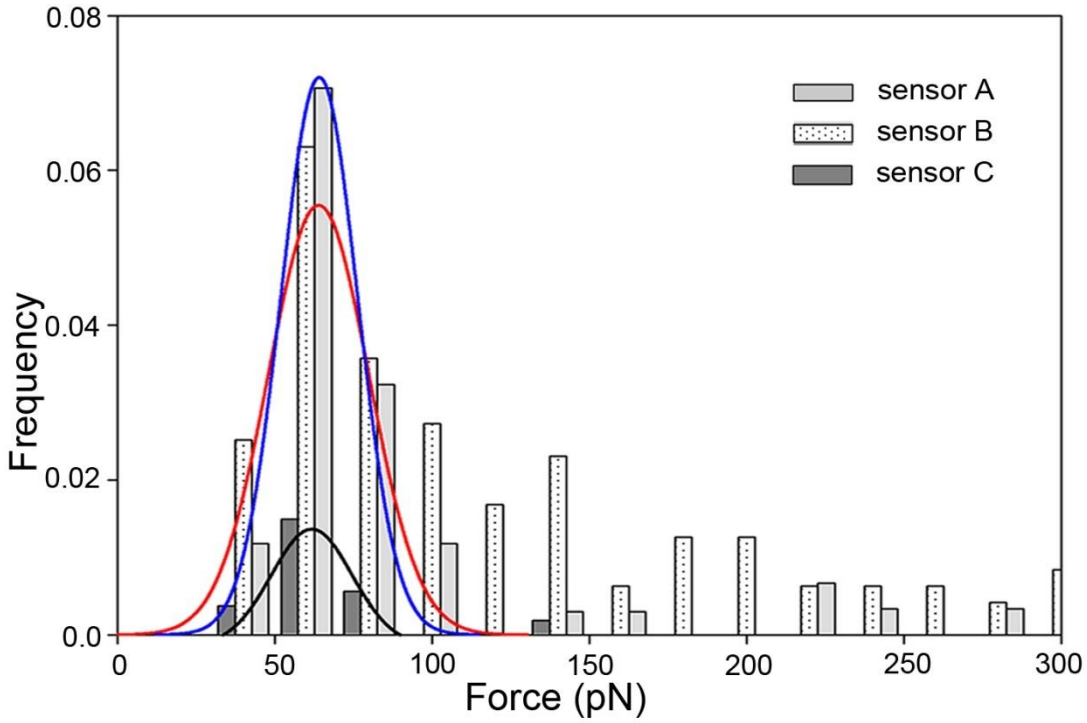

Figure 4.7. Force distribution of IgE immobilized tip towards different mixed SAM surfaces. Gaussians represent force peaks of 64.1 ±0.9 pN, 64.0 ±2.9 pN and 61.7 ±0.7 pN for sensors A, B and C respectively.

4.3.4 Aptamer surface density, accessibility and affinity towards its target

The rupture forces from all surfaces obtained via force spectroscopy were found to be at 60-65 pN. This implies that, at the *molecular level*, the immobilized aptamers retained their similar biophysical characteristics and structure, even though they had been attached via different strategies. It was therefore hypothesized that the

different affinity values from QCM experiments are likely caused by the interactions and aptamer accessibility due to the surrounding OEG thiols. The length, the density and the regularity of the OEG thiol coverage depends on the type of thiols and also on the immobilization process. These factors determine the ability of the surface to resist nonspecific adsorption of IgE and affect the accessibility of the aptamer towards its target. The theoretical thickness of monolayers formed by EG_3 and EG_6 thiols are 22.4 Å and 30.8 Å respectively.[150] The co-adsorbent thiol can reduce the nonspecific adhesion between DNA and gold surface, while improving the orientation of aptamer. Compared to the EG_6 thiol, the EG_3 thiol is shorter, allowing most of the stem structure to be exposed resulting in a better binding to the protein target. It has also been demonstrated earlier that OEG thiols have the ability to stabilize and control the orientation of DNA on a surface[224], further increasing the utility of this strategy.

Although the 1:40 molar ratio of aptamer : OEG used to prepare Sensor C is 100 times higher than that used in Sensor B, the total binding was estimated to be 80.9 ng, which is 56 % of that in Sensor B. This implies that the surface coverage of the aptamer immobilized in this one-step modification procedure is dilute compared to Sensor B. The calculated K_A of the aptamers by these two methods are almost similar, although Sensor C shows a slightly higher affinity than Sensor B. This difference is likely due to a better separation of the aptamer on the surface, resulting in easier adaptive binding towards the protein target. Suitable optimization of the molar ratios of the aptamer and OEG can therefore be used to increase both the

binding and affinity of the immobilized aptamer.

Table 4.1. Summary of the AFM and QCM results of anti-IgE aptamer and IgE system by different modification strategy

sensor	modification	Aptamer Conc.	OEG	K_A(nM^{-1})	Rupture force (pN)
A	Two-step	0.25 μM	EG_6	0.058±0.009	64.1±0.9
B	Two-step	0.25 μM	EG_3	0.030±0.002	64.0±2.9
C	One-step	25 μM	EG_3	0.041±0.003	61.7±0.7

4.3.5 Comparison with VEGF Binding to mixed SAMs of thiolated Anti-VEGF DNA aptamer and OEG thiol

Based on these results, the optimal thiol strategy could be adapted from the model system to the system of interest - the angiogenic protein vascular endothelial growth factor (VEGF). Because DNA aptamers against IgE were used as the model system described in the previous section, the experiments focused on DNA aptamers instead of the RNA aptamers as had been studied in Chapter 3. Instead of the anti-VEGF RNA aptamer characterized in Chapter 3, an anti-VEGF DNA aptamer selected against VEGF was used as a comparison to the IgE/IgE DNA aptamer system.[180] In these experiments, the QCM measurements were conducted with the sensor modified with an anti-VEGF DNA aptamer and EG_3 thiol by incubating with 0.25 μM aptamer followed by 1 mM EG_3 (Scheme 2). The rupture force between the aptamer and target (VEGF) was measured on the same surface using a VEGF

functionalized AFM cantilever (Figure 4.8, inset B). From the frequency response of the QCM experiment (Figure 4.8), the K_A= 0.043 nM^{-1}. This value is higher than the K_A of 0.029 nM^{-1} for the IgE aptamer/IgE system by the same modification. The K_A is close to the reported value of the affinity constant (0.092 nM^{-1}) obtained earlier for the DNA aptamer using SPR.[180]

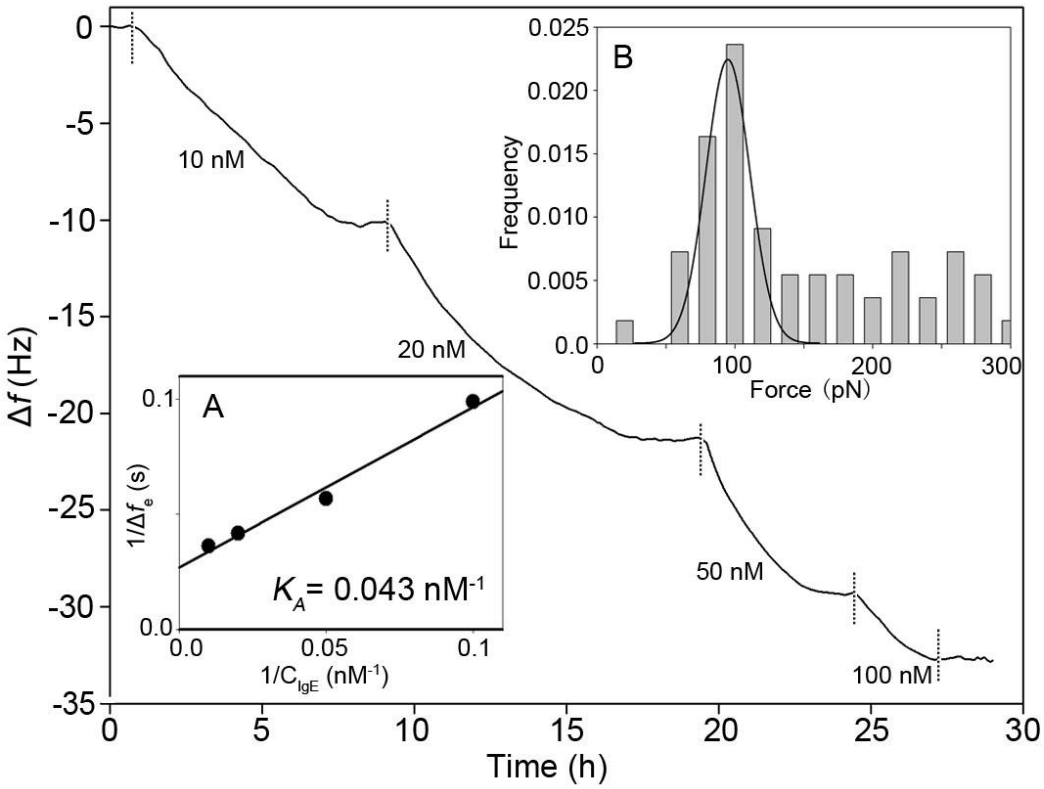

Figure 4.8. QCM frequency response of sensor to varying concentrations of VEGF. Inset A - K_A estimated from $1/\Delta f_e$ as a function of $1/C_{IgE}$; Inset B - AFM rupture force distribution of VEGF and anti-VEGF aptamer on Sensor B for IgE/anti-IgE system.

As measured earlier, the unbinding/rupture force for an antigen/antibody pair can be determined from the free enthalpy ΔH and the effective range of the potential

d, given by $F = \Delta H/d$. For a K_A between 10^2 and 10^{10} M^{-1}, the rupture force is therefore estimated to be between 35 and 165 pN.[226] In these experiments, the K_A ~ 3 x 10^7 M^{-1}, and rupture force ~65 pN for the IgE system and 4 x 10^7 M^{-1}, and rupture force ~95 pN for the VEGF system, showing that the aptamer/protein pairs behave in a similar and consistent fashion. This was consistent to that observed earlier by force spectroscopy of the IgE aptamer/IgE.[49]

It is interesting to note that the higher affinity of the VEGF pair is also accompanied by a much larger rupture force for this system, compared with the values analyzed from the IgE system under identical experimental conditions. As mentioned above, bridging the gap between the two scales (ensemble and single-molecule scales) is the challenge to correlate the information obtained from these two scales. The rupture force analysis from the force spectroscopy describes the dissociation process under an external force, where it is far from equilibrium kinetics. On the other hand, the binding affinity is an averaging property describes the reactions that proceed at equilibrium.

Evans and Ritchie had established a model based on the binding of biotin and streptavidin, which described the thermodynamic process of unbinding kinetics at single molecule level by calculating the free energy of the reaction from the applied external force. Based on this model, the dissociation rate can be extracted from single molecule force measurements.[102] Both the affinity (ensemble level) and rupture force (molecular level) describes how strong the binding between the biomolecular pair. However, there have been no direct correlations established

between the affinity property and the rupture force. Although, extensive experiments are required to draw firm conclusions, based on a survey of the literature, this is the first study showing the possible correlation to bridge the gap between the two scales.

4.3.6 Effect of Mg^{2+} on the binding at ensemble scale using QCM

As one of the central themes of this dissertation, the information provided from the single molecule level is of great importance in trying to understand (and eventually engineer) the fundamental biophysical properties of the binding biomolecular pairs. As has been investigated in the previous chapter, divalent cations such as Mg^{2+} play a vital role as structural stabilizers for functional nucleic acid aptamers. With higher concentrations of Mg^{2+}, aptamers are more rigid, which require higher rupture force to separate the aptamer-protein pair. The question therefore is whether this information can be used to tune the ensemble level interactions of the aptamer and protein as measured using QCM.

Here, the effect of Mg^{2+} on the anti-VEGF RNA and VEGF pair was evaluated, and the affinity and kinetics analysis were carried out. It has been reported that RNA ligands to VEGF exhibit biphasic binding to the protein and the RNA is hypothesized to be partitioned between two components.[227] Based on this model, the equilibrium dissociation constant K_D of these two conformers of the anti-VEGF RNA aptamer were reported as 0.42 ± 0.04 nM (conformer 1) and 182 ± 94 nM (conformer 2), with a molar fraction of conformer 1 as 0.76.[187] Since conformer 1 shows over 400 times higher affinity toward VEGF than conformer 2, and is the

majority of the two-conformer mixture, an approximation, assuming only one component exists instead of two, was made to simplify the kinetic analysis.

The binding reaction between anti-VEGF RNA aptamer and VEGF protein was described in a manner of ligand and receptor binding in this study. Typically, in biomolecular interactions in solution, ligands and receptors reversibly form ligand–receptor complexes. In the QCM measurements, aptamers were immobilized on the sensor surface, and the percentage of ligands bound to receptors present on the surface (θ_t) is a function of time of the ligand solution injection as shown in Equation (9): [228-230]

$$\theta_t = \theta_e(1 - e^{-1(1/\tau)t}) \tag{9}$$

where τ is a relaxation time and θ_e is an equilibrium percentage of bound ligands at the certain ligands concentration. The relaxation time (τ) is related to the ligand concentration injected, which is described by Equation (10):

$$\tau^{-1} = k_{+1}[ligand] + k_{-1} \tag{10}$$

where k_{+1} and k_{-1} represent the association rate constant and the dissociation rate constant, respectively. The mass gain of the sensor during the QCM experiment is proportionally related to the percentage of bound ligands. As a result, the mass gain at a given time (m_t) and the mass gain at equilibrium (m_e) can be described as in Equation (11):

$$\Delta m_t = \Delta m_e(1 - e^{-(1/\tau)t}) \tag{11}$$

As previously introduced, the mass change of the quartz crystal sensor is reflected by the frequency shift (Δf), thus:

$$\frac{\Delta f_t}{\Delta f_e} = (1 - e^{-(1/\tau)t}) \tag{12}$$

where Δf_t and Δf_e represent the frequency change of crystal sensor at a given time t and after it reaches equilibrium, respectively.

QCM measurements were carried out under different Mg^{2+} concentrations in a similar manner to the previously described experiments, using the optimal sensor fabrication strategy investigated above (two-step modification, back filling with EG_3). The curves showed in Figure 4.9 are the normalized frequency response ($\Delta f_t/\Delta f_e$) to 5 nM VEGF recorded as a function of time at different Mg^{2+} concentrations, ranging from 0 to 10 mM. By fitting Equation (12) to these data, a relaxation time (τ) could be obtained for each condition.

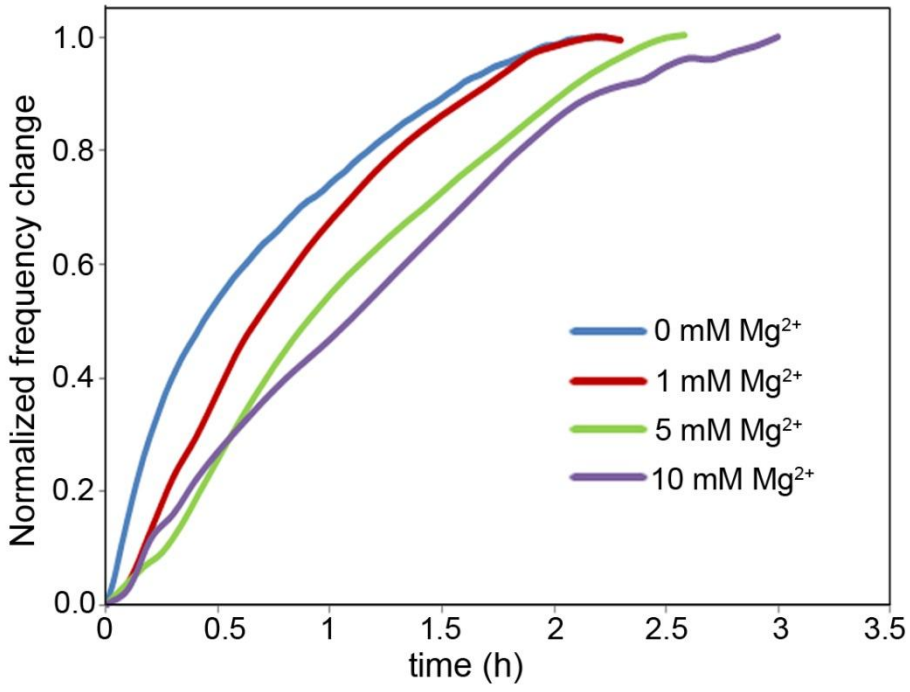

Figure 4.9. Normalized frequency response ($\Delta f_t/\Delta f_e$) as a function of time with different Mg^{2+} in presence. These normalized curves were used to fit Equation (12).

The total frequency responses to different VEGF concentration after the reaction reached equilibrium (Δf_e) are summarized in Table 4.2. Based on Equation (9), the equilibrium constant K_A was analyzed in the presence of different concentrations of Mg^{2+}. Furthermore, the association and dissociation rate constant k_{+1} and k_{-1} were obtained by Equations (7) and (10). Figure 4.10 shows the impact of the Mg^{2+} on the K_A and k_{-1} analyzed from QCM measurements. It can be concluded that in the presence of higher Mg^{2+} concentrations, the affinity between anti-VEGF RNA aptamer and VEGF protein increased more than 3 times, from 0.029 nM^{-1} at 0 mM Mg^{2+} to 0.105 nM^{-1} at 10 mM Mg^{2+}. However, the dissociation rate decreased from 3.18×10^{-4} s^{-1} to 1.50×10^{-4} s^{-1}.

Table 4.2. The equilibrium frequency response (Δf_e) of anti-VEGF RNA aptamer functionalized sensor corresponding to different VEGF concentration under different Mg^{2+} concentration

Mg Conc. (mM)	Δf_e			$K_A(nM^{-1})$
	5 nM VEGF	10 nM VEGF	20 nM VEGF	
0	3.47	4.69	9.36	0.030
1	2.17	9.24	14.53	0.016
5	3.33	7.99	NA	0.028
10	4.00	5.92	7.92	0.105

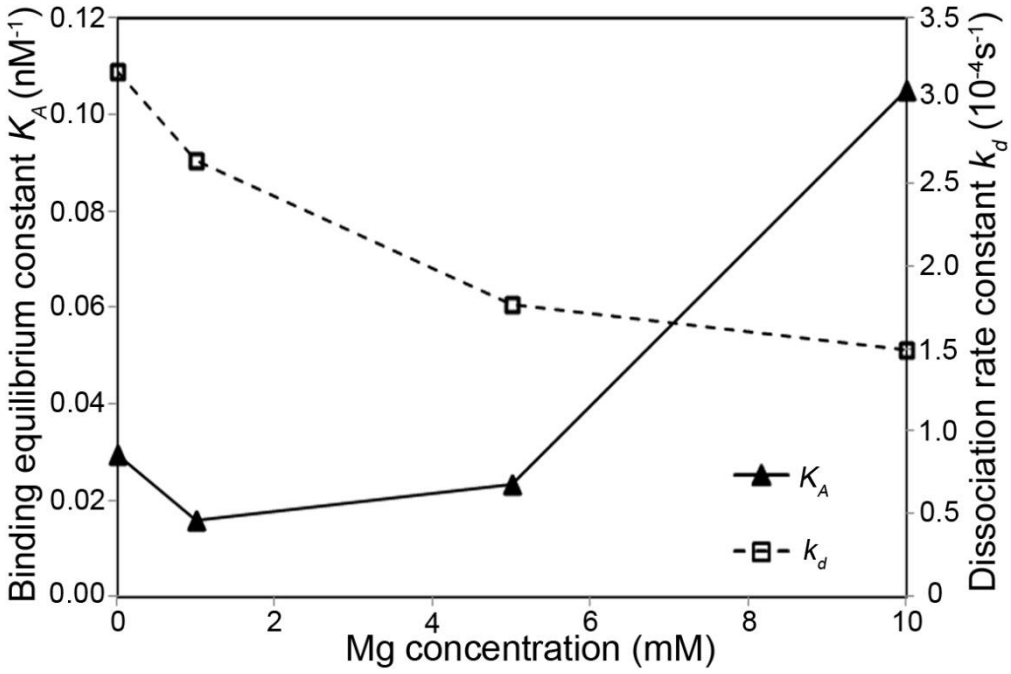

Figure 4.10. Analysis based on QCM measurements showing the effect of Mg^{2+} on the affinity and kinetics of the binding between anti-VEGF RNA aptamer and VEGF protein using QCM

The effect of the Mg^{2+}, which acts as structural stabilizer of aptamer was investigated at the molecular level in Chapter 3. It was concluded the rigidity of the aptamer conformation significantly affects the binding at this level. The work shown in this chapter, indicated the effect of Mg^{2+} on the aptamer/protein binding is also manifested at ensemble level. Specifically, with higher Mg^{2+} in presence, the binding between this aptamer and target protein is stronger, which is reflected as a higher rupture force and a higher affinity (larger K_A). Furthermore, the kinetic property of this reaction was also influenced by this conformational factor, manifested as a slower dissociation rate (smaller k_{-1}). In previous chapter, it was hypothesized that with a more rigid structure, aptamers are less likely to adaptively adjust their

structure in response to the target. This hypothesis can also explain the fact that it took a longer time to reach equilibrium in presence of higher concentration of Mg^{2+} (Figure 4.9). These results demonstrate how the biophysical properties obtained from single-molecule experiments can be translated to ensemble level, and can be used to guide the ensemble level sensing techniques.

4.4 Conclusion

Different modification strategies for immobilizing thiol-modified aptamers directly on gold surfaces were studied using QCM and AFM force spectroscopy. Mixed SAMs with aptamer and OEG thiols as co-adsorbents improved the sensing performance of the sensors by imparting a resistance to nonspecific protein adsorption. Using the optimal modification strategy from these experiments, the sensors showed a high sensitivity and dynamic range. While the EG_6 thiol has better resistance to nonspecific protein adsorption compared to the EG_3 thiol, the longer length of the alkyl chain results in a reduced accessibility of the aptamer. In the different systems, similar rupture forces were required to unbind aptamer and protein and the relationship between the force and the affinity constant were consistent with energy calculations shown for antigen-antibody binding. These simple and versatile strategies can be used in aptamer platforms for ultrasensitive analyte detection with minimal non-specific binding.

Furthermore, based on the fabrication strategy established above, the experimental results of aptamer/protein systems obtained from single-molecule level

and ensemble level were correlated. The system required higher rupture force but also showed a correspondingly higher affinity. The environment-induced (Mg^{2+}) conformational property of the aptamer obtained from single molecule level analysis significantly affected the binding behavior at the ensemble level, manifested in different affinities and binding kinetics. These results can help to bridge the gap between the two sensing scales, and further enable the design of aptamer-based biosensors and biodiagnostic devices.

[This chapter contains results that have been previously published in the paper "Surface immobilization of DNA aptamers for biosensing and protein interaction analysis" in Biosensors and Bioelectronics, 2011]

CHAPTER 5

APTAMER-TAGGED FUNCTIONAL DNA NANOSTRUCTURES FOR MOLECULAR RECOGNITION

5.1 Introduction

In the previous chapters the biomolecular recognition function of aptamers were investigated at multiple length scales using different model systems and different techniques. These studies uncovered unique properties of aptamers including their flexible adaptive binding and specificity. All these experiments were conducted in systems where the aptamer was tethered to a surface by means of a linker at one end. However, a fundamental question that could be asked is on how it may be possible to further adapt these unique reagents to advanced high-throughput applications that may not require any surface attachment and still can take advantage of their unique properties. One approach is to organize aptamers into programmable nanoconstructs. The chemical nature of aptamers as nucleic acids, allows us to take

advantage of their intrinsic programmability, and various reported DNA/RNA structural motifs to fabricate aptamer functionalized nanostructures. In this chapter, different aptamer-functionalized DNA nanostructures are reported. The fabrication and the functionality of these aptamer functionalized nanostructures are discussed. These can further facilitate the development of molecular nanosensors, nanoscale catalysts for reactions, or delivery systems.

As been introduced in Chapter 1, DNA is an attractive natural material for fabricating diverse nanoshapes and nanostructures because of unique and precise hybridization.[231, 232] Pioneering works on DNA nano-architectures have resulted in strategies such as complementary end cohesion and branched junctions to fabricate precise geometries, periodic lattices, and nanoscale shapes and patterns in all three dimensions.[134] Structural motifs such as hairpins, junctions and loops function as modular units that can be assembled and modeled to construct well-defined and designed architectures from a vast set of synthesized or modified sequences.[125, 233] Over the past few years, a number of works have demonstrated a variety of geometric shapes including DNA cubes, knots and supramolecular polyhedra.[234] These shapes have been proposed for applications ranging from enabling spatially periodic networks and nanoarrays and as molecular cages for drug delivery to DNA-based computation. [235]

Typically, engineered DNA and RNA designs have been either tile-based designs assembled from chemically synthesized oligonucleotides, [125, 129] or origami designs that employ a scaffold strand and synthetic staple strands.[134, 135]

The former utilize networked architectures to fabricate contiguous lattices and self-assembled protein arrays.[125, 128, 129, 236] The latter, referred to as "DNA origami", fold long, single-stranded DNA into 2 and 3D shapes.[134, 237] Some challenges in translating these DNA and RNA nanoarchitectures to applications lie in developing facile synthesis strategies and enabling function in addition to unique geometry. One route is to take advantage of the programmable construction and ease of modification in nanodesign using nucleic acids, which allow attachment or synthesis of motifs and groups to predefined nanostructures to add functionality.

DNA nanoarrays with attached aptamers have been demonstrated to organize proteins and form addressable architectures.[236, 238] While arrays and lattices of varying complexity have wide applications in protein positioning including aptamer-directed assembly or as 'nanobreadboards',[134] they are limited to applications *in situ* on controlled substrates. The assemblies are primarily treated as scaffolds and functionality is restricted to the site of formation with limited portability, as separation from the continuous scaffold may result in a loss in biological function. Fabricating portable architectures that can be used away from the production site could potentially address this challenge. Along these lines, hexagonal self-assembling RNA nanorings based on RNAI/Iii kissing complexes were described with potential as delivery vehicles for siRNA.[239] DNA polyhedra with chemical modification of the backbone with phosphorothiolate and with short hairpin 'spikes' on their exterior surfaces to act as docking sites for guest objects have been reported.[240, 241] DNA origami designs, that tend to be computationally

intensive are only recently being used as functional devices.[242] Another challenge involves the fabrication of biologically functional architectures. While a number of structures have been visualized in air, it is additionally necessary to ensure that they are capable of performance in an aqueous environment. Herein, in this work, a strategy that moves away from linking together tiles to larger supramolecular assemblies and instead exploits the individual units themselves as unique shaped-defined functional nanoarchitectures in aqueous environments.

In this chapter, utilizing the recognition function of aptamer, a strategy to construct large numbers of precisely formed, discrete 2D DNA shapes for molecular recognition is reported. The DNA was used both for construction of nanoshapes and as the recognition agent via DNA aptamers. It was demonstrated the coupling of two different aptamers to predefined DNA nanostructures in the shapes of an ′X′ and ′Y′. Each shape is engineered to contain a core, assembled from single strands of designed sequences, with receptor-binding aptamers arms (Figure 5.1). These functional and stable nanostructures are easily fabricated, are stable in aqueous environments. They can be produced in large numbers to a variety of different shapes, and can be used to recognize specific protein targets. Multiple shapes with different targets can be mixed together enabling multiplexing on the same platform. This strategy can therefore be adapted to form a variety of different DNA shapes as functional nanoparticles for applications including biosensing and therapeutic delivery.

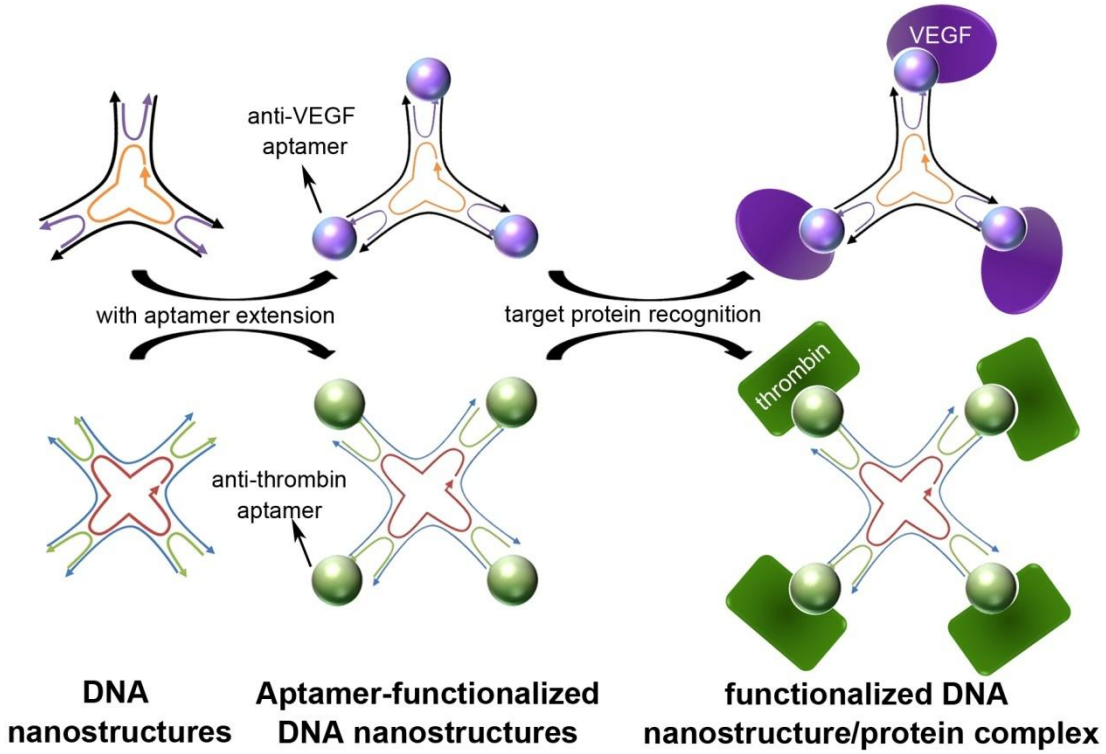

Figure 5.1. Schematic of the aptamer-functionalized DNA nanostructure, and the DNA/protein complex

5.2 Experimental section

5.2.1 Materials

DNA strands for assembly and aptamer were custom synthesized by Integrated DNA Technologies, Inc. (Coralville, IA). Vascular endothelial growth factor (VEGF) and thrombin were purchased from Biovision, Inc. (Mountain View, CA) and Abcam, Inc. (Cambridge, MA). Tris/acetic acid/EDTA buffer, Tris/boric acid/EDTA buffer, PBS buffer, Tris-HCl (pH 7.4), and $Mg(AcO)_2$ and Ethanol (200-proof) were purchased from Fisher Scientific. DEPC treated RNase free water was used for all experiments.

5.2.2 DNA structural and sequence design

Sequence design of the 3-point and 4-point DNA nanostructure core (without aptamer) was adapted from a previous design reported by Sun et al.[243] Sequences were modified to ensure that two different structures do not hybridize or connect. The secondary structure of DNA complex was verified using the software NUPACK (Nucleic Acid Package).[244] Each DNA nanostructure was assembled from three different strands, including one center strand (C3 or C4) and a pair of side strands (S1/S2 pair or S1b/S2b pair) as shown in Figure 5.2 A, E. Functionalized DNA nanostructures with aptamers were assembled using side strands with the extension of DNA aptamer sequences and 2Ts as a linker at the 3′-end. For example, S2Va contains the S2 strand sequence and the extension of anti-VEGF aptamer at 3′-end; S2bTa comprise the S2b strand sequence and anti-thrombin aptamer sequences [245], respectively (Figure 5.2 A, E).

Table 5.1. Sequences used to construct the 3-point and 4-point star DNA nanostructures used in this study. The letters C and S are used to represent the center and side strand, respectively. Aptamers are coupled to the side strands by means of a TT linker (green). Red letters denote the sequences of the aptamers used in this study (DNA aptamer to VEGF (Va) and DNA aptamer to thrombin (Ta))

	Strand	Sequence
3-point star	C3	5′-AGG CAC CAT CGT AGG TTT TCT TGC CAG GCA CCA TCG TAG GTT TTC TTG CCA GGC ACC ATC GTA GGT TTT CTT GCC-3′
	S1	5′-ACT ATG CAA CCT GCC TGG CAA GCC TAC GAT GGA CAC GGT AAC G-3′
	S2	5′-CGT TAC CGT GTG GTT GCA TAG T-3′
	S2Va	5′-CGT TAC CGT GTG GTT GCA TAG TTT **CCG TCT TCC AGA CAA GAG TGC AGG G**-3′
	S2Ta	5′-CGT TAC CGT GTG GTT GCA TAG T **TTA GTC CGT GGT AGG GCA GGT TGG GGT GAC T**-3′
4-point star	C4	5′-AGG CAC CAT CGT AGG TTT TCT TGC CAG GCA CCA TCG TAG GTT TTC TTG CCA GGC ACC ATC GTA GGT TTT CTT GCC AGG CAC CAT CGT AGG TTT TCT TGC C-3′
	S1b	5′-GAC TGA GCC CTG CCT GGC AAG CCT ACG ATG GAC TAC TCA TCC-3′
	S2b	5′-GGA TGA GTA GTG GGC TCA GTC-3′
	S2bTa	5′-GGA TGA GTA GTG GGC TCA GTC **TTA GTC CGT GGT AGG GCA GGT TGG GGT GAC T**-3′

Table 5.2. Sequences used to construct the "square", "triangle" and "diamond" DNA nanostructure used in this study, which is adapted from the design reported by Jaeger et al. [132] Letters in blue are the sticky end used for aptamer attachment. Anti-IgE aptamer (Ia) sequence (letter in red) is extended with sticky end 1' (complimentary to sticky 1, letters in blue)

	strand	Sequence
square	A + stick end 1	5′-GGGAAAGCCTGGATGAAGTGGACACGTCCAGGCAAG TCTCGTAGAAGGAGGCACTACGAGGCAA**GCATCC**-3′
	B	5′-GGGAAAGCCTGGATGAAGTCCACACGTCCAGGCAAG TCTCGTAGAAGCCTGCACTACGAGGCACT-3′
	C + stick end 1	5′-GGGAAAGCCTGGATGAAGCGAGCACGTCCAGGCAAG TCTCGTAGAAGCAGGCACTACGAGGCAA**GCATCC**-3′
	D	5′GGGAAAGCCTGGATGAAGCTCGCACGTCCAGGCAAGT CTCGTAGAAGCCTCCACTACGAGGCACT-3′
	Ia + 1'	5′-**GGATGC GGG GCA CGT TTATCC GTC CCT CCT AGT GGC GTG CCC C**-3′
triangle	A + stick end 1	5′-GGGCTAACGCAGACCGATGAAGTGGACACGTCGGTCT GCGGACAGCCGTGCATTGAAGCAGGCACGATGCACGGC TGCCC**GCATCC** -3′
	B	5′-CGGACATGGTGAAGTCCACACGCCATGTCCGCGAACG TGAAGCCTGCACGCGTTCG-3′
diamond	A + stick end 1	5′-GGGCTAACGCAGACCGATGAAGGAGGCACGTCGGTC TGCGGACAGCCGTGCATTGAAGCCTCCACGATGCACGG CTGCCC**GCATCC**-3′

5.2.3 DNA self-assembly formation

DNA assembly formation was performed using different protocols described earlier.[132, 139] The assembling protocol was further optimized. 10 μM center strand and two side strands were mixed in a DNA assembling buffer (40 mM Tris base, pH 8.0, 40 mM acetic acid, 1 mM EDTA, and 15 mM $Mg(Ac)_2$) in a molar ratio of 1:3:3 or 1:4:4 for the 3-point star or 4-point star assembly, respectively. In the case of square DNA assembly, an equal amount of the DNA strands were mixed in Tris-borate pH 8.2 (TB) with 0.2 mM $Mg(OAc)_2$, 15 mM KCl buffer. The mixture was heated at 95 ℃ for 5 minutes, and then slowly cooled down to 20 ℃ in 48 hours to allow self-assembly of the DNA sequences.

5.2.4 Native polyacrylamide gel electrophoresis (PAGE)

Non-denaturing 10 % polyacrylamide gels containing TBE buffer were typically pre-run in running buffer (TBE buffer + 2 mM $Mg(OAc)_2$) for 30 minutes, and then run at 90V or 2 hrs 2 mM after the sample were loaded. After electrophoresis, the gels were stained with SYBR green and exposure to UV light for documentation.

5.2.5 Electrophoretic mobility shift assay (EMSA)

EMSA analysis was carried out monitor the formation of the DNA/protein complexes. In principle, due to the larger size of the complex compared with free DNA, the band of the complex should migrate much slower than that of free DNA. Various concentrations of protein were mixed with 4 μL, 0.1 μM DNA assembly in

Tris/HCl, pH 8.0 buffer, and incubated for 20 min at 20^{o}C. Samples were loaded onto 4-20% gradient or 10% native PAGE in TBE buffer. The gels were run at 120 V for 90 min. After electrophoresis, the DNA was stained with SYBR green stain for 20 min.

5.2.6 Atomic force microscopy imaging

Aminopropyl-mica (AP-mica) with a net positive surface charge was used to immobilize negatively charged DNA assembly. Freshly cleaved mica was incubated in the vapor of 3-aminopropyltriethoxysilane (APTES) in a vacuumed desiccator for 2 hours.[246] 10 μl of solution containing 3 nM DNA assemblies in assembling buffer was deposited onto AP-mica for two minutes right after the AP-modification procedure, and then rinsed with assembly buffer. The DNA assembly/protein complexes were prepared as described in the EMSA experiment, and diluted 20 times before deposition. Imaging was performed under a liquid environment in non-contact mode by an Asylum MFP-3D atomic force microscope (AFM, Asylum Research, Santa Barbara, CA). Super sharp CSG cantilevers from NT-MDT (Moscow, Russia) and SNL cantilevers from Bruker (Camarillo, CA) were used for AFM imaging with nominal radii of curvature ~ 5 nm were used for imaging these small features at a high resolution.

5.3 Results and discussion

5.3.1 3-point and 4-point star DNA nanostructures design and assembly

Periodic DNA nanoarrays with attached aptamers have been shown to direct protein organization and form addressable architectures.[236, 238] However, the structural rigidity and charge of the DNA arrays can influence aptamer function.[236] These connected or contiguous DNA architectures often involve complex fabrication strategies or must be formed at the application site. One approach that moves away from this paradigm is to form discrete, portable DNA shapes in 2 or 3 dimensions. Individual, square-shaped RNA structural motifs were reported in elegant works, but were used in turn as tiles to form larger assemblies.[132, 247] DNA origami can form discrete shapes but these often require complex assembly strategies. Aptamer conjugated DNA icosahedra were recently reported as nanocarriers for the anticancer drug doxorubicin.[248] The hierarchical self-assembly of DNA into supramolecular polyhedra was reported as a one-pot synthesis via the control of flexibility and concentration of basic DNA tiles.[234] However, to the best of my knowledge, functional discrete nanostructures have not been reported. Here nanostructures that exhibit high stability and distinguishing conformations are reported, with programmable and functional modification that allows them to recognize and bind specific protein targets. Utilizing single-step assembly, we outline unconnected DNA nanostructures as a facile and versatile method to attach a variety of molecular recognition agents to basic core ‘shapes’. These can utilize the unique binding capabilities of aptamers while rendering new applications in targeted recognition.

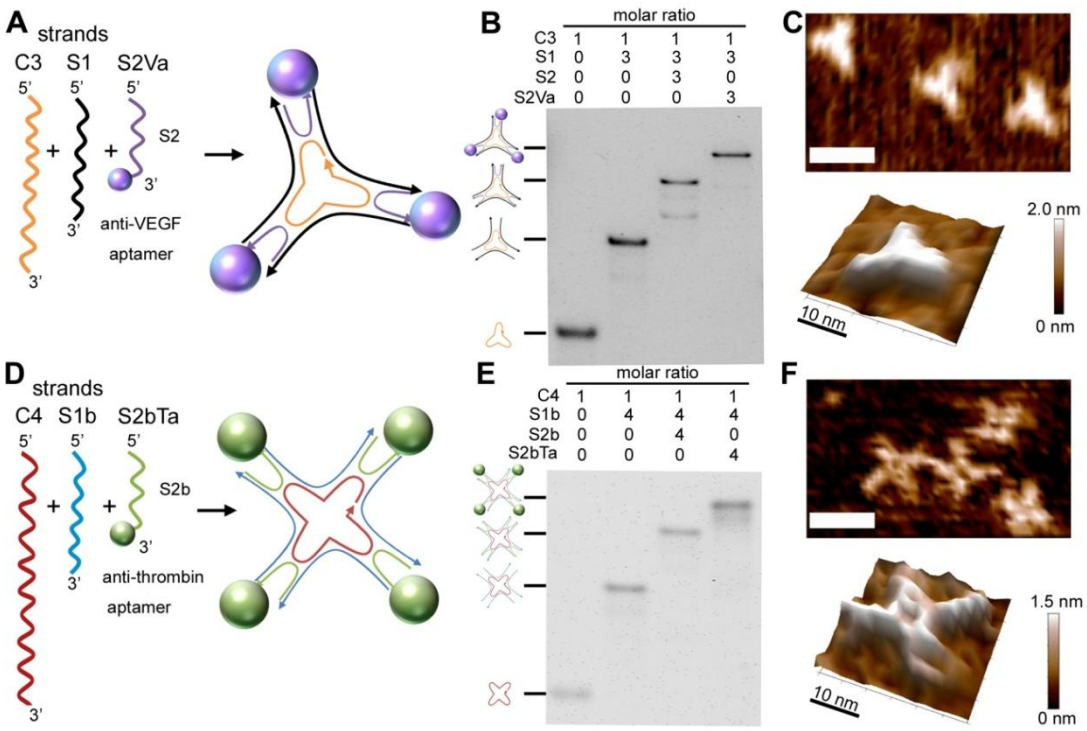

Figure 5.2. DNA assembly schematics and characterization. Aptamers are represented by the colored spheres. (A) 3-PSVa assembly. (B) Native PAGE analysis for 3-PSVa. DNA strands and the molar ratio are indicated above the gel. (C) AFM images for the 3-PSVa in solution (Scale bar = 25 nm); 3D image of single 3-PSVa. (D) 4-PSTa assembly. (E) Native PAGE analysis of 4-PSTa. DNA strands and the molar ratio are indicated above the gel. (F) AFM images for the 4-PSTa in solution (Scale bar = 25 nm); 3D image of single 4-PSTa.

To demonstrate this, we show the formation of two basic shapes ("X" – 4 point star (4-PS) and a "Y" – 3 point star (3-PS)) functionalized with two different aptamers. The target proteins in this study are thrombin and vascular endothelial growth factor (VEGF). Design sequences for the DNA nanostructures reported in this work – assembly to a 3-point star (3-PS) and 4-point star (4-PS) (Figure 5.2)

were modified and adapted from previously reported core sequences. [128, 249] Similar sequences have been well characterized and utilized as DNA tiles that can assemble into hierarchical nanoarrays [128, 139, 249] or polyhedra.[234] In a one step process, 3-PS and 4-PS DNA nanostructures were annealed from one center strand and two side strands, in the ratio of 1:3:3 or 1:4:4 respectively (Figure 5.2A, D). To form unconnected DNA shapes, the so-called "sticky ends" in each side strand were deleted. This prevents the assembly or connection of individual tiles into an array and provides greater flexibility in designing different shapes.

Another design modification is introduction of functionality via the attachment of different molecular recognition aptamers to the core shape. There are two possible approaches to modify such architectures with aptamers – post-modification after the construction of the DNA assembly and pre-modification, where the aptamer sequences are attached to the outsides of the DNA architectures.[248] The strategy used in this work follows the latter, achieved by encoding the aptamer sequence with 2Ts as linkers at the 3′ end of the side 2 strand. Thus each DNA nanostructure is created with pendant ligand-binding aptamers. It is necessary to ensure that the modification of the aptamer sequence does not interfere with the folding of the aptamer. The secondary structure of this side 2 strand with the aptamer sequence extension as well as the hybridization between this strand with center strand and side strand 1 is predicted by NUPACK. The extended aptamer can maintain its free state by not hybridizing with the core assembly. It is important to note that due to the large section of complimentary sequences between the strands, this basic core DNA

nanostructure is a robust design, which facilitates the flexibility of applying these designs to the aptamer systems.

Post-assembly, the DNA nanostructures were monitored by native polyacrylamide gel electrophoresis analysis (Figure 5.2 B, E). The lanes loaded with assemblies without aptamer functionalization are in good agreement with previous reports. [235, 249] The last lanes of both of the gels are the assemblies with aptamer functionalization, which are 3-PS extended with anti-VEGF aptamer, (hereby referred to as 3-PSVa) and 4-PS extended with anti-thrombin aptamer (4-PSTa). These migrate slower than those without aptamer extension, suggesting the success of the aptamer modification of the DNA nanostructures.

5.3.2 AFM characterization of the 3-point and 4-point Star DNA Nanostructures

Due to the small size of the DNA nanostructures (typically less than 20 nm, with branches less than 5 nm), the visualization of their detailed features is extremely challenging. Given the typical radius of the AFM tip between 10 to 20 nm, the resolution provided by these tips is definitely too low to visualize the exact structure of these DNA nanostructures (Figure 5.3 A). As a result, instead of the well defined branched structures, diffuse dot-shaped features were observed from the image (Figure 5.3 C).

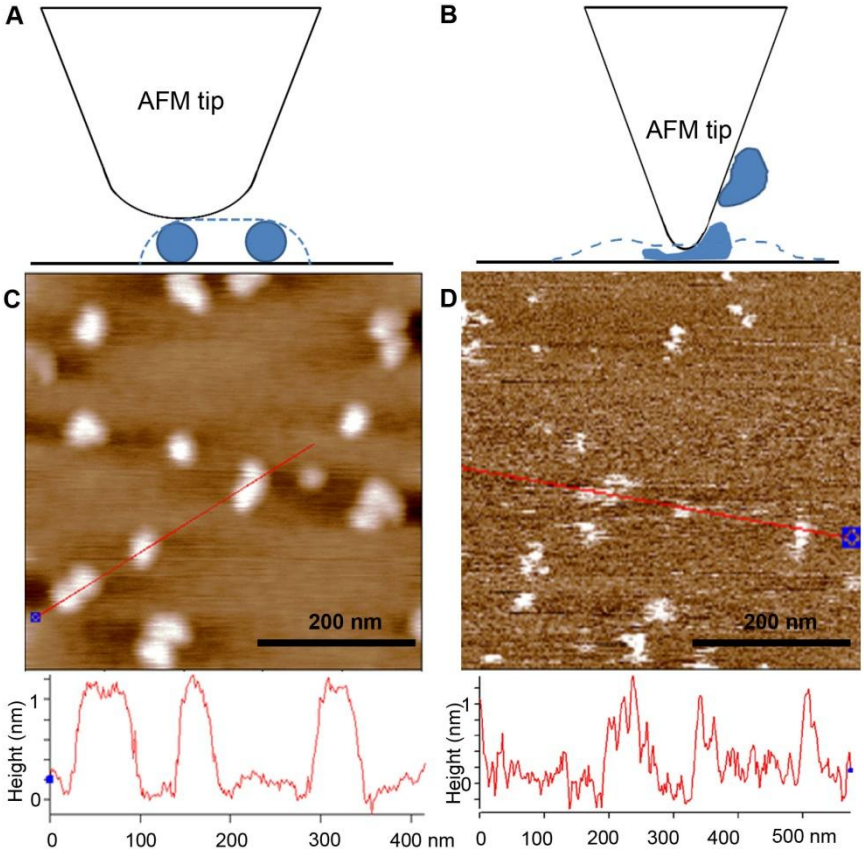

Figure.5.3. The effect of the AFM tip deconvolution and the stiffness on the AFM imaging. The schematic (A) and an example of AFM image (C) AFM tip with a typical radius of curvature greater than 10 nm cannot provide a high resolution image capable of distinguishing two features close together. The schematic (B) and AFM image (D) represent the possibility of damaging the sample during the imaging due to too much force applied by a sharp AFM tip.

Besides the sharpness of the tip, another critical parameter is the stiffness of the cantilever. With a stiff AFM tip, during the image, higher force is applied to the sample, which might result in either "sweeping away" the samples from the surface, or damaging the sample (Figure 5.3 B and D). This problem is more critical in

biological samples such as proteins and DNA, especially when the imaging is carried out in solution, where the biomolecules exist in their soft and native state. Based on these considerations, soft cantilevers (spring constant <0.5 nN/nm) with a smaller radius (<5 nm) were chosen to image these nanostructures in buffer condition. However, although softer cantilevers were used to minimize the force of the tip against the sample, the pressure applied by a sharp AFM tip could still be much higher due to the smaller contact area between surface and the tip. Extensive experiments were therefore carried out to optimize the imaging condition. With the suitable imaging parameters, a high resolution visualization of the DNA nanostructure can be obtained.

Another problem observed frequently during the AFM imaging of these nanostructures was the formation of unexpected networks, such as the example shown in Figure 5.4. As discussed above, the goal of this research was to form unconnected nanostructures by the removal of the "sticky ends" that allow different strands to link together. The mechanism for the formation of networks is not clear. Since no network assembly was formed in the solution indicated by native PAGE assay, it is likely that the surface could affect the assembly and cause a hierarchical network structure. It was previously reported that the surface-mediated self assembly can fundamentally change the assembling behavior of the DNA molecules.[243] The transient inter DNA nanostructure interactions can be stabilized by DNA/solid surface interaction. These stabilized transient tile assemblies could act as nuclei to

initiate further DNA assembling on the surface, resulting in the large 2D arrays observed on the surfaces. With a higher yield of the formation by optimizing the DNA assembling process, along with a strong positively charged surface (AP mica), it was possible to eliminate this network assembly formation on the surface.

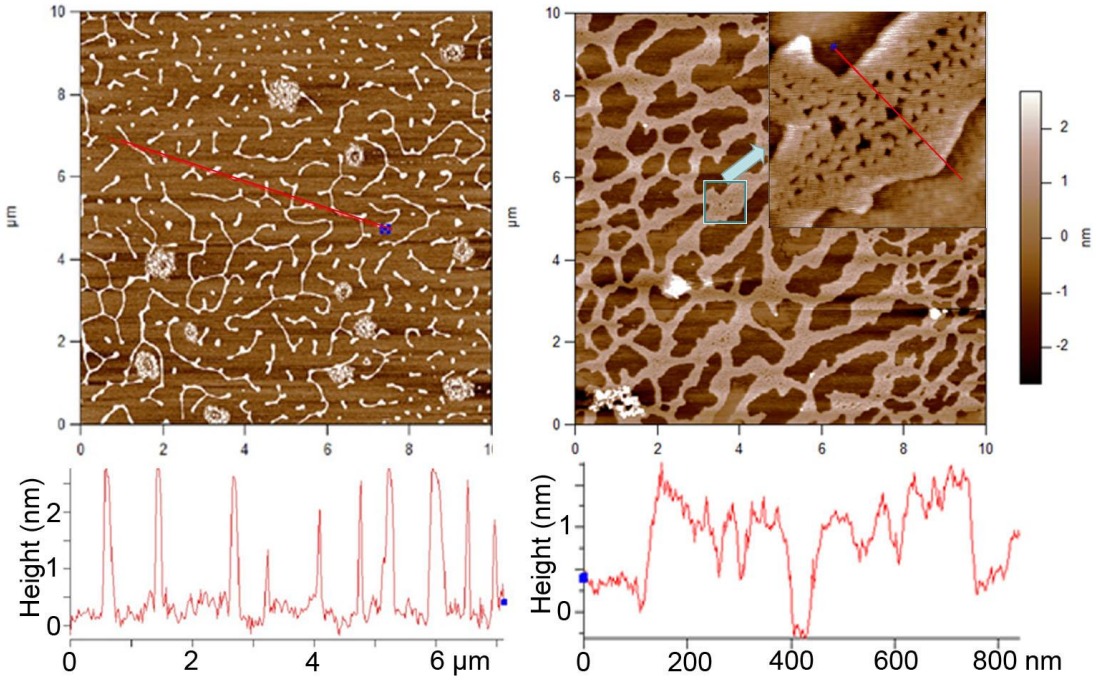

Figure 5.4. Examples of network structures formed on the surface based on the branched discrete DNA nanostructures assembled in solution. The inset in the right image shows the large scale network features consist of small branched structures.

The AFM characterization for all assemblies and protein conjugations were conducted in buffer condition, where the aptamer ligands retain a biologically favorable state. This is an advance from earlier reported works which primarily imaged nanostructures that were dried on mica surfaces. AFM images confirmed the formation of well defined and discrete DNA nanostructures (Figure 5.2 C, F). The height of the features is ~1.5 nm (Figure 5.5). The end-to-end arm length of DNA

nanostructures was analyzed to estimate their sizes (Figure 5.6 A, B, D, and E). Statistical analysis of the AFM images reveals that the end-to-end arm length of the 3-PS and 3-PSVa DNA nanostructures show a narrow distribution, with peaks at 18 nm and 24 nm, respectively (Figure 5.6 C). This result for 3-PS DNA is consistent with the calculated value of 13.0 nm (7.5 nm for each arm assuming 0.34 nm per base pair), also considering the finite size of the AFM tip (radius of curvature < 5 nm). Because of the aptamer extension at each end of arm of 3-PSVa, the end-to-end arm length of the aptamer functionalized DNA nanostructures is 6 nm longer than 3-PS, consistent with the expected hydrodynamic radii of the aptamers (typically around 2-3 nm).[250] Similarly, 4-PS nanostructures were analyzed to be 20 nm, consistent with the theoretical value of 18.2 nm (7.1 nm for each arm and 2 nm for the diameter of each helix). The assemblies with attached anti-thrombin aptamer are larger, with a measured end-to-end length of 4-PSTa of 26 nm (Figure 5.6 F).

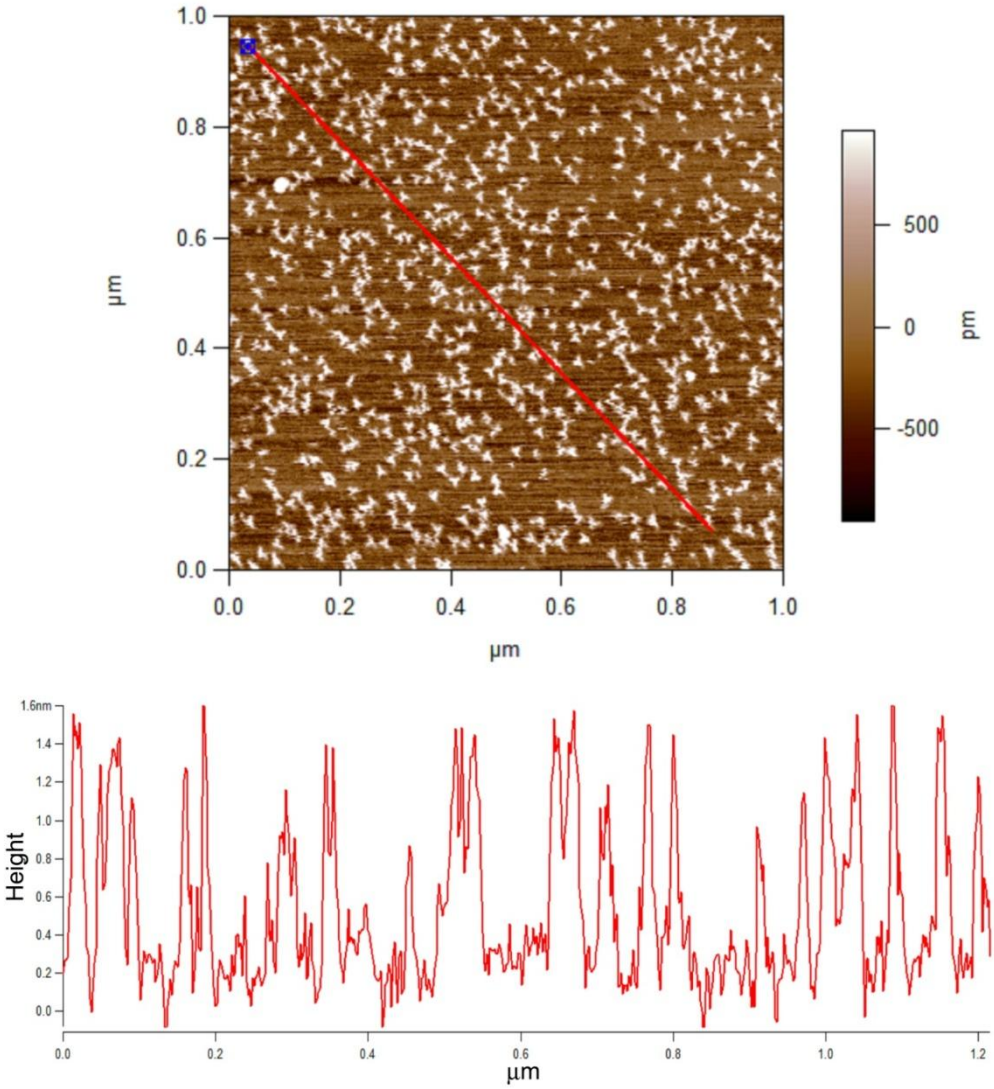

Figure 5.5. Height analysis of an AFM scan of the 3-PS assembly as an example. As expected from the design of the nanostructures, the heights are uniform and consistent at ~ 1.5 nm.

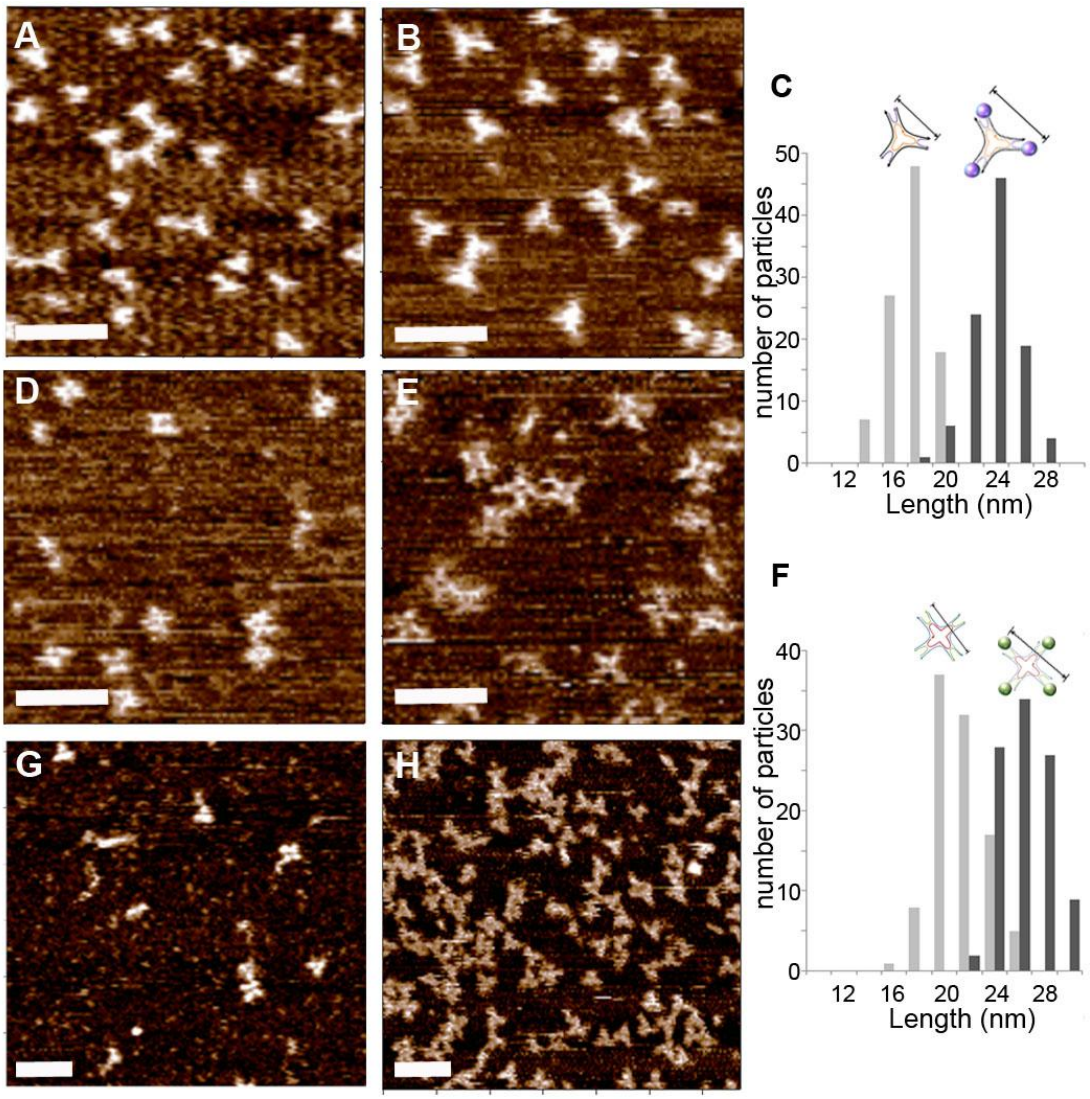

Figure 5.6. AFM image of discrete DNA nanostructures and the size characterization. (A, B) AFM image of 3-PS and 3-PSVa DNA. (C) End-to-end arm length of 3-PS and 3-PSVa. *(n = 100)* (D, E) AFM image of 4-PS and 4-PSTa. (F) End-to-end arm length of 3-PS and 3-PSVa. *(n = 100)* (G) Image of mixture of 3-PS and 4-PS. (H) Image of mixture of 3-PSVa and 4-PSTa. Scale bar = 50 nm.

The results above, including the AFM imaging, clearly demonstrated the success of aptamer functionalized DNA nanostructure formation. No further purification was needed to achieve a high yield of nanostructures that can be imaged over large areas

(Figure 5.7-5.10). This is therefore useful to potentially enable a one-pot synthesis of large numbers of molecular shapes that can be harvested for recognition. AFM Images of the sample with the mixture of 3-PS and 4-PS as well as the mixture of 3-PSVa and 4-PSTa after assembly are shown in Figure 5.6 G, H. As seen the different assemblies can maintain their distinct shapes, and do not interfere with each other. It is also possible to modulate the numbers of each shape by simply controlling the ratios prior to deposition on a surface. This indicates that the reported platform can enable location and differentiation of different aptamers and potentially be used to organize or identify multiple targets simultaneously.

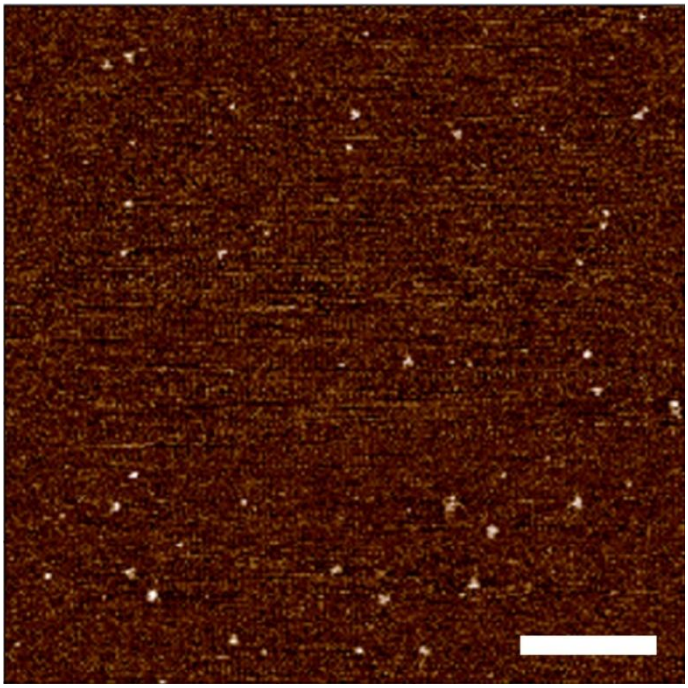

Figure 5.7. 1 μm^2 AFM scan of the 3-PS DNA assembly on mica surface in buffer condition (scale bar = 200 nm). A lower concentration is shown for clarity.

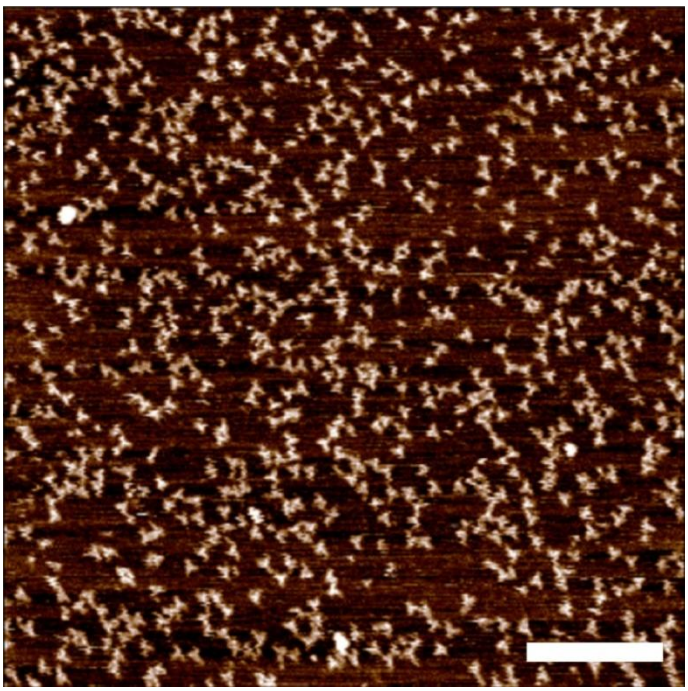

Figure 5.8. 1 μm^2 AFM scan of the VEGF aptamer-tagged 3-PS - 3-PSVa DNA assembly on mica surface in buffer condition (scale bar = 200 nm)

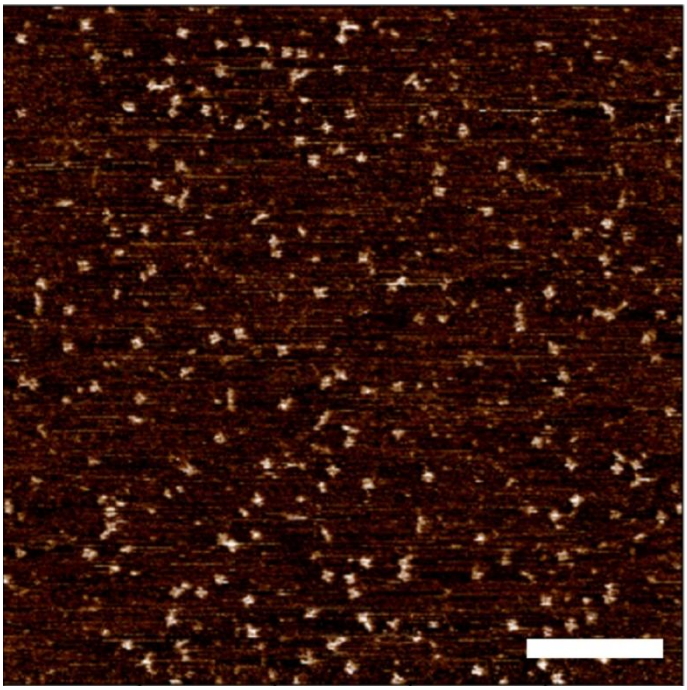

Figure 5.9. 1 μm^2 AFM scan of the 4-PS DNA assembly on mica surface in buffer condition (scale bar = 200 nm)

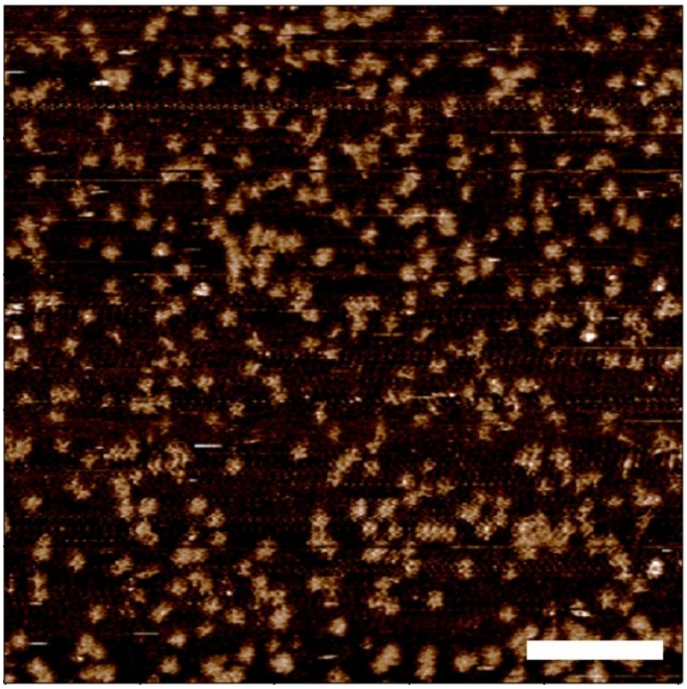

Figure 5.10. 1 μm^2 AFM scan of the thrombin aptamer-tagged 4-PS - 4-PSTa DNA assembly on mica surface in buffer condition (scale bar = 200 nm)

Aptamers linked to DNA arrays or tiles were previously reported for molecular recognition [251] and protein positioning.[236, 238] In comparison to these nanoarray strategies, the reported DNA assemblies have the following advantages:

a) DNA nanostructures are potentially less likely to interfere with aptamer bioactivity than nanoarrays due to the reduced steric hindrance or surface charge. [236] This design is also versatile enough to allow extension of the aptamer at the free end of each arm, providing significant flexibility to the aptamers which adaptively fold in the presence of their target.[252]

b) The single-pot assembly of these nanostructures enables a facile strategy for the development of large numbers of different shapes that are portable and can be harvested as molecular sensors that do not need to be used on a controlled surface or

array.

c) Unlinked and discrete DNA nanoparticles of various shapes can enable further investigations on potential applications in drug delivery or *in vivo* diagnostics.[234, 248] This also provides the ability to fabricate libraries of diverse shapes that can be mixed for potential multiplexing of different functionalities on the same platform.

5.3.3 Design and characterization of DNA nanostructures based on a "kissing-loop" interaction

Besides 3-point and 4-point star designs, other DNA nanostructure designs were also modified and applied in this research as a core shapes for attachment of aptamers. These designs are based on a common assembly principle-the "kissing-loop" interaction.[253] Specifically, single DNA or RNA can form stem-loop structures due to partially self-complementary sequences. When the sequence in two hairpin loops are complimentary for several base pairs, specific "loop-loop kissing" structure formed.[253]

Based on this design principle, first, a square DNA nanostructure was designed and demonstrated. The sequence design is based on the RNA square nanostructure reported by Chworos et al. (Figure 5.11 B).[132] Because the sequence is partially self-complementary, each chain may form two stems, two interacting hairpin-loop structures and a small motif that can specifically form a right angle (RA) (Figure 5.11). Since the sequences in two hairpin loops are complimentary for 5 base pairs, the loop-loop kissing structure formed between the adjacent two DNA chains, and

further resulting in the formation of the "square-shaped" DNA nanostructure. Assisted by the NUPACK web server[254], four DNA sequences were designed for "square" shape DNA assembly (Table 5.2). Besides this design, a "triangle" and "diamond" shape DNA nanostructures were also designed as core shapes for aptamer attachment based on this principle (Figure 5.12).

In order to attach the aptamer to each nanostructure, two identical "sticky ends" are added to the sequence of two chains to allow aptamer with a complementary tail attached there (Figure 5.11 A Figure 5.12). "Sticky ends" enable different sequences of RNA and DNA to act as attachment sites for the complementary sequences via hybridization.[255] The feasibility of several sticky ends with lengths of 6 bases was tested by NUPACK prediction. The advantage of using "sticky ends" to attach aptamers compared with the encoding method used for the previous set of designs (3-PS or 4-PS above) is that the aptamer can attach to the core shape structure after formation, which may minimize the effect of the aptamer sequence on the nanostructure assembly. However, it was found that the folding of aptamer might be affected by the sticky end extension. As shown in Figure 5.13 A, anti-IgE aptamer with a long stem forms a stable secondary structure, and is not affected by the sticky end extension. However, in the case of anti-VEGF DNA aptamer, the secondary structure is easily affected by the sticky end extension, due to the relatively floppy structure of this aptamer. Figure 5.13 B is one example, where the stick end sequence is 5′-GGATGC-3′, but this effect was commonly observed with other sticky ends as well. These is a crucial issue not just because it can reduce the yield of the DNA

nanostructures, but also result in the loss of the functionality of the aptamer, which is closely related with its structure. Hence, the utilization of these designs has to be limited to those aptamers with a more stable structure. (More specifically, with a stem structure at the 3′ and 5′)

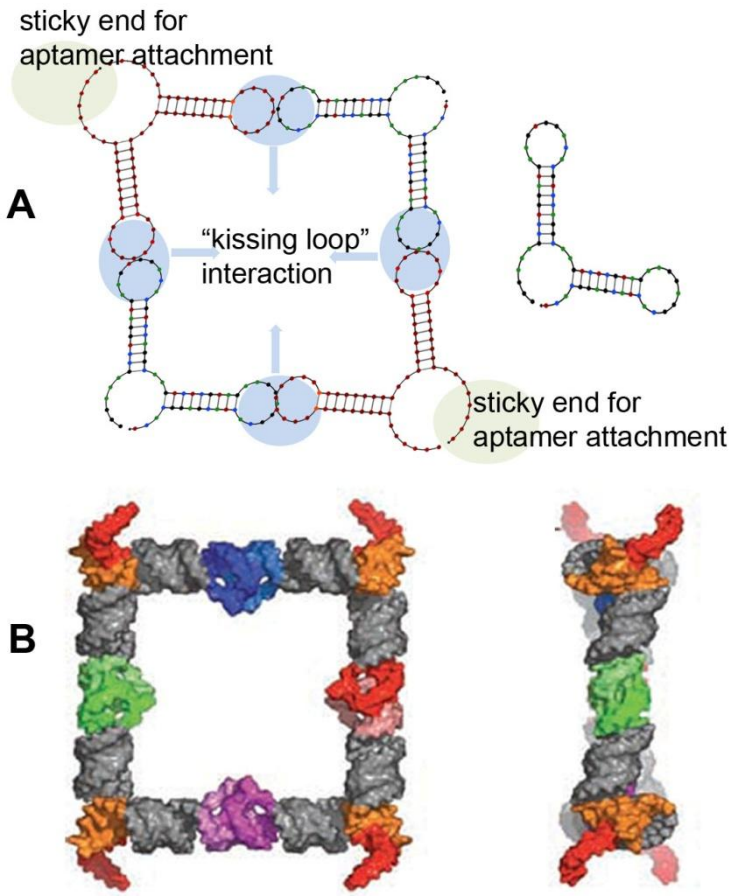

Figure 5.11. Predicted square DNA nanostructure. (A), secondary structure of chain A predicted by NUPACK web server, and DNA square assembly based on "kissing loop" interaction; (B) 3D model of square DNA assembly;[132]

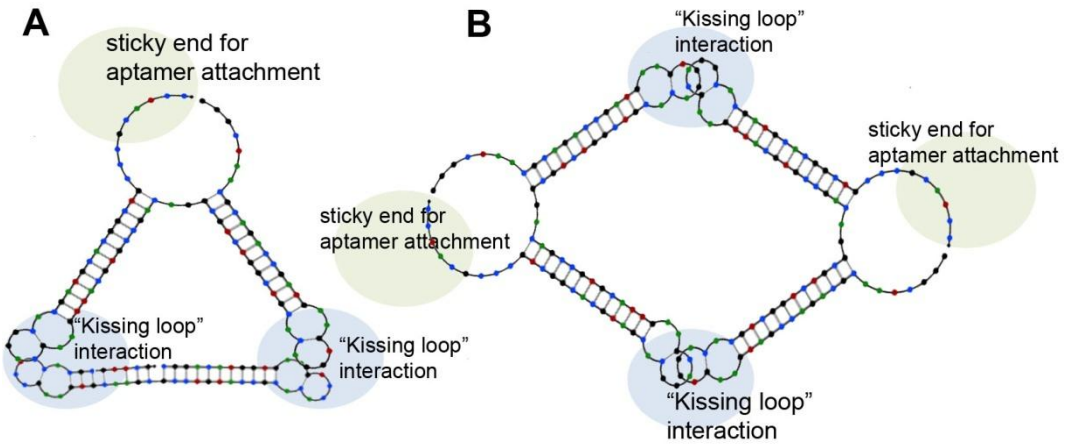

Figure 5.12. Predicted "triangle" and "diamond" DNA assembly based on "kissing-loop" interaction by NUPACK web server. (A), "triangle" DNA assembly; (B) "diamond" DNA assembly,

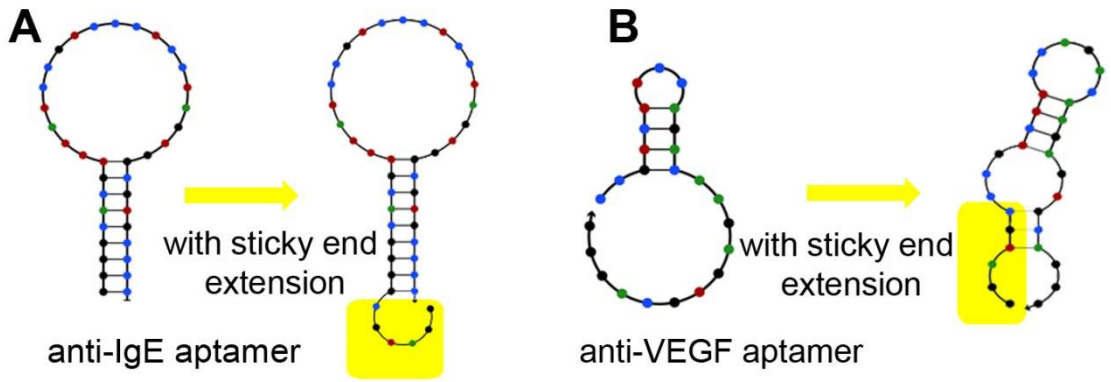

Figure 5.13. Predicted secondary structure of the aptamers with and without sticky end extension. In each panel, the "sticky end" extensions have been highlighted in yellow.

Different assembly processes were carried out to form the "square", "triangle" and "diamond" DNA nanostructures. These include the protocols used to form RNA assembly based on a "kissing loop" interaction, and also the protocol used for branched DNA assembly. [132, 133, 239, 249] However, the yield of the assembly was not enough to be used for further study. Using the "square" shape nanostructure

as an example, as shown in Figure 5.14 A, multiple, distinct bands migrated much faster than the assembly band indicating that the byproduct formed after the assembling process. Another challenge is that the aptamer sequence (in this design, an anti-IgE DNA aptamer was used) with the complimentary sticky end extended at 5′ failed to attach to the core square-structure. Figure 5.14 A shows the last lane was loaded with the sample assembled with the aptamer strand. However, the assembly migrated to the same location of the assembly formed without aptamer strand (the second last lane), which indicates the failure of the aptamer attachment. The AFM characterization of these DNA assemblies (Figure 5.14 B) showed that square-shaped nanostructures were formed, but lots of linear features were also observed from the images due to such non-preferential assembly. The AFM characterization results are consistent with the native PAGE results.

The formation and assembly process were ultimately optimized based on the thermal property of the strands, resulting in a small improvement in overall yield. However, the yield is still much lower than the 3-point and 4-point star designs described above. The low yield of these "kiss-loop" based DNA assemblies was hypothesized to be because of the assembly being based on the recognition of the kissing loops in the adjacent chains. This is a relatively weaker interaction compared with hybridization between DNA single strands. Due to these drawbacks, these designs based on "kissing-loop" interaction were discarded to minimize the uncertainty of such nanostructures formed. The research focused on the more successful 3-PS and 4-PS designs as described below.

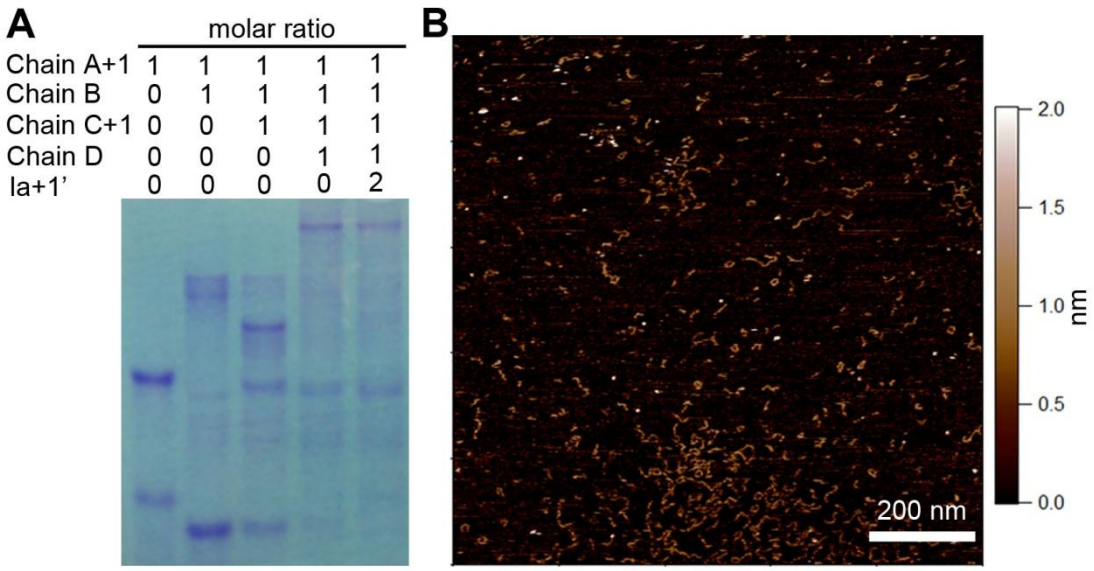

Figure 5.14. Square DNA assembly formation. (A) square DNA assembly formation monitored by native PAGE electrophoresis. DNA strands and the molar ratio are indicated above the gel. (B) AFM images for the square in solution.

5.3.4 Functionalized DNA nanostructure and protein conjugation

Following the attachment of functional aptamers, the biofunction and use of aptamer-tagged DNA nanostructures for molecular recognition and binding was investigated. Initially, the DNA-aptamer nanostructures were incubated with the target proteins (3-PSVa with VEGF and 4-PSTa with thrombin). Electrophoretic mobility shift assay (EMSA) was conducted to explore the binding between the nanostructures and the protein. As shown in Figure 5.15 A and C (protein:DNA ratios between 2:1 to 24:1), with higher concentrations of protein for the VEGF-3-PSVa and thrombin-4-PSTa systems, the bands corresponding to the free DNA nanostructures were fainter, and bands corresponding to the slower migrating

DNA/protein complexes appeared instead. These results indicate the formation of nanostructures bound to protein molecules (control experiment below). Since each aptamer-functionalized DNA nanostructure can have multiple protein binding sites (for example, 3 binding sites for 3PSVa assembly, and 4 binding sites for 3-PSVa assembly), conjugation with upto 3 or 4 protein molecules can occur in the described systems.

The formation of DNA/protein complexes with different molecular weights were confirmed by multiple discrete bands observed in the EMSA results. More specifically, the binding between the aptamers attached to the DNA nanostructures and their targets is analyte-concentration dependent, which is consistent with previously reported binding phenomena between aptamers and target proteins.[256] At even higher protein concentrations, multiple EMSA experiments showed that when the molar ratio of protein to DNA nanostructure was higher than 24:1 for 3-PSVa and 32:1 for 4-PSTa, the presence of single bands suggested saturation of the DNA assemblies (Figure 5.16). It is interesting to note that the discrete bands of DNA/protein complexes are fainter and more smeared than that of the free DNA nanostructures, especially at molecular conjugations of more than one protein molecule. This is likely due to the large size of the complexes - the maximal molecular weight of 200 and 300 KDa for 3-PSVa/VEGF and 4-PSTa/thrombin respectively, potentially resulting in the difficulty of the complex to migrate into the gel. It is also likely that the branched structure of the complexes affects this process as well.

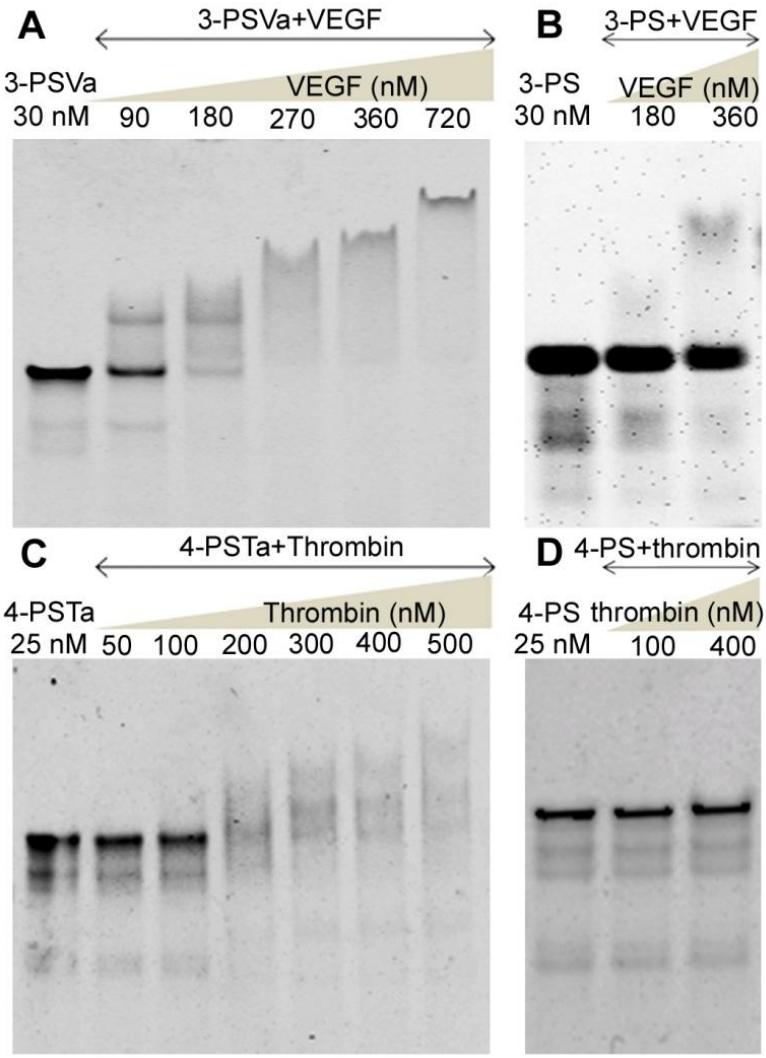

Figure 5.15. EMSA assay confirming binding between aptamer functionalized DNA nanostructures and target proteins. (A) Analysis of 3-PSVa and VEGF. (B) Analysis of 3-PS and VEGF to investigate specificity. (C) Analysis of 4-PSTa and thrombin. (D) Analysis of 4-PS and thrombin to investigate the specificity. The concentration of sample loaded in each lane is indicated above the gel. In all the gels, the left lane was loaded with DNA nanostructures without protein.

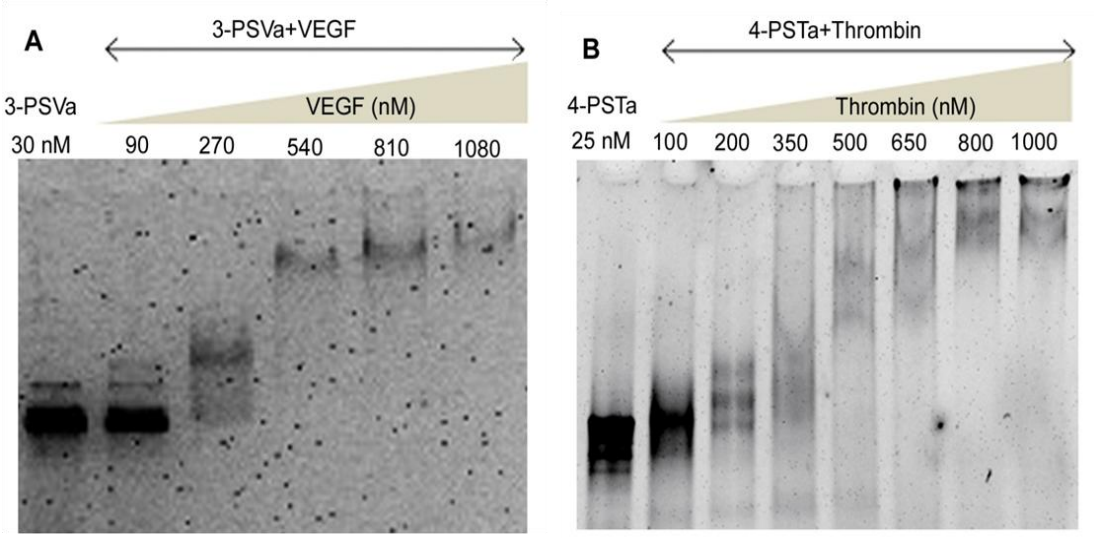

Figure 5.16. EMSA assay showing the saturation of the binding between 3-PSVa DNA assembly and VEGF and 4-PSTa DNA assembly and thrombin. The concentration of sample loaded in each lane is indicated above the gel.

To confirm that the DNA nanostructure/protein complex was formed by the specific recognition between the aptamer and the protein target, DNA nanostructures without aptamers were characterized by EMSA (Figure 5.15 B and D). The intensity of free assembly bands were similar in the lanes loaded with the sample incubated with and without protein. This showed that there is no significant binding between the DNA assemblies and protein. At a much higher protein concentrations, some non-specific binding may occur, resulting in a faint band with a higher molecular weight (Figure 5.15B). This nonspecific adhesion between protein and DNA is somewhat expected and likely caused by the weak association between the protein and DNA to counterbalance the electrostatic attraction at the interface.[257] This possibility of nonspecific adhesion between a non-preferential DNA ligand and

VEGF protein was also described earlier in Chapter 3.

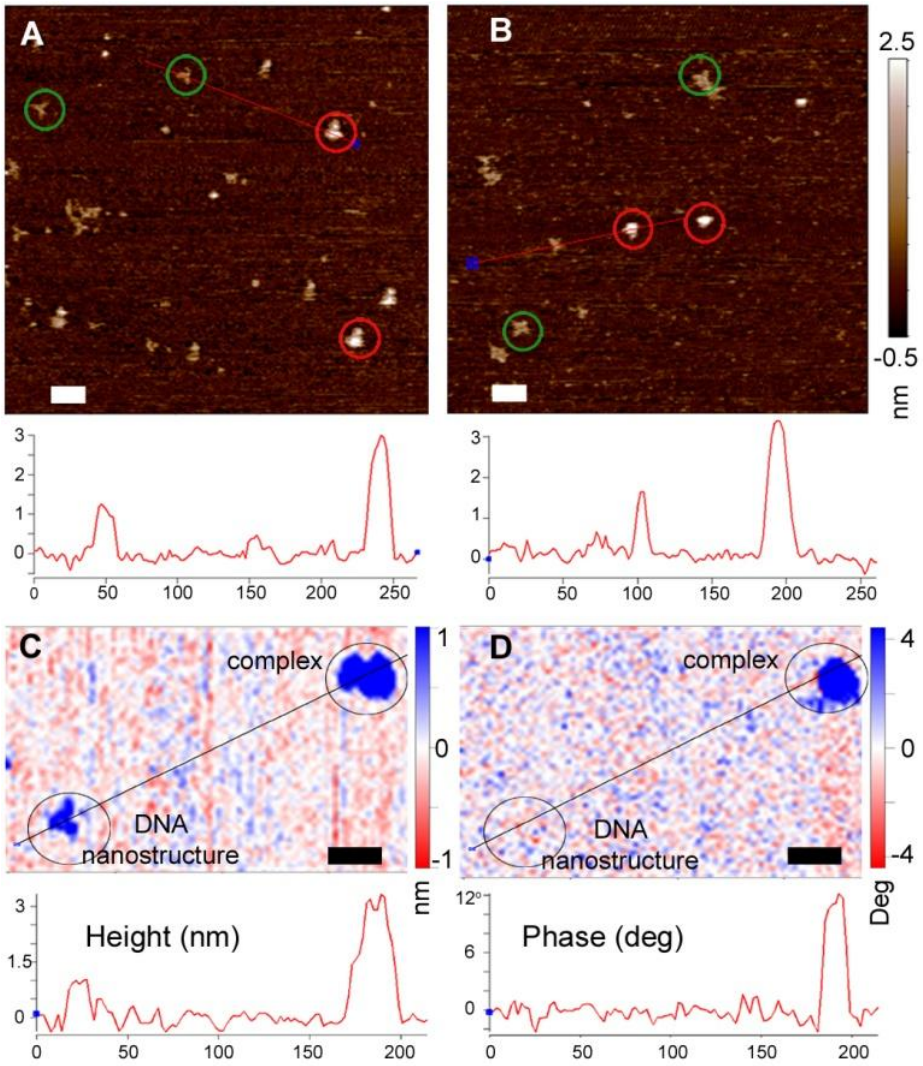

Figure 5.17. AFM image of aptamer functionalized DNA/target protein complex. (A, B) 3-PSVa/VEGF complex at the molar ratio of 9:1 (VEGF:3-PSVa). (B) 4-PSTa/Thrombin complex at the molar ratio of 12:1 (thrombin: 4-PSTa). Nanostructures without (green) and with attached proteins (red) are circled. The cross section analyses below reflect increased height on protein binding. (C, D) Comparison of height and phase AFM images for the 3-PSVa/VEGF complex. Color scale changed for clarity. The softer protein, shows a significant phase shift in comparison to the stiffer DNA nanostructure. Scale bar = 20 nm.

To visually verify the ligand binding ability of the aptamer-DNA assemblies, the nanostructures were incubated with the target proteins (3-PSVa with VEGF and 4-PSTa with thrombin as above). Based on the EMSA results, an excess of protein was used in these experiments, (9:1 ratio VEGF to 3-PSVa and 12:1 thrombin to 4-PSTa). The AFM images demonstrate that in the presence of protein, assemblies of 3-PSVa and 4-PSTa show an increased height, ~3-4 nm, consistent with the expected dimensions of VEGF and thrombin (Figure 5.17 A, B). In addition to the height differences observed from the AFM topography, the stiffness of the features with and without protein are also distinct from each other, which can be observed from the phase images, obtained during tapping-mode imaging.

During scanning, phase images record the oscillation amplitude peak shift of the cantilever, which associates with the viscous dissipation at the interface. Hence, phase imaging via AFM can be used to characterize the relative stiffness of domains in composite materials, as well as discriminate biological molecules, including DNA and protein.[258, 259] For example, Figure 5.17 C, D shows the imaging of the 3PSVa-VEGF complex. Free and complexed DNA nanostructures (lower phase shift) are visible in topography images but not observed in phase images. The protein molecules (higher phase shift) are clearly observed in both. Profiles of complexes show DNA present in topography but absent in the phase images, indicating that observed height differences are not due to protein physisorption alone. This well-defined phase contrast between the stiffer DNA nanostructure and the softer

protein can be correlated to height differences, further confirming the conjugation between the nanostructure and the protein.

Interestingly, compared to the EMSA result, a reduced degree of protein/DNA assembly conjugation was observed on the mica surfaces. Under the imaging condition in the buffer (pH 7.4), both proteins are positively charged. This may impact the association of the complex on a positively charged AP-mica surface. However, DNA nanostructures both complexed and uncomplexed (with and without attached protein) are clearly seen in each image and further optimization is possible. Successful ligand recognition indicates that such aptamer-functionalized nanostructures may be inversely used as molecular sensors to spatially locate specific targets on heterogeneous surfaces.

5.3.5 Exploring the versatility of DNA nanostructure functionalization

The above results on two distinct DNA assemblies (3-PSVa and 4-PSTa) confirm the formation and the recognition function of the aptamer attached to each functional DNA. To further evaluate the potential effect of DNA nanostructures on the aptamer function, the DNA assembly for attaching anti-thrombin aptamer was switched. Specifically, the anti-thrombin aptamer used to attached to 4-PS DNA assembly in the previous experiment was attached to 3-PS DNA assembly (notated as 3-PSTa). As above, the assembly formation was monitored by the native PAGE electrophoresis and AFM image (Figure 5.18 A and B). The binding between anti-thrombin aptamer and thrombin protein was verified by the EMSA assay

(Figure 5.18 C). Multiple bands were observed with the sample of mixture of 3-PSTa DNA assembly and thrombin protein, which indicate conjugation with one, two or three proteins.

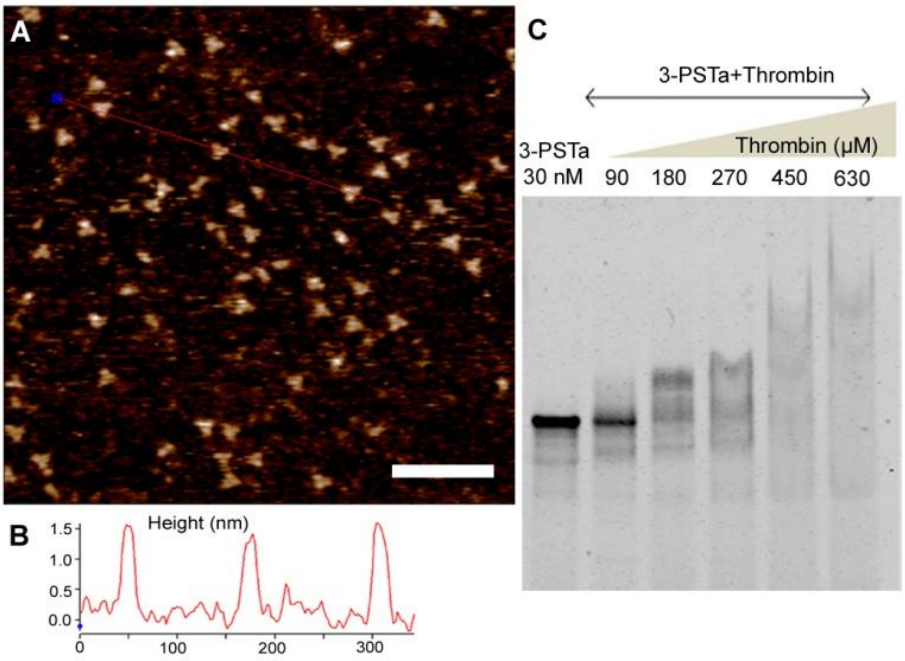

Figure 5.18. Structural and functional characterization of 3-PS DNA functionalized with anti-thrombin aptamer. (A) AFM image of 3-PSTa. (B) the cross section analysis of DNA nanostructures. (C) EMSA analysis confirming the binding between 3-PSTa and thrombin. The concentration of the sample loaded in each lane is indicated above the gel. Scale bar = 100 nm.

These results confirm that shapes of the DNA assembly (3-PS and 4-PS) do not interfere with the aptamer's biofunction significantly. Moreover, these results also reflect the programmability and flexibility of this strategy, in that it is possible to take various predefined nanoarchitectures and functionalize them with different aptamers by simple sequence extension. This versatility of design can open up facile

synthesis strategies for labeling various shapes as molecular recognition agents. More existing DNA and RNA nanostructures are under exploration currently. It is also important to note that that in terms of stability, the functional DNA assemblies with aptamer extension are similar to the assemblies without aptamer extension. All the DNA assemblies characterized above can be stored at 4^{o}C for over two months without any significant dissociation of the assembly and inactivation of the aptamer.

5.4 Conclusions

In this chapter, in order to demonstrate that aptamers can be further adapted to more advanced and high-throughput recognition applications, functional nucleic acids were organized into programmable, discrete nanoconstructs. This presents a novel approach that can combine the merits of structural DNA architectonics with exquisite aptamer molecular recognition. Specifically, DNA nanostructures assembled by different principles were modified and applied as a "key chain" for aptamer attachment, and the aptamers were attached by sequence extension or via sticky ends. Different DNA nanostructures were investigated in this work to evaluate the feasibility of being applied as "key chain". While this study demonstrates basic shapes such as an 'X' or 'Y', it is feasible to construct libraries of diverse shapes that may be mixed together enabling multiplexed sensing platforms.

It is shown that these discrete aptamer-tagged DNA shapes and nanostructures can recognize and bind protein targets in an aqueous environment. These nanostructures are stable over long periods of time and capable of binding

different target proteins. The facile construction modality enables adaptation of suitable designs for the on-demand production of oligonucleotide nanostructures. Further studies are ongoing to examine the sensitivity, selectivity, stability and effect of shape on binding as well as to enable quantitative measurements of ligand concentrations. These nanostructures can be envisioned as molecular nanosensors for ligand recognition, catalyzing reactions, or for enabling the development of ultrasensitive molecular sensors in complex environments.

[This chapter contains results that have been submitted to the journal Nanoscale].

CHAPTER 6

CONCLUSION AND FUTURE WORKS

6.1 Conclusion

The work described in this dissertation aimed at investigating the interactions of diverse biomolecular recognition systems based on reliable methodological platforms, and further enabling sensing and molecular recognition tools:

a. Using a strategy of mixed-self-assembled monolayers to create different functionalities on a solid substrate, a reliable and versatile platform to investigate the biomolecular interaction was established. This not only enabled biomolecule immobilization but also the ability to interrogate the interactions of these biomolecules at the single molecule level via AFM based force spectroscopy.

b. Based on this platform, different binding systems could be investigated including a lectin-carbohydrate system and importantly, several newly developed aptamer-target protein systems. The energy landscape, the specificity, the conformational properties of these systems was characterized. These results helped better understand the hitherto unstudied recognition forces between aptamers and their target proteins at the molecular level.

c. The unique properties of aptamer-target protein interactions were further adapted to ensemble level binding systems, investigated by QCM analysis. The affinity and kinetics of several aptamer/target protein systems were investigated using similar self-assembled monolayer methods as in a) and b). This binding information obtained at both the molecular scale and the ensemble scale contributes to bridging the gap across length scales, and helps to correlate and utilize the single molecular dynamic behaviors with ensemble-averaging properties.

d. Finally, using DNA nanostructures, aptamers were used to develop a novel shape-based sensing strategy. The formation and the functionality of these nanostructures to bind proteins were investigated. The results indicated that these aptamers tagged with distinct nanoconstructs are a flexible strategy, and have potential to be developed as shape-based ultrasensitive molecular sensors in complex environments.

6.2 Recommendations for future work

Uncovering fundamental properties in aptamer and protein binding

During the investigation of the aptamer/target interaction, several important issues had been addressed, including the specificity of the aptamer against its preferential targets, the energy landscape, the dynamic strength of the bond under increasing loading rate, and the effect of the conformational property of aptamer on the bond

strength. While different aptamer/target protein systems were investigated, in order to verify whether these conclusions are the universal property of all aptamer/protein interactions or specific to some systems, many more aptamer systems need to be investigated. For example, by adding divalent cations such as Mg^{2+}, the rigidity of anti-VEGF RNA aptamer (which is not selected in a buffer containing Mg^{2+}) could be regulated, which further resulted in a higher affinity and higher rupture force. However, how this conformational effect affects other aptamer/protein systems, especially when the aptamers are originally selected in the presence of Mg^{2+}? This is related to more fundamental questions on how the rigidity/flexibility of aptamers affects their binding and how this can be modulated externally.

Force Mapping based on specific aptamer protein interactions

One of the most powerful features of AFM is that it can record the adhesion force between the AFM tip and surface while scanning across the surface. The generation of *x*,*y* maps of these adhesive forces is referred to as "force mapping". The unique advantage of this technique is its capability of localizing specific binding sites on the surface. Combined with different self-assembled monolayers or nanografting lithography, different aptamer protein interactions can be detected in specific regions with high lateral resolution at the nanoscale. This could therefore provide a technique to study high-throughput aptamer or protein arrays from a binding force perspective.

Biosensing based on aptamer functionalized DNA nanostructures

In Chapter 5, preliminary works showing the feasibility of fabricating aptamer-functionalized DNA nanostructures was presented. Future work would need to demonstrate actual qualitative and quantitative sensing applications with these nanostructures. Hence, a user friendly sensing format would need to be established. For example, a chip-based sensing format could be developed with multiple aptamer-functionalized DNA nanostructures immobilized on and also displayed in a well-controlled fashion to detect for multiple proteins on a single platform. Similarly, effective and optimal fabrication strategies could be developed to fabricate such functional nanostuctures in large quantities and against multiple targets.

3D DNA Nanostructures Development for Drug Delivery Applications

Extending the concept of the functional 2D nanostructures, it would be advantageous to adapt these designs to 3D DNA nanostructures, which would not only significantly expand the available DNA designs for tagging aptamers, but also enables different applications such as using them as target drug delivery agents. This would combine the recognition ability of aptamers attached to the 3D DNA nanostructures with therapeutic agents loaded within the nanostructure to delivery drugs as and where needed.

LIST OF REFERENCES

LIST OF REFERENCES

1. Jayaraman, A.; Yarmush, M. L.; Roth, C. M. Molecular bioengineering. *Industrial & Engineering Chemistry Research.* **2002**, 41, 441-455.

2. Wyttenbach, T.; Bowers, M. T., Intermolecular interactions in biomolecular systems examined by mass spectrometry. In *Annual Review of Physical Chemistry*, Annual Reviews: Palo Alto, 2007; Vol. 58, pp 511-533.

3. Liu, Y.; Han, B.-H.; Qi, A.-D.; Chen, R.-T. Molecular Recognition Study of a Supramolecular System. *Bioorganic Chemistry.* **1997**, 25, 155-162.

4. Lalonde, S.; Ehrhardt, D. W.; Loque, D.; Chen, J.; Rhee, S. Y.; Frommer, W. B. Molecular and cellular approaches for the detection of protein-protein interactions: latest techniques and current limitations. *Plant Journal.* **2008**, 53, 610-635.

5. Cusick, M. E.; Klitgord, N.; Vidal, M.; Hill, D. E. Interactome: gateway into systems biology. *Human Molecular Genetics.* **2005**, 14, R171-R181.

6. Ryu, D. D. Y.; Nam, D. H. Recent progress in biomolecular engineering. *Biotechnology Progress.* **2000**, 16, 2-16.

7. Vadgama, P.; Crump, P. W. Biosensors: recent trends. A review. *Analyst.* **1992**, 117, 1657-1670.

8. Shah, V. P. The history of bioanalytical method validation and regulation: Evolution of a guidance document on bioanalytical methods validation. *Aaps Journal.* **2007**, 9, E43-E47.

9. Neuman, K. C.; Nagy, A. Single-molecule force spectroscopy: optical tweezers, magnetic tweezers and atomic force microscopy. *Nature Methods.* **2008**, 5, 491-505.

10. Baran, J.; Barnes, A. J.; Handke, M.; Ratajczak, H. Special issue: From molecules to molecular biological systems and molecular materials: the role of non covalent interactions and molecular recognition in supramolecular systems. Preface.

Journal of Molecular Structure. **2002**, 614, 1-1.

11. Kooistra, D. A.; Smallcombe, S. H.; Richards, J. H. Binding dynamics in biological systems. Interaction of MOPC-315 with ^{19}F labelled nitrophenyl haptens. *Organic Magnetic Resonance.* **1980**, 13, 1-8.

12. Turner, A. P. F. Biochemistry - Biosensors sense and sensitivity. *Science.* **2000**, 290, 1315-1317.

13. Hinterdorfer, P.; Dufrene, Y. F. Detection and localization of single molecular recognition events using atomic force microscopy. *Nature Methods.* **2006**, 3, 347-355.

14. Reed, A. E.; Curtiss, L. A.; Weinhold, F. Intermolecular interactions from a natural bond orbital, donor-acceptor viewpoint. *Chemical Reviews.* **1988**, 88, 899-926.

15. Simon, Z., *Quantum biochemistry and specific interactions*. Abacus Press: Tunbbridge Wells, Kent, 1976.

16. Ziegler, C.; Gopel, W. Biosensor development. *Current Opinion in Chemical Biology.* **1998**, 2, 585-591.

17. Hall, E. A. H. Recent progress in biosensor development. *International Journal of Biochemistry.* **1988**, 20, 357-362.

18. Yalow, R. S.; Berson, S. A. Assay of Plasma Insulin in Human Subjects by Immunological Methods. *Nature.* **1959**, 184, 1648-1649.

19. Rogers, K. R. Principles of affinity-based biosensors. *Molecular Biotechnology.* **2000**, 14, 109-129.

20. Briones, C.; Martin-Gago, J. A. Nucleic acids and their analogs as nanomaterials for biosensor development. *Current Nanoscience.* **2006**, 2, 257-273.

21. Gibson, T. D.; Woodward, J. R. Protein stabilization in biosensor systems. *Acs Symposium Series.* **1992**, 487, 40-55.

22. Oliver, N. S.; Toumazou, C.; Cass, A. E. G.; Johnston, D. G. Glucose sensors: a review of current and emerging technology. *Diabetic Medicine.* **2009**, 26, 197-210.

23. Marshall, A.; Hodgson, J. DNA chips: An array of possibilities. *Nature Biotechnology.* **1998**, 16, 27-31.

24. Kruger, K.; Grabowski, P. J.; Zaug, A. J.; Sands, J.; Gottschling, D. E.; Cech, T. R. Self-splicing RNA: autoexcision and autocyclization of the ribosomal RNA intervening sequence of Tetrahymena. *Cell.* **1982**, 31, 147-157.

25. Stark, B. C.; Kole, R.; Bowman, E. J.; Altman, S. Ribonuclease P: an enzyme with an essential RNA component. *Proceedings of the National Academy of Sciences of the United States of America.* **1978**, 75, 3717-3721.

26. Breaker, R. R. Natural and engineered nucleic acids as tools to explore biology. *Nature.* **2004**, 432, 838-845.

27. Nudler, E.; Mironov, A. S. The riboswitch control of bacterial metabolism. *Trends in Biochemical Sciences.* **2004**, 29, 11-17.

28. Siomi, H.; Siomi, M. C. On the road to reading the RNA-interference code. *Nature.* **2009**, 457, 396-404.

29. Tuerk, C.; Gold, L. Systematic evolution of ligands by exponential enrichment: RNA ligands to bacteriophage T4 DNA polymerase. *Science.* **1990**, 249, 505-510.

30. Ellington, A. D.; Szostak, J. W. In vitro selection of RNA molecules that bind specific ligands. *Nature.* **1990**, 346, 818-822.

31. Robertson, D. L.; Joyce, G. F. Selection *in vitro* of an RNA enzyme that specifically cleaves single-stranded DNA. *Nature.* **1990**, 344, 467-468.

32. Jayasena, S. D. Aptamers: An emerging class of molecules that rival antibodies in diagnostics. *Clinical Chemistry.* **1999**, 45, 1628-1650.

33. Luzi, E.; Minunni, M.; Tombelli, S.; Mascini, M. New trends in affinity sensing: aptamers for ligand binding. *Trac-Trends in Analytical Chemistry.* **2003**, 22, 810-818.

34. Jhaveri, S.; Rajendran, M.; Ellington, A. D. In vitro selection of signaling aptamers. *Nature Biotechnology.* **2000**, 18, 1293-1297.

35. Strehlitz, B.; Nikolaus, N.; Stoltenburg, R. Protein detection with aptamer biosensors. *Sensors.* **2008**, 8, 4296-4307.

36. Bunka, D. H. J.; Stockley, P. G. Aptamers come of age - at last. *Nature Reviews Microbiology.* **2006**, 4, 588-596.

37. Zhou, J.; Battig, M. R.; Wang, Y. Aptamer-based molecular recognition for biosensor development. *Analytical and Bioanalytical Chemistry.* **2010**, 398,

2471-2480.

38. Famulok, M.; Hartig, J. S.; Mayer, G. Functional aptamers and aptazymes in biotechnology, diagnostics, and therapy. *Chemical Reviews.* **2007**, 107, 3715-3743.

39. Lee, J. H.; Yigit, M. V.; Mazumdar, D.; Lu, Y. Molecular diagnostic and drug delivery agents based on aptamer-nanomaterial conjugates. *Advanced Drug Delivery Reviews.* **2010**, 62, 592-605.

40. Yan, A. C.; Levy, M. Aptamers and aptamer targeted delivery. *Rna Biology.* **2009**, 6, 316-320.

41. Ng, E. W. M.; Shima, D. T.; Calias, P.; Cunningham, E. T.; Guyer, D. R.; Adamis, A. P. Pegaptanib, a targeted anti-VEGF aptamer for ocular vascular disease. *Nature Reviews Drug Discovery.* **2006**, 5, 123-132.

42. Cho, E. J.; Lee, J. W.; Ellington, A. D. Applications of Aptamers as Sensors. *Annual Review of Analytical Chemistry.* **2009**, 2, 241-264.

43. Navani, N. K.; Li, Y. F. Nucleic acid aptamers and enzymes as sensors. *Current Opinion in Chemical Biology.* **2006**, 10, 272-281.

44. Hermann, T.; Patel, D. J. Biochemistry - Adaptive recognition by nucleic acid aptamers. *Science.* **2000**, 287, 820-825.

45. Nutiu, R.; Li, Y. F. Aptamers with fluorescence-signaling properties. *Methods.* **2005**, 37, 16-25.

46. Nutiu, R.; Li, Y. F. Structure-switching signaling aptamers. *Journal of the American Chemical Society.* **2003**, 125, 4771-4778.

47. Li, N.; Ho, C. M. Aptamer-based optical probes with separated molecular recognition and signal transduction modules. *Journal of the American Chemical Society.* **2008**, 130, 2380-2381.

48. Nick Taylor, J.; Darugar, Q.; Kourentzi, K.; Willson, R. C.; Landes, C. F. Dynamics of an anti-VEGF DNA aptamer: A single-molecule study. *Biochemical and Biophysical Research Communications.* **2008**, 373, 213-218.

49. Jiang, Y. X.; Zhu, C. F.; Ling, L. S.; Wan, L. J.; Fang, X. H.; Bai, C. Specific aptamer-protein interaction studied by atomic force microscopy. *Analytical Chemistry.* **2003**, 75, 2112-2116.

50. Yu, J. P.; Jiang, Y. X.; Ma, X. Y.; Lin, Y.; Fang, X. H. Energy landscape of

aptamer/protein complexes studied by single-molecule force spectroscopy. *Chemistry-an Asian Journal.* **2007**, 2, 284-289.

51. He, X. X.; Jin, R.; Yang, L.; Wang, K. M.; Li, W.; Tan, W. H.; Li, H. M. Study on the specific interaction between angiogenin and aptamer by atomic force microscopy (AFM). *Chinese Science Bulletin.* **2008**, 53, 198-203.

52. Basnar, B.; Elnathan, R.; Willner, I. Following aptamer-thrombin binding by force measurements. *Analytical Chemistry.* **2006**, 78, 3638-3642.

53. Lazcka, O.; Del Campo, F. J.; Munoz, F. X. Pathogen detection: A perspective of traditional methods and biosensors. *Biosensors & Bioelectronics.* **2007**, 22, 1205-1217.

54. Mann, M.; Hendrickson, R. C.; Pandey, A. Analysis of proteins and proteomes by mass spectrometry. *Annual Review of Biochemistry.* **2001**, 70, 437-473.

55. Yoshinobu, T.; Iwasaki, H.; Ui, Y.; Furuichi, K.; Ermolenko, Y.; Mourzina, Y.; Wagner, T.; Nather, N.; Schoning, M. J. The light-addressable potentiometric sensor for multi-ion sensing and imaging. *Methods.* **2005**, 37, 94-102.

56. Bruns, T.; Strauss, W. S. L.; Sailer, R.; Wagner, M.; Schneckenburger, H. Total internal reflectance fluorescence reader for selective investigations of cell membranes. *Journal of Biomedical Optics.* **2006**, 11, 1-7.

57. Nice, E. C.; Catimel, B. Instrumental biosensors: new perspectives for the analysis of biomolecular interactions. *Bioessays.* **1999**, 21, 339-352.

58. Cooper, M. A.; Singleton, V. T. A survey of the 2001 to 2005 quartz crystal microbalance biosensor literature: applications of acoustic physics to the analysis of biomolecular interactions. *Journal of Molecular Recognition.* **2007**, 20, 154-184.

59. Wohltjen, H. Mechanism of operation and design considerations for surface acoustic wave device vapour sensors. *Sensors and Actuators.* **1984**, 5, 307-325.

60. Liu, Y.; Yu, X.; Zhao, R.; Shangguan, D. H.; Bo, Z. Y.; Liu, G. Q. Quartz crystal biosensor for real-time monitoring of molecular recognition between protein and small molecular medicinal agents. *Biosensors & Bioelectronics.* **2003**, 19, 9-19.

61. Kosslinger, C.; Uttenthaler, E.; Drost, S.; Aberl, F.; Wolf, H.; Brink, G.; Stanglmaier, A.; Sackmann, E. Comparison of the QCM and the SPR method for surface studies and immunological applications. *Sensors and Actuators B-Chemical.* **1995**, 24, 107-112.

62. Hianik, T.; Ostatna, V.; Zajacova, Z.; Stoikova, E.; Evtugyn, G. Detection of aptamer-protein interactions using QCM and electrochemical indicator methods. *Bioorganic & Medicinal Chemistry Letters.* **2005**, 15, 291-295.

63. Yao, C. Y.; Qi, Y. Z.; Zhao, Y. H.; Xiang, Y.; Chen, Q. H.; Fu, W. L. Aptamer-based piezoelectric quartz crystal microbalance biosensor array for the quantification of IgE. *Biosensors & Bioelectronics.* **2009**, 24, 2499-2503.

64. Yao, C. Y.; Zhu, T. Y.; Qi, Y. Z.; Zhao, Y. H.; Xia, H.; Fu, W. L. Development of a Quartz Crystal Microbalance Biosensor with Aptamers as Bio-recognition Element. *Sensors.* **2010**, 10, 5859-5871.

65. sauerbrey, G. Z. Verwendung von Schwingquarzen zur Wägung dünner Schichten und zur Mikrowägung *Physics.* **1959**, 155.

66. Ferreira, G. N. M.; Da-Silva, A. C.; Tome, B. Acoustic wave biosensors: physical models and biological applications of quartz crystal microbalance. *Trends in Biotechnology.* **2009**, 27, 689-697.

67. Liss, M.; Petersen, B.; Wolf, H.; Prohaska, E. An aptamer-based quartz crystal protein biosensor. *Analytical Chemistry.* **2002**, 74, 4488-4495.

68. Tombelli, S.; Minunni, A.; Luzi, E.; Mascini, M. Aptamer-based biosensors for the detection of HIV-1 Tat protein. *Bioelectrochemistry.* **2005**, 67, 135-141.

69. Min, K.; Cho, M.; Han, S. Y.; Shim, Y. B.; Ku, J.; Ban, C. A simple and direct electrochemical detection of interferon-gamma using its RNA and DNA aptamers. *Biosensors & Bioelectronics.* **2008**, 23, 1819-1824.

70. van Oijen, A. M. Cutting the forest to see a single tree? *Nature Chemical Biology.* **2008**, 4, 440-443.

71. Clausen-Schaumann, H.; Seitz, M.; Krautbauer, R.; Gaub, H. E. Force spectroscopy with single bio-molecules. *Current Opinion in Chemical Biology.* **2000**, 4, 524-530.

72. Smith, S. B.; Finzi, L.; Bustamante, C. Direct mechanical measurements of the elasticity of single DNA molecules by using magnetic beads. *Science.* **1992**, 258, 1122-1126.

73. Kuo, S. C.; Sheetz, M. P. Force of single kinesin molecules measured with optical tweezers. *Science.* **1993**, 260, 232-234.

74. Brampton, C.; Wahab, O.; Batchelor, M. R.; Allen, S.; Williams, P. M.

Biomembrane force probe investigation of RNA dissociation. *European Biophysics Journal with Biophysics Letters.* **2011**, 40, 247-257.

75. Moy, V. T.; Florin, E. L.; Gaub, H. E. Adhesive forces between ligand and receptor measured by AFM. *Biophysical Journal.* **1994**, 66, A340-A340.

76. Ng, S. P.; Rounsevell, R. W. S.; Steward, A.; Geierhaas, C. D.; Williams, P. M.; Paci, E.; Clarke, J. Mechanical unfolding of TNfn3: The unfolding pathway of a fnIII domain probed by protein engineering, AFM and MD simulation. *Journal of Molecular Biology.* **2005**, 350, 776-789.

77. Borgia, A.; Williams, P. M.; Clarke, J., Single-molecule studies of protein folding. In *Annual Review of Biochemistry*, 2008; Vol. 77, pp 101-125.

78. Puchner, E. M.; Gaub, H. E. Force and function: probing proteins with AFM-based force spectroscopy. *Current Opinion in Structural Biology.* **2009**, 19, 605-614.

79. Evans, E. Probing the relation between force - Lifetime - and chemistry in single molecular bonds. *Annual Review of Biophysics and Biomolecular Structure.* **2001**, 30, 105-128.

80. Seo, Y.; Jhe, W. Atomic force microscopy and spectroscopy. *Reports on Progress in Physics.* **2008**, 71, 1-23.

81. Binnig, G.; Quate, C. F.; Gerber, C. Atomic force microscope *Physical Review Letters.* **1986**, 56, 930-933.

82. Francis, L. W.; Lewis, P. D.; Wright, C. J.; Conlan, R. S. Atomic force microscopy comes of age. *Biology of the Cell.* **2010**, 102, 133-143.

83. Giessibl, F. J.; Quate, C. F. Exploring the nanoworld with atomic force microscopy. *Physics Today.* **2006**, 59, 44-50.

84. Marti, O.; Elings, V.; Haugan, M.; Bracker, C. E.; Schneir, J.; Drake, B.; Gould, S. A. C.; Gurley, J.; Hellemans, L.; Shaw, K.; Weisenhorn, A. L.; Zasadzinski, J.; Hansma, P. K. Scanning probe microscopy of biological samples and other surfaces. *Journal of Microscopy-Oxford.* **1988**, 152, 803-809.

85. Shao, Z. F.; Yang, J.; Somlyo, A. P. Biological atomic force microscopy: From microns to nanometers and beyond. *Annual Review of Cell and Developmental Biology.* **1995**, 11, 241-265.

86. Kada, G.; Kienberger, F.; Hinterdorfer, P. Atomic force microscopy in

bionanotechnology. *Nano Today.* **2008**, 3, 12-19.

87. Zlatanova, J.; Lindsay, S. M.; Leuba, S. H. Single molecule force spectroscopy in biology using the atomic force microscope. *Progress in Biophysics & Molecular Biology*. **2000**, 74, 37-61.

88. Yang, J. AFM as a high-resolution imaging tool and a molecular bond force probe. *Cell Biochemistry and Biophysics.* **2004**, 41, 435-449.

89. Fang, H. H. P.; Chan, K. Y.; Xu, L. C. Quantification of bacterial adhesion forces using atomic force microscopy (AFM). *Journal of Microbiological Methods.* **2000**, 40, 89-97.

90. Dammer, U.; Hegner, M.; Anselmetti, D.; Wagner, P.; Dreier, M.; Huber, W.; Guntherodt, H. J. Specific antigen/antibody interactions measured by force microscopy. *Biophysical Journal.* **1996**, 70, 2437-2441.

91. Paquim, A. M. C.; Diculescu, V. C.; Oretskaya, T. S.; Brett, A. M. O. AFM and electroanalytical studies of synthetic oligonucleotide hybridization. *Biosensors & Bioelectronics.* **2004**, 20, 933-944.

92. Ratto, T. V.; Langry, K. C.; Rudd, R. E.; Balhorn, R. L.; Allen, M. J.; McElfresh, M. W. Force spectroscopy of the double-tethered concanavalin-A mannose bond. *Biophysical Journal.* **2004**, 86, 2430-2437.

93. Baumgartner, W.; Hinterdorfer, P.; Ness, W.; Raab, A.; Vestweber, D.; Schindler, H.; Drenckhahn, D. Cadherin interaction probed by atomic force microscopy. *Proceedings of the National Academy of Sciences of the United States of America.* **2000**, 97, 4005-4010.

94. Li, F. Y.; Redick, S. D.; Erickson, H. P.; Moy, V. T. Force measurements of the alpha(5)beta(1) integrin-fibronectin interaction. *Biophysical Journal.* **2003**, 84, 1252-1262.

95. Sewald, N.; Wilking, S. D.; Eckel, R.; Albu, S.; Wollschlager, K.; Gaus, K.; Becker, A.; Bartels, F. W.; Ros, R.; Anselmetti, D. Probing DNA-peptide interaction forces at the single-molecule level. *Journal of Peptide Science.* **2006**, 12, 836-842.

96. Wright, C. J.; Armstrong, I. The application of atomic force microscopy force measurements to the characterisation of microbial surfaces. *Surface and Interface Analysis.* **2006**, 38, 1419-1428.

97. Favre, M.; Polesel-Maris, J.; Overstolz, T.; Niedermann, P.; Dasen, S.; Gruener, G.; Ischer, R.; Vettiger, P.; Liley, M.; Heinzelmann, H.; Meister, A. Parallel AFM

imaging and force spectroscopy using two-dimensional probe arrays for applications in cell biology. *Journal of Molecular Recognition.* **2011**, 24, 446-452.

98. Hugel, T.; Seitz, M. The study of molecular interactions by AFM force spectroscopy. *Macromolecular Rapid Communications.* **2001**, 22, 989-1016.

99. Wakayama, J.; Sekiguchi, H.; Akanuma, S.; Ohtani, T.; Sugiyama, S. Methods for reducing nonspecific interaction in antibody-antigen assay via atomic force microscopy. *Analytical Biochemistry.* **2008**, 380, 51-58.

100. Brogan, K. L.; Shin, J. H.; Schoenfisch, M. H. Influence of surfactants and antibody immobilization strategy on reducing nonspecific protein interactions for molecular recognition force microscopy. *Langmuir.* **2004**, 20, 9729-9735.

101. Bell, G. I. Models for the Specific Adhesion of Cells to Cells. *Science.* **1978**, 200, 618-627.

102. Evans, E.; Ritchie, K. Dynamic strength of molecular adhesion bonds. *Biophysical Journal.* **1997**, 72, 1541-1555.

103. Evans, E.; Ritchie, K.; Merkel, R. Sensitive force technique to probe molecular adhesion and structural linkages at biological interfaces. *Biophysical Journal.* **1995**, 68, 2580-2587.

104. Rusmini, F.; Zhong, Z. Y.; Feijen, J. Protein immobilization strategies for protein biochips. *Biomacromolecules.* **2007**, 8, 1775-1789.

105. Beaucage, S. L. Strategies in the preparation of DNA oligonucleotide arrays for diagnostic applications. *Current Medicinal Chemistry.* **2001**, 8, 1213-1244.

106. Lyubchenko, Y. L. Preparation of DNA and nucleoprotein samples for AFM imaging. *Micron.* **2011**, 42, 196-206.

107. Lyubchenko, Y. L.; Shlyakhtenko, L. S. AFM for analysis of structure and dynamics of DNA and protein-DNA complexes. *Methods.* **2009**, 47, 206-213.

108. Neish, C. S.; Martin, I. L.; Henderson, R. M.; Edwardson, J. M. Direct visualization of ligand-protein interactions using atomic force microscopy. *British Journal of Pharmacology.* **2002**, 135, 1943-1950.

109. Hinterdorfer, P.; Gruber, H. J.; Kienberger, F.; Kada, G.; Riener, C.; Borken, C.; Schindler, H. Surface attachment of ligands and receptors for molecular recognition force microscopy. *Colloids and Surfaces B-Biointerfaces.* **2002**, 23, 115-123.

110. Dufrene, Y. F. AFM for nanoscale microbe analysis. *Analyst.* **2008**, 133, 297-301.

111. Nuzzo, R. G.; Allara, D. L. Adsorption of bifunctional organic disulfides on gold surfaces. *Journal of the American Chemical Society.* **1983**, 105, 4481-4483.

112. Love, J. C.; Estroff, L. A.; Kriebel, J. K.; Nuzzo, R. G.; Whitesides, G. M. Self-assembled monolayers of thiolates on metals as a form of nanotechnology. *Chemical Reviews.* **2005**, 105, 1103-1169.

113. Samanta, D.; Sarkar, A. Immobilization of bio-macromolecules on self-assembled monolayers: methods and sensor applications. *Chemical Society Reviews.* **2011**, 40, 2567-2592.

114. Wink, T.; vanZuilen, S. J.; Bult, A.; vanBennekom, W. P. Self-assembled monolayers for biosensors. *Analyst.* **1997**, 122, R43-R50.

115. Ulman, A. Formation and structure of self-assembled monolayers. *Chemical Reviews.* **1996**, 96, 1533-1554.

116. Bain, C. D.; Whitesides, G. M. Modeling organic-sufaces with self-assembled monolayers. *Angewandte Chemie-International Edition in English.* **1989**, 28, 506-512.

117. Folkers, J. P.; Laibinis, P. E.; Whitesides, G. M. Self-assembled monolayers of alkanethiols on gold-comparisons of monolayers containing mixtures of short-chain and long-chain constituents with CH_3 and CH_2OH terminal groups. *Langmuir.* **1992**, 8, 1330-1341.

118. Yadavalli, V. K.; Forbes, J. G.; Wang, K. Functionalized self-assembled monolayers on ultraflat gold as platforms for single molecule force spectroscopy and imaging. *Langmuir.* **2006**, 22, 6969-6976.

119. Balamurugan, S.; Obubuafo, A.; Soper, S. A.; McCarley, R. L.; Spivak, D. A. Designing highly specific biosensing surfaces using aptamer monolayers on gold. *Langmuir.* **2006**, 22, 6446-6453.

120. Jiang, Y. X.; Fang, X. H.; Bai, C. L. Signaling aptamer/protein binding by a molecular light switch complex. *Analytical Chemistry.* **2004**, 76, 5230-5235.

121. Stojanovic, M. N.; de Prada, P.; Landry, D. W. Aptamer-based folding fluorescent sensor for cocaine. *Journal of the American Chemical Society.* **2001**, 123, 4928-4931.

122. Modi, S.; Bhatia, D.; Simmel, F. C.; Krishnan, Y. Structural DNA Nanotechnology: From Bases to Bricks, From Structure to Function. *Journal of Physical Chemistry Letters.* **2010**, 1, 1994-2005.

123. Seeman, N. C. Nucleic acid junctions and lattices. *Journal of Theoretical Biology.* **1982**, 99, 237-247.

124. Li, H. Y.; Carter, J. D.; LaBean, T. H. Nanofabrication by DNA self-assembly. *Materials Today.* **2009**, 12, 24-32.

125. Lin, C.; Liu, Y.; Yan, H. Designer DNA Nanoarchitectures. *Biochemistry.* **2009**, 48, 1663-1674.

126. Ko, S. H.; Su, M.; Zhang, C. A.; Ribbe, A. E.; Jiang, W.; Mao, C. D. Synergistic self-assembly of RNA and DNA molecules. *Nature Chemistry.* **2010**, 2, 1050-1055.

127. Hays, F. A.; Watson, J.; Ho, P. S. Caution! DNA crossing: crystal structures of Holliday junctions. *Journal of Biological Chemistry.* **2003**, 278, 49663-49666.

128. Yan, H.; Park, S. H.; Finkelstein, G.; Reif, J. H.; LaBean, T. H. DNA-templated self-assembly of protein arrays and highly conductive nanowires. *Science.* **2003**, 301, 1882-1884.

129. Lin, C. X.; Liu, Y.; Rinker, S.; Yan, H. DNA tile based self-assembly: Building complex nanoarchitectures. *Chemphyschem.* **2006**, 7, 1641-1647.

130. Chen, J. H.; Seeman, N. C. Synthesis from DNA of a Molecule with the Connectivity of a Cube. *Nature.* **1991**, 350, 631-633.

131. He, Y.; Ye, T.; Su, M.; Zhang, C.; Ribbe, A. E.; Jiang, W.; Mao, C. D. Hierarchical self-assembly of DNA into symmetric supramolecular polyhedra. *Nature.* **2008**, 452, 198-U41.

132. Chworos, A.; Severcan, I.; Koyfman, A. Y.; Weinkam, P.; Oroudjev, E.; Hansma, H. G.; Jaeger, L. Building programmable jigsaw puzzles with RNA. *Science.* **2004**, 306, 2068-2072.

133. Severcan, I.; Geary, C.; Chworos, A.; Voss, N.; Jacovetty, E.; Jaeger, L. A polyhedron made of tRNAs. *Nature Chemistry.* **2010**, 2, 772-779.

134. Rothemund, P. W. K. Folding DNA to create nanoscale shapes and patterns. *Nature.* **2006**, 440, 297-302.

135. Hansen, M. N.; Zhang, A. M.; Rangnekar, A.; Bompiani, K. M.; Carter, J. D.; Gothelf, K. V.; LaBean, T. H. Weave Tile Architecture Construction Strategy for DNA Nanotechnology. *Journal of the American Chemical Society.* **2010**, 132, 14481-14486.

136. He, Y.; Tian, Y.; Chen, Y.; Deng, Z.; Ribbe, A. E.; Mao, C. Sequence symmetry as a tool for designing DNA nanostructures. *Angewandte Chemie. International Ed. In English.* **2005**, 44, 6694-6.

137. Chhabra, R.; Sharma, J.; Ke, Y. G.; Liu, Y.; Rinker, S.; Lindsay, S.; Yan, H. Spatially addressable multiprotein nanoarrays templated by aptamer-tagged DNA nanoarchitectures. *Journal of the American Chemical Society.* **2007**, 129, 10304-+.

138. Erben, C. M.; Goodman, R. P.; Turberfield, A. J. Single-molecule protein encapsulation in a rigid DNA cage. *Angewandte Chemie-International Edition.* **2006**, 45, 7414-7417.

139. Park, S. H.; Yin, P.; Liu, Y.; Reif, J. H.; LaBean, T. H.; Yan, H. Programmable DNA self-assemblies for nanoscale organization of ligands and proteins. *Nano Letters.* **2005**, 5, 729-733.

140. Abu-Lail, N. I.; Camesano, T. A. Specific and nonspecific interaction forces between Escherichia coli and silicon nitride, determined by Poisson statistical analysis. *Langmuir.* **2006**, 22, 7296-7301.

141. Willemsen, O. H.; Snel, M. M. E.; Kuipers, L.; Figdor, C. G.; Greve, J.; De Grooth, B. G. A physical approach to reduce nonspecific adhesion in molecular recognition atomic force microscopy. *Biophysical Journal.* **1999**, 76, 716-724.

142. Silberzan, P.; Leger, L.; Ausserre, D.; Benattar, J. J. Silanation of silica surfaces. A new method of constructing pure or mixed monolayers. *Langmuir.* **1991**, 7, 1647-1651.

143. Ros, R.; Schwesinger, F.; Anselmetti, D.; Kubon, M.; Schafer, R.; Pluckthun, A.; Tiefenauer, L. Antigen binding forces of individually addressed single-chain Fv antibody molecules. *Proceedings of the National Academy of Sciences of the United States of America.* **1998**, 95, 7402-7405.

144. Strunz, T.; Oroszlan, K.; Schafer, R.; Guntherodt, H. J. Dynamic force spectroscopy of single DNA molecules. *Proceedings of the National Academy of Sciences of the United States of America.* **1999**, 96, 11277-11282.

145. Yersin, A.; Hirling, H.; Steiner, P.; Magnin, S.; Regazzi, R.; Huni, B.; Huguenot, P.; De Los Rios, P.; Dietler, G.; Catsicas, S.; Kasas, S. Interactions

between synaptic vesicle fusion proteins explored by atomic force microscopy. *Proceedings of the National Academy of Sciences of the United States of America.* **2003**, 100, 8736-8741.

146. Dammer, U.; Popescu, O.; Wagner, P.; Anselmetti, D.; Guntherodt, H. J.; Misevic, G. N. Binding strength between cell-adhesion proteoglycans measured by atomic-force microscopy. *Science.* **1995**, 267, 1173-1175.

147. Touhami, A.; Hoffmann, B.; Vasella, A.; Denis, F. A.; Dufrene, Y. F. Aggregation of yeast cells: direct measurement of discrete lectin-carbohyd rate interactions. *Microbiology-Sgm.* **2003**, 149, 2873-2878.

148. Guiomar, A. J.; Guthrie, J. T.; Evans, S. D. Use of mixed self-assembled monolayers in a study of the effect of the microenvironment on immobilized glucose oxidase. *Langmuir.* **1999**, 15, 1198-1207.

149. Frutos, A. G.; Brockman, J. M.; Corn, R. M. Reversible protection and reactive patterning of amine- and hydroxyl-terminated self-assembled monolayers on gold surfaces for the fabrication of biopolymer arrays. *Langmuir.* **2000**, 16, 2192-2197.

150. Harder, P.; Grunze, M.; Dahint, R.; Whitesides, G. M.; Laibinis, P. E. Molecular conformation in oligo(ethylene glycol)-terminated self-assembled monolayers on gold and silver surfaces determines their ability to resist protein adsorption. *Journal of Physical Chemistry B.* **1998**, 102, 426-436.

151. Biebricher, A.; Paul, A.; Tinnefeld, P.; Golzhauser, A.; Sauer, M. Controlled three-dimensional immobilization of biomolecules on chemically patterned surfaces. *Journal of Biotechnology.* **2004**, 112, 97-107.

152. Lou, X. H.; He, L. Surface passivation using oligo(ethylene glycol) in ATRP-assisted DNA detection. *Sensors and Actuators B-Chemical.* **2008**, 129, 225-230.

153. Brandley, B. K.; Schnaar, R. L. Cell-surface carbohydrates in cell recognition and response. *J Leukoc Biol.* **1986**, 40, 97-111.

154. Lis, H.; Sharon, N. Lectins: Carbohydrate-specific proteins that mediate cellular recognition. *Chemical Reviews.* **1998**, 98, 637-674.

155. Fuster, M. M.; Esko, J. D. The sweet and sour of cancer: Glycans as novel therapeutic targets. *Nature Reviews Cancer.* **2005**, 5, 526-542.

156. Sharon, N.; Lis, H. Lectins as cell recognition molecules. *Science.* **1989**,

246, 227-234.

157. Kiessling, L. L.; Pohl, N. L. Strength in numbers: Non-natural polyvalent carbohydrate derivatives. *Chemistry & Biology.* **1996**, 3, 71-77.

158. Shinohara, Y.; Kim, F.; Shimizu, M.; Goto, M.; Tosu, M.; Hasegawa, Y. Kinetic measurement of the interaction between an oligosaccharide and lectins by a biosensor based on surface-plasmon resonance. *European Journal of Biochemistry.* **1994**, 223, 189-194.

159. Kuno, A.; Uchiyama, N.; Koseki-Kuno, S.; Ebe, Y.; Takashima, S.; Yamada, M.; Hirabayashi, J. Evanescent-field fluorescence-assisted lectin microarray: a new strategy for glycan profiling. *Nature Methods.* **2005**, 2, 851-856.

160. Lekka, M.; Laidler, P.; Dulinska, J.; Labedz, M.; Pyka, G. Probing molecular interaction between concanavalin A and mannose ligands by means of SFM. *European Biophysics Journal with Biophysics Letters.* **2004**, 33, 644-650.

161. Touhami, A.; Hoffmann, B.; Vasella, A.; Denis, F. A.; Dufrene, Y. F. Probing specific lectin-carbohydrate interactions using atomic force microscopy imaging and force measurements. *Langmuir.* **2003**, 19, 1745-1751.

162. Vetter, D.; Gallop, M. A. Strategies for the Synthesis and Screening of Glycoconjugates. 1. A Library of Glycosylamines. *Bioconjugate Chemistry.* **1995**, 6, 316-318.

163. Brun, M. A.; Disney, M. D.; Seeberger, P. H. Miniaturization of microwave-assisted carbohydrate functionalization to create oligosaccharide microarrays. *Chembiochem.* **2006**, 7, 421-424.

164. Wagner, P.; Hegner, M.; Kemen, P.; Zaugg, F.; Semenza, G. Covalent immobilization of native biomolecules onto Au(111) via N-hydroxysuccinimide ester functionalized self-assembled monolayers for scanning probe microscopy. *Biophysical Journal.* **1996**, 70, 2052-2066.

165. Hutter, J. L.; Bechhoefer, J. Calibration of Atomic-Force Microscope Tips. *Review of Scientific Instruments.* **1993**, 64, 1868-1873.

166. Lis, H.; Sharon, N., *Lectins*. 2 ed.; Springer: 2007.

167. Weatherman, R. V.; Mortell, K. I.; Chervenak, M.; Kiessling, L. L.; Toone, E. J. Specificity of C-glycoside complexation by mannose glucose specific lectins. *Biochemistry.* **1996**, 35, 3619-3624.

168. Folkers, J. P.; Laibinis, P. E.; Whitesides, G. M. Self-Assembled Monolayers of Alkanethiols on Gold - the Adsorption and Wetting Properties of Monolayers Derived from 2 Components with Alkane Chains of Different Lengths. *Journal of Adhesion Science and Technology*. **1992**, 6, 1397-1410.

169. Prime, K. L.; Whitesides, G. M. Adsorption of proteins onto surfaces containing end-attached oligo(ethylene oxide): A model system using self-assembled monolayers. *Journal of the American Chemical Society*. **1993**, 115, 10714-10721.

170. Hardman, K. D.; Wood, M. K.; Schiffer, M.; Edmundso.Ab; Ainswort.Cf Structure of Concanavalin-a at 4.25-Angstrom Resolution - (X-Ray Diffraction/Electron Density Map/Isomorphous Replacement/Subunits/Molecular Weight). *Proceedings of the National Academy of Sciences of the United States of America*. **1971**, 68, 1393-&.

171. Senear, D. F.; Teller, D. C. Thermodynamics of Concanavalin-a Dimer-Tetramer Self-Association - Sedimentation Equilibrium Studies. *Biochemistry*. **1981**, 20, 3076-3083.

172. Florin, E. L.; Rief, M.; Lehmann, H.; Ludwig, M.; Dornmair, C.; Moy, V. T.; Gaub, H. E. Sensing specific molecular-interactions with the atomic-force microscope. *Biosensors & Bioelectronics*. **1995**, 10, 895-901.

173. Israelachvili, J., *Intermolecular and surface forces*. 2nd ed.; Academic Press: San Diego, CA, 1992.

174. Clifford, C. A.; Seah, M. P. The determination of atomic force microscope cantilever spring constants via dimensional methods for nanomechanical analysis. *Nanotechnology*. **2005**, 16, 1666-1680.

175. Evans, E.; Ritchie, K. Dynamic strength of molecular adhesion bonds. *Biophys J*. **1997**, 72, 1541-55.

176. Wolfenden, M. L.; Cloninger, M. J. Carbohydrate-functionalized dendrimers to investigate the predictable tunability of multivalent interactions. *Bioconjugate Chemistry*. **2006**, 17, 958-966.

177. Ellington, A. D.; Szostak, J. W. Selection Invitro of Single-Stranded-DNA Molecules That Fold into Specific Ligand-Binding Structures. *Nature*. **1992**, 355, 850-852.

178. Tuerk, C.; Gold, L. Systematic Evolution of Ligands by Exponential Enrichment - Rna Ligands to Bacteriophage-T4 DNA-Polymerase. *Science*. **1990**, 249, 505-510.

179. Ellington, A. D.; Szostak, J. W. Invitro selection of RNA molecules that bind specific ligands *Nature.* **1990**, 346, 818-822.

180. Potty, A. S. R.; Kourentzi, K.; Fang, H.; Jackson, G. W.; Zhang, X.; Legge, G. B.; Willson, R. C. Biophysical Characterization of DNA Aptamer Interactions with Vascular Endothelial Growth Factor. *Biopolymers.* **2009**, 91, 145-156.

181. Taylor, J. N.; Darugar, Q.; Kourentzi, K.; Willson, R. C.; Landes, C. F. Dynamics of an anti-VEGF DNA aptamer: A single-molecule study. *Biochemical and Biophysical Research Communications.* **2008**, 373, 213-218.

182. Basnar, B.; Elnathan, R.; Willner, I. Following aptamer-thrombin binding by force measurements. *Analytical Chemistry.* **2006**, 78, 3638-42.

183. Carothers, J. M.; Oestreich, S. C.; Szostak, J. W. Aptamers selected for higher-affinity binding are not more specific for the target ligand. *Journal of the American Chemical Society.* **2006**, 128, 7929-7937.

184. Carmeliet, P. Angiogenesis in life, disease and medicine. *Nature.* **2005**, 438, 932-936.

185. Muller, Y. A.; Christinger, H. W.; Keyt, B. A.; deVos, A. M. The crystal structure of vascular endothelial growth factor (VEGF) refined to 1.93 angstrom resolution: multiple copy flexibility and receptor binding. *Structure.* **1997**, 5, 1325-1338.

186. Park, J. E.; Keller, G. A.; Ferrara, N. The vascular endothelial growth factor (VEGF) isoforms: differential deposition into the subepithelial extracellular matrix and bioactivity of extracellular matrix-bound VEGF. *Molecular Biology of the Cell.* **1993**, 4, 1317-1326.

187. Jellinek, D.; Green, L. S.; Bell, C.; Janjic, N. Inibition of receptor-binding by high-affnity RNA ligands to vascular endothelial growth-factor. *Biochemistry.* **1994**, 33, 10450-10456.

188. Ferrara, N.; Houck, K. A.; Jakeman, L. B.; Winer, J.; Leung, D. W. The Vascular Endothelial Growth-Factor Family of Polypeptides. *Journal of Cellular Biochemistry.* **1991**, 47, 211-218.

189. Ruckman, J.; Green, L. S.; Beeson, J.; Waugh, S.; Gillette, W. L.; Henninger, D. D.; Claesson-Welsh, L.; Janjic, N. 2 '-fluoropyrimidine RNA-based aptamers to the 165-amino acid form of vascular endothelial growth factor (VEGF(165)) - Inhibition of receptor binding and VEGF-induced vascular permeability through interactions requiring the exon 7-encoded domain. *Journal of*

Biological Chemistry. **1998**, 273, 20556-20567.

190. Lo, Y. S.; Zhu, Y. J.; Beebe, T. P. Loading-rate dependence of individual ligand-receptor bond-rupture forces studied by atomic force microscopy. *Langmuir*. **2001**, 17, 3741-3748.

191. Cha, T.; Guo, A.; Jun, Y.; Pei, D. Q.; Zhu, X. Y. Immobilization of oriented protein molecules on poly(ethylene glycol)-coated Si(111). *Proteomics*. **2004**, 4, 1965-1976.

192. Ikeda, T.; Hata, Y.; Ninomiya, K.; Ikura, Y.; Takeguchi, K.; Aoyagi, S.; Hirota, R.; Kuroda, A. Oriented immobilization of antibodies on a silicon wafer using Si-tagged protein A. *Analytical Biochemistry*. **2009**, 385, 132-137.

193. Hodneland, C. D.; Lee, Y. S.; Min, D. H.; Mrksich, M. Selective immobilization of proteins to self-assembled monolayers presenting active site-directed capture ligands. *Proceedings of the National Academy of Sciences of the United States of America*. **2002**, 99, 5048-5052.

194. Hofacker, I. L. Vienna RNA secondary structure server. *Nucleic Acids Research*. **2003**, 31, 3429-3431.

195. Li, Y.; Lee, H. J.; Corn, R. M. Detection of protein biomarkers using RNA aptamer microarrays and enzymatically amplified surface plasmon resonance imaging. *Analytical Chemistry*. **2007**, 79, 1082-1088.

196. Zuker, M. Mfold web server for nucleic acid folding and hybridization prediction. *Nucleic Acids Research*. **2003**, 31, 3406-3415.

197. Keyt, B. A.; Nguyen, H. V.; Berleau, L. T.; Duarte, C. M.; Park, J.; Chen, H.; Ferrara, N. Identification of vascular endothelial growth factor determinants for binding KDR and FLT-1 receptors - Generation of receptor-selective VEGF variants by site-directed mutagenesis. *Journal of Biological Chemistry*. **1996**, 271, 5638-5646.

198. Merkel, R.; Nassoy, P.; Leung, A.; Ritchie, K.; Evans, E. Energy landscapes of receptor-ligand bonds explored with dynamic force spectroscopy. *Nature*. **1999**, 397, 50-53.

199. Lo, Y. S.; Huefner, N. D.; Chan, W. S.; Stevens, F.; Harris, J. M.; Beebe, T. P. Specific interactions between biotin and avidin studied by atomic force microscopy using the Poisson statistical analysis method. *Langmuir*. **1999**, 15, 1373-1382.

200. Evans, E.; Leung, A.; Hammer, D.; Simon, S. Chemically distinct transition states govern rapid dissociation of single L-selectin bonds under force. *Proceedings of the National Academy of Sciences of the United States of America.* **2001**, 98, 3784-3789.

201. Yu, Z. B.; Schonhoft, J. D.; Dhakal, S.; Bajracharya, R.; Hegde, R.; Basu, S.; Mao, H. B. ILPR G-Quadruplexes Formed in Seconds Demonstrate High Mechanical Stabilities. *Journal of the American Chemical Society.* **2009**, 131, 1876-1882.

202. Draper, D. E.; Grilley, D.; Soto, A. M. Ions and RNA folding. *Annual Review of Biophysics and Biomolecular Structure.* **2005**, 34, 221-243.

203. Draper, D. E.; Misra, V. K. RNA shows its metal. *Nature Structural Biology.* **1998**, 5, 927-930.

204. Tinoco, I.; Bustamante, C. How RNA folds. *Journal of Molecular Biology.* **1999**, 293, 271-281.

205. Gonzalez, R. L.; Tinoco, I. Solution structure and thermodynamics of a divalent metal ion binding site in an RNA pseudoknot. *Faseb Journal.* **1999**, 13, A1326-A1326.

206. Cho, E. J.; Collett, J. R.; Szafranska, A. E.; Ellington, A. D. Optimization of aptamer microarray technology for multiple protein targets. *Analytica Chimica Acta.* **2006**, 564, 82-90.

207. Cho, E. J.; Lee, J.-W.; Ellington, A. D. Applications of aptamers as sensors. *Annual Reviews in Analytical Chemistry.* **2009**, 2, 12.1-12.24.

208. Liu, M.; Amro, N. A.; Liu, G. Y., Nanografting for surface physical chemistry. In *Annual Review of Physical Chemistry*, Annual Reviews: Palo Alto, 2008; Vol. 59, pp 367-386.

209. Liu, M. Z.; Amro, N. A.; Chow, C. S.; Liu, G. Y. Production of nanostructures of DNA on surfaces. *Nano Letters.* **2002**, 2, 863-867.

210. Castronovo, M.; Radovic, S.; Grunwald, C.; Casalis, L.; Morgante, M.; Scoles, G. Control of Steric Hindrance on Restriction Enzyme Reactions with Surface-Bound DNA Nanostructures. *Nano Letters.* **2008**, 8, 4140-4145.

211. Niemeyer, C. M. Functional devices from DNA and proteins. *Nano Today.* **2007**, 2, 42-52.

212. Bano, F.; Fruk, L.; Sanavio, B.; Glettenberg, M.; Casalls, L.; Niemeyer, C. M.; Scoles, G. Toward Multiprotein Nanoarrays Using Nanografting and DNA Directed Immobilization of Proteins. *Nano Letters.* **2009**, 9, 2614-2618.

213. Balamurugan, S.; Obubuafo, A.; Soper, S. A.; Spivak, D. A. Surface immobilization methods for aptamer diagnostic applications. *Analytical and Bioanalytical Chemistry.* **2008**, 390, 1009-1021.

214. Fang, X. H.; Sen, A.; Vicens, M.; Tan, W. H. Synthetic DNA aptamers to detect protein molecular variants in a high-throughput fluorescence quenching assay. *Chembiochem.* **2003**, 4, 829-834.

215. Huizenga, D. E.; Szostak, J. W. A DNA aptamer that binds adenosine and ATP. *Biochemistry.* **1995**, 34, 656-665.

216. Sassanfar, M.; Szostak, J. W. An RNA motif that binds ATP. *Nature.* **1993**, 364, 550-553.

217. Caruso, F.; Rodda, E.; Furlong, D. F.; Niikura, K.; Okahata, Y. Quartz crystal microbalance study of DNA immobilization and hybridization for nucleic acid sensor development. *Analytical Chemistry.* **1997**, 69, 2043-2049.

218. Yamaguchi, S.; Shimomura, T.; Tatsuma, T.; Oyama, N. Adsorption, Immobilization, and Hybridization of DNA Studied by the Use of Quartz-Crystal Oscillators. *Analytical Chemistry.* **1993**, 65, 1925-1927.

219. Peterlinz, K. A.; Georgiadis, R. M.; Herne, T. M.; Tarlov, M. J. Observation of hybridization and dehybridization of thiol-tethered DNA using two-color surface plasmon resonance spectroscopy. *Journal of the American Chemical Society.* **1997**, 119, 3401-3402.

220. Eichler, D. C.; Eales, S. J. The effect of RNA secondary structure on the action of a nucleolar endoribonuclease. *Journal of Biological Chemistry.* **1983**, 258, 49-53.

221. Bruckenstein, S.; Michalski, M.; Fensore, A.; Li, Z.; Hillman, A. R. Dual Quartz Crystal Microbalance Oscillator Circuit. Minimizing Effects due to Liquid Viscosity, Density, and Temperature. *Analytical Chemistry.* **1994**, 66, 1847-1852.

222. Wiegand, T. W.; Williams, P. B.; Dreskin, S. C.; Jouvin, M. H.; Kinet, J. P.; Tasset, D. High-affinity oligonucleotide ligands to human IgE inhibit binding to Fc epsilon receptor I. *Journal of Immunology.* **1996**, 157, 221-230.

223. Herne, T. M.; Tarlov, M. J. Characterization of DNA probes immobilized

on gold surfaces. *Journal of the American Chemical Society.* **1997**, 119, 8916-8920.

224. Boozer, C.; Chen, S. F.; Jiang, S. Y. Controlling DNA orientation on mixed ssDNA/OEG SAMs. *Langmuir.* **2006**, 22, 4694-4698.

225. Li, L.; Chen, S.; Zheng, J.; Ratner, B. D.; Jiang, S. Protein adsorption on oligo(ethylene glycol) terminated alkanethiolate self-assembled monolayers: The molecular basis for non fouling behavior. *Journal of Physical Chemistry B.* **2005**, 109, 2934-2941.

226. Dammer, U.; Hegner, M.; Anselmetti, D.; Wagner, P.; Dreier, M.; Huber, W.; Guntherodt, H. J. Specific antigen/antibody interactions measured by force microscopy. *Biophysical Journal.* **1996**, 70, 2437-41.

227. Jellinek, D.; Lynott, C. K.; Rifkin, D. B.; Janjic, N. High-affinity RNA ligands to basic fibroblast growth-factor inhibit receptor-binding. *Proceedings of the National Academy of Sciences of the United States of America.* **1993**, 90, 11227-11231.

228. Ebara, Y.; Okahata, Y. A kinetic-study of Concanavalin-A binding to glycolipid monolayers by using a quartz-crystal microbalance. *Journal of the American Chemical Society.* **1994**, 116, 11209-11212.

229. Mao, Y.; Wei, W.; He, D.; Nie, L.; Yao, S. Monitoring and Kinetic Parameter Estimation for the Binding Process of Berberine Hydrochloride to Bovine Serum Albumin with Piezoelectric Quartz Crystal Impedance Analysis. *Analytical Biochemistry.* **2002**, 306, 23-30.

230. Lebed, K.; Kulik, A. J.; Forro, L.; Lekka, M. Lectin-carbohydrate affinity measured using a quartz crystal microbalance. *Journal of Colloid and Interface Science.* **2006**, 299, 41-48.

231. Seeman, N. C. DNA in a material world. *Nature.* **2003**, 421, 427-431.

232. Aldaye, F. A.; Palmer, A. L.; Sleiman, H. F. Assembling materials with DNA as the guide. *Science.* **2008**, 321, 1795-1799.

233. Jaeger, L.; Chworos, A. The architectonics of programmable RNA and DNA nanostructures. *Current Opinion in Structural Biology.* **2006**, 16, 531-543.

234. He, Y.; Ye, T.; Su, M.; Zhang, C.; Ribbe, A. E.; Jiang, W.; Mao, C. D. Hierarchical self-assembly of DNA into symmetric supramolecular polyhedra. *Nature.* **2008**, 452, 198-202.

235. He, Y.; Tian, Y.; Chen, Y.; Deng, Z.; Ribbe, A. E.; Mao, C. Sequence Symmetry as a Tool for Designing DNA Nanostructures. *Angewandte Chemie-International Edition.* **2005**, 44, 6694-6696.

236. Chhabra, R.; Sharma, J.; Ke, Y. G.; Liu, Y.; Rinker, S.; Lindsay, S.; Yan, H. Spatially addressable multiprotein nanoarrays templated by aptamer-tagged DNA nanoarchitectures. *Journal of the American Chemical Society.* **2007**, 129, 10304-10306.

237. Sanderson, K. Bioengineering: What to make with DNA origami. *Nature.* **2010**, 464, 158-159.

238. Rinker, S.; Ke, Y. G.; Liu, Y.; Chhabra, R.; Yan, H. Self-assembled DNA nanostructures for distance-dependent multivalent ligand-protein binding. *Nature Nanotechnology.* **2008**, 3, 418-422.

239. Grabow, W. W.; Zakrevsky, P.; Afonin, K. A.; Chworos, A.; Shapiro, B. A.; Jaeger, L. Self-Assembling RNA Nanorings Based on RNAI/II Inverse Kissing Complexes. *Nano Letters.* **2011**, 11, 878-887.

240. Zhang, C. A.; Su, M.; He, Y.; Leng, Y. J.; Ribbe, A. E.; Wang, G. S.; Jiang, W.; Mao, C. D. Exterior modification of a DNA tetrahedron. *Chemical Communications.* **2010**, 46, 6792-6794.

241. Wong, N. Y.; Zhang, C.; Tan, L. H.; Lu, Y. Site-Specific Attachment of Proteins onto a 3D DNA Tetrahedron through Backbone-Modified Phosphorothioate DNA. *Small.* **2011**, 7, 1427-1430.

242. Shen, W. Q.; Zhong, H.; Neff, D.; Norton, M. L. NTA Directed Protein Nanopatterning on DNA Origami Nanoconstructs. *Journal of the American Chemical Society.* **2009**, 131, 6660-6661.

243. Sun, X. P.; Ko, S. H.; Zhang, C. A.; Ribbe, A. E.; Mao, C. D. Surface-Mediated DNA Self-Assembly. *Journal of the American Chemical Society.* **2009**, 131, 13248-13249.

244. Zadeh, J. N.; Steenberg, C. D.; Bois, J. S.; Wolfe, B. R.; Pierce, M. B.; Khan, A. R.; Dirks, R. M.; Pierce, N. A. NUPACK: Analysis and design of nucleic acid systems. *Journal of Computational Chemistry.* **2011**, 32, 170-173.

245. Tasset, D. M.; Kubik, M. F.; Steiner, W. Oligonucleotide inhibitors of human thrombin that bind distinct epitopes. *Journal of Molecular Biology.* **1997**, 272, 688-698.

246. Lyubchenko, Y. L.; Gall, A. A.; Shlyakhtenko, L. S.; Harrington, R. E.; Jacobs, B. L.; Oden, P. I.; Lindsay, S. M. Atomic force microscopy imaging of double stranded DNA and RNA. *Journal of Biomolecular Structure & Dynamics.* **1992**, 10, 589-606.

247. Severcan, I.; Geary, C.; Verzemnieks, E.; Chworos, A.; Jaeger, L. Square-Shaped RNA Particles from Different RNA Folds. *Nano Letters.* **2009**, 9, 1270-1277.

248. Chang, M.; Yang, C. S.; Huang, D. M. Aptamer-Conjugated DNA Icosahedral Nanoparticles As a Carrier of Doxorubicin for Cancer Therapy. *ACS Nano.* **2011**, 5, 6156-6163.

249. He, Y.; Chen, Y.; Liu, H. P.; Ribbe, A. E.; Mao, C. D. Self-assembly of hexagonal DNA two-dimensional (2D) arrays. *Journal of the American Chemical Society*. **2005**, 127, 12202-12203.

250. Lee, J. F.; Stovall, G. M.; Ellington, A. D. Aptamer therapeutics advance. *Current Opinion in Chemical Biology*. **2006**, 10, 282-289.

251. Lin, C.; Katilius, E.; Liu, Y.; Zhang, J.; Yan, H. Self-Assembled Signaling Aptamer DNA Arrays for Protein Detection. *Angewandte Chemie-International Edition.* **2006**, 45, 5296-5301.

252. Hermann, T.; Patel, D. J. Adaptive recognition by nucleic acid aptamers. *Science.* **2000**, 287, 820-825.

253. Gago, S.; de la Pena, M.; Flores, R. A kissing-loop interaction in a hammerhead viroid RNA critical for its in vitro folding and in vivo viability. *Rna-a Publication of the Rna Society.* **2005**, 11, 1073-1083.

254. Dirks, R. M.; Pierce, N. A. An algorithm for computing nucleic acid base-pairing probabilities including pseudoknots. *Journal of Computational Chemistry.* **2004**, 25, 1295-1304.

255. Seeman, N. C. An overview of structural DNA Nanotechnology. *Molecular Biotechnology.* **2007**, 37, 246-257.

256. Savran, C. A.; Knudsen, S. M.; Ellington, A. D.; Manalis, S. R. Micromechanical detection of proteins using aptamer-based receptor molecules. *Analytical Chemistry.* **2004**, 76, 3194-3198.

257. Dahirel, V.; Paillusson, F.; Jardat, M.; Barbi, M.; Victor, J.-M. Nonspecific DNA-Protein Interaction: Why Proteins Can Diffuse along DNA. *Physical Review*

Letters. **2009**, 102, 228101-1-228101-4.

258. Krausch, G.; Lysetska, M.; Zettl, H.; Oka, I.; Lipps, G.; Krauss, G. Site-specific binding of the 9.5 kilodalton DNA-binding protein ORF80 visualized by atomic force microscopy. *Biomacromolecules.* **2005**, 6, 1252-1257.

259. Chakrabarty, S.; Zhang, X. J.; Bharti, P.; Chujo, Y.; Miyake, J.; Wynne, K. J.; Yadavalli, V. K. Processing dependence of surface morphology in condensation cured PDMS nanocomposites. *Polymer.* **2010**, 51, 5756-5763.

APPENDIX

Permits of Using Figures and Tables in this Dissertation

Supplier	Elsevier Limited The Boulevard,Langford Lane Kidlington,Oxford,OX5 1GB,UK
Registered Company Number	1982084
Customer name	Xiaojuan Zhang
Customer address	5300 Glenside Dr. Apt 312 Henrico, VA 23228
License number	2780610022668
License date	Nov 02, 2011
Licensed content publisher	Elsevier
Licensed content publication	Analytica Chimica Acta
Licensed content title	Functionalized self-assembled monolayers for measuring single molecule lectin carbohydrate interactions
Licensed content author	Xiaojuan Zhang,Vamsi K. Yadavalli
Licensed content date	1 September 2009
Licensed content volume number	649
Licensed content issue number	1
Number of pages	7
Start Page	1
End Page	7
Type of Use	reuse in a thesis/dissertation
Portion	full article
Format	electronic
Are you the author of this Elsevier article?	Yes
Will you be translating?	No
Order reference number	
Title of your thesis/dissertation	Investigation of biomolecular interactions for the development of sensors and diagnostics
Expected completion date	Dec 2011
Estimated size (number of pages)	150
Elsevier VAT number	GB 494 6272 12
Permissions price	0.00 USD
VAT/Local Sales Tax	0.0 USD / 0.0 GBP
Total	0.00 USD
Terms and Conditions	

Supplier	Elsevier Limited The Boulevard,Langford Lane Kidlington,Oxford,OX5 1GB,UK
Registered Company Number	1982084
Customer name	Xiaojuan Zhang
Customer address	5300 Glenside Dr. Apt 312 Henrico, VA 23228
License number	2780611091000
License date	Nov 02, 2011
Licensed content publisher	Elsevier
Licensed content publication	Biosensors and Bioelectronics
Licensed content title	Surface immobilization of DNA aptamers for biosensing and protein interaction analysis
Licensed content author	Xiaojuan Zhang,Vamsi K. Yadavalli
Licensed content date	15 March 2011
Licensed content volume number	26
Licensed content issue number	7
Number of pages	6
Start Page	3142
End Page	3147
Type of Use	reuse in a thesis/dissertation
Intended publisher of new work	other
Portion	full article
Format	both print and electronic
Are you the author of this Elsevier article?	Yes
Will you be translating?	No
Order reference number	
Title of your thesis/dissertation	Investigation of biomolecular interactions for the development of sensors and diagnostics
Expected completion date	Dec 2011
Estimated size (number of pages)	150
Elsevier VAT number	GB 494 6272 12
Permissions price	0.00 USD
VAT/Local Sales Tax	0.0 USD / 0.0 GBP
Total	0.00 USD

VITA

Xiaojuan Zhang was born on May 8, 1982 in Hohhot, Inner Mongolia, China. She is Chinese citizen. She attended Jiangnan University, Wuxi, China from September 2001 to June 2005 earning the Bachelor of Engineering in Biotechnology, followed by Master of Science in Engineering, majoring in Fermentation Engineering in June 2007. She started her graduate studies in Chemical and Life Engineering at Virginia Commonwealth University in Fall 2008.